

# Synthesis and Characterisation of P- or As- containing Nanoparticle Precursors



Dissertation zur Erlangung des  
DOKTORGRADES DER NATURWISSENSCHAFTEN

(Dr. rer. nat.)

der Fakultät für Chemie und Pharmazie

der Universität Regensburg

Vorgelegt von

**Reinhard Rund**

aus Massing

**Regensburg 2020**



Diese Arbeit wurde angeleitet von Prof. Dr. Manfred Scheer.

Promotionsgesuch eingereicht am: 03.03.2020

Tag der mündlichen Prüfung: 05.06.2020

Vorsitzender: Prof. Dr. Hubert Motschman

Prüfungsausschuss: Prof. Dr. Manfred Scheer

Prof. Dr. Henri Brunner

Prof. Dr. Frank-Michael Matysik



Universität Regensburg

## Eidesstattliche Erklärung

Ich erkläre hiermit an Eides statt, dass ich die vorliegende Arbeit ohne unzulässige Hilfe Dritter und ohne Benutzung anderer als der angegebenen Hilfsmittel angefertigt habe; die aus anderen Quellen direkt oder indirekt übernommenen Daten und Konzepte sind unter Angabe des Literaturzitats gekennzeichnet.

---

Reinhard Rund

This thesis was elaborated within the period from November 2014 until March 2020 in the Institute of Inorganic Chemistry at the University of Regensburg under the supervision of Prof. Dr. Manfred Scheer.



*Meinen Eltern gewidmet*

*Erschaffe Meisterwerke*



## Table of Contents

1. Introduction.....	1
1.1. Definition and History of Nanoparticles .....	1
1.2. Properties of Nanomaterials .....	7
1.3. Production of Nanomaterials .....	9
1.4. Applications and Dangers of Nanoparticles .....	13
1.5. References .....	15
2. Conceptual Formulation .....	18
3. The Parent Diarsene $\text{HAs=AsH}$ as Side-on Bound Ligand in an Iron Carbonyl Complex.....	19
3.1. Preface .....	19
3.2. Author contribution .....	19
3.3. Abstract.....	19
3.4. Introduction .....	20
3.5. Results and Discussion .....	21
3.6. Conclusion .....	27
3.7. Supporting Information .....	28
3.8. Miscellaneous and Outlook .....	47
3.9. References .....	50
4. Examination of Indium Triphospholyls as Precursors for Nanoparticle Syntheses.....	53
4.1. Author contribution .....	53
4.2. Abstract.....	53
4.3. Introduction .....	53
4.4. Results and Discussion .....	54
4.5. Conclusion .....	62
4.6. Supporting Information .....	63
4.7. References .....	78
5. Conclusion.....	80
5.1. A Parent Diarsene $\text{HAs=AsH}$ Complex as AsH Unit Source to Novel Compounds.....	80
5.2. Indium Triphospholyls Examined as Precursor for Nanoparticle Synthesis.....	83
6. Appendix .....	85
6.1. List of Numbered Compounds.....	85
6.2. List of Abbreviations .....	87
6.3. Danksagung.....	90



# 1. Introduction

## 1.1. Definition and History of Nanoparticles

The word *nános* derives from the ancient Greek *vávoç*, which can be translated into dwarf. Accordingly, nanotechnology deals with very small materials in the range of 1 to 100 nm. 3D materials can be described as materials with an unrestricted latitude in all three dimensions. The restriction of one of the three dimensions (latitude is below 100 nm) leads to two dimensional (2D) layers. A further restriction of another dimension leads to nanowires or nanotubes. Finally, the restriction of the latitude in all three dimensions leads to zero dimensional (0D) nanoparticles (NP), which are often called quantum dots in the case of semiconductors. Figure 1 shows four carbon-based examples for the above described restrictions.

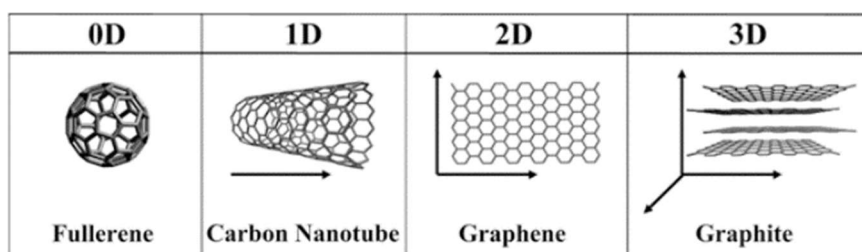


**Figure 1:** Examples for 0D, 1D, 2D, and 3D carbon nanostructures. Reprinted with permission from Springer International Publishing: Carbon Nanomaterials as Adsorbents for Environmental and Biological Applications by Carlos P. Bergmann and Fernando Machado Machado, Copyright 2015

In space, NP exist since billions of years and can be detected by methods such as emission light analysis or the investigation of meteorites. As example, silicon nanoparticles with a of 1 nm were detected through their blue luminescence in planetary nebulae, which is identified in addition to the red emission wavelengths (Figure 2).<sup>[1]</sup> <sup>54</sup>Cr nanoparticles were found in the Orgueil meteorite<sup>[2]</sup> and fullerenes were detected in the Allende meteorite, the largest carbonaceous chondrite ever found on earth.<sup>[3]</sup>

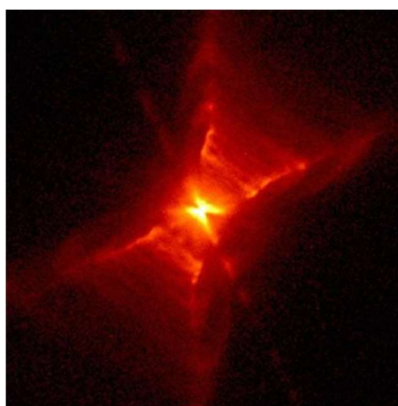


**Figure 2:** Image of a proto-planetary nebula as Red Rectangle. Image from <https://commons.wikimedia.org/w/index.php?curid=15307726>.

On earth, nanomaterials (NM) exist in various forms. They could naturally develop through volcanic eruptions or forest fires as fine dust.<sup>[4]</sup> First „earth made“ nanomaterials were released in the atmosphere 3.5 billion years ago, as volcanic eruption took place as side effect of the starting plate tectonics.<sup>[5]</sup>

Like the german philosopher Andreas Tenzer stated: „The most creative artist is the nature.“, and so the nature is full of amazing examples which are caused by nanomaterial effects.

There are several effects, which can be attributed to nanomaterial effects, such as the white appearance of milk. This emulsion in nanoscale is causing the so-called Tyndall effect, which describes the light scattering of particles in a colloid. In opals, a mineraloid, the characteristic colour originates from the reflection and interference of very small particles of silica gel (Figure 3).

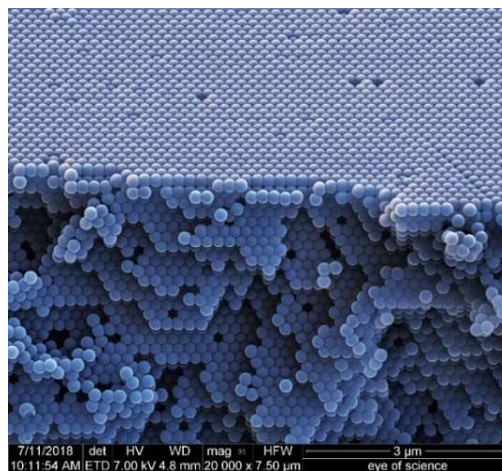


**Figure 3:** Scanning Electron Microscope (SEM) Image of the particles of an opaline. © eye of science, Meckes & Ottawa.

One further example is the mother of pearl, nacre, which is produced by some molluscs as inner shell. Nacre consists of layers of thin platelets of aragonite ( $\text{CaCO}_3$ ) and an organic matrix (Figure 4). Each of these layers reflect and transmit light, which leads to change in colour depending on the angle of the observer.<sup>[6]</sup>

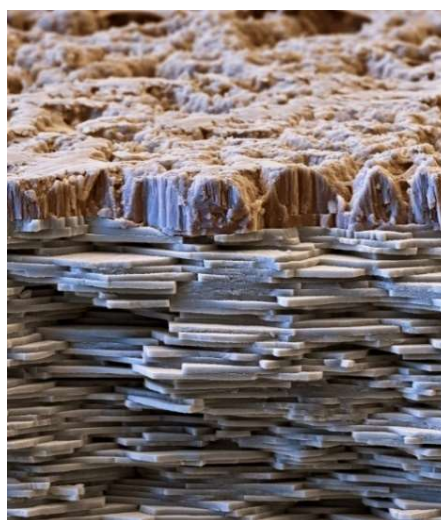


**Figure 4:** SEM Image of the shell of a nautilus, 5000x magnification. © eye of science, Meckes & Ottawa.

Noteworthy, the bright and shining colour of the butterfly wings of some butterfly species is also attributed to NM effects. The colour does not derive from pigments, since the material of the wing is colourless. The bright blue colour of the *Morpho peleides* or the green colour of the *Papilio palinurus* evolves from the small nanoscopic grooves in its scales (Figure 5). These nanoscopic arrangements cause coherent scattering of the light, causing these beautiful colours.<sup>[7][8]</sup>

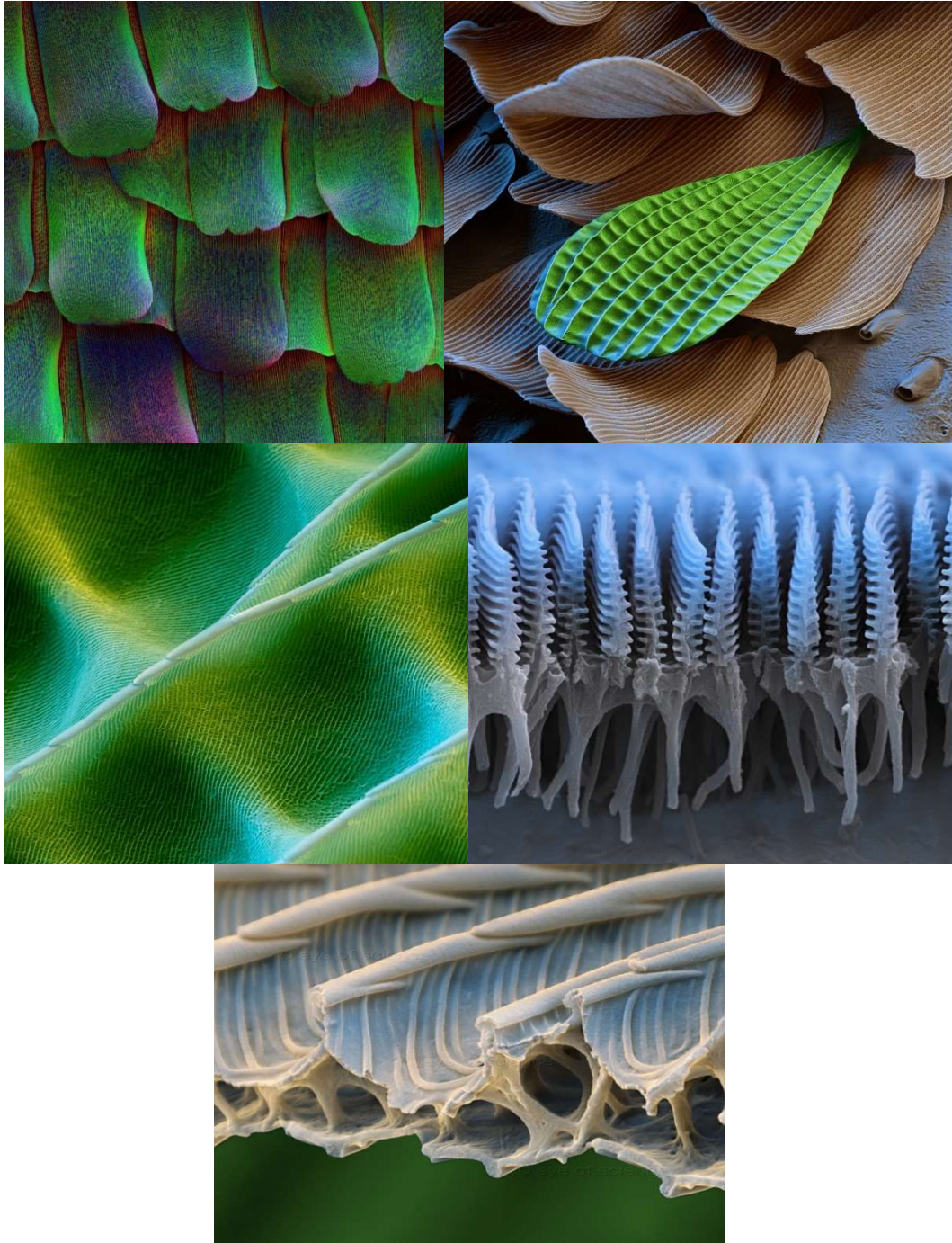


**Figure 5:** SEM Images the wing of butterflys. Top left: 260x magnification of a wing of the Papilio Palinurus. Top right: 800x magnification of a wing of the Papilio Palinurus. Middle left: 10 000x magnification of a wing of the Papilio Palinurus. Middle right: 20 000x magnification of the shed of the Morpho Peleides. Bottom: 32000x magnification of a butterfly wing scale (15 cm image width). All Images: © eye of science, Meckes & Ottawa.



Aristoteles already described the ability of geckos to run down trees.<sup>[9]</sup> The toes of some geckos end up in millions of small adhesive hairs, the setae. The myriads of setae, which sum up to a huge surface, provide strong van der Waals interactions, causing strong adhesion (Figure 6).<sup>[10]</sup>



**Figure 6:** SEM Image of the setae on the foot of a gecko. Left: 120x magnification. Right top: image width ~200  $\mu\text{m}$ . Right bottom: 20 000x magnification. All images: © eye of science, Meckes & Ottawa.

Another example of nature made nanomaterials is found in the microscopic dimension. Some bacteria possess nano-sized magnets which help them to navigate like a compass (Figure 7).<sup>[11]</sup>

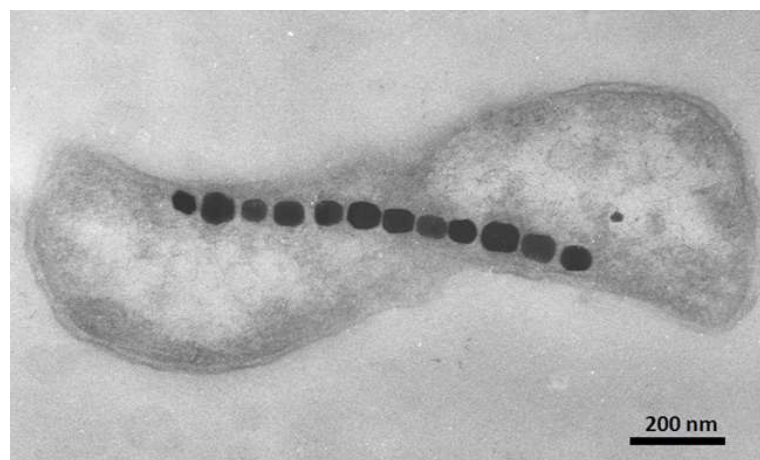


**Figure 7:** Transmission Electron Microscope (TEM) image of twelve magnetite nanoparticles ( $\text{Fe}_3\text{O}_4\text{-NP}$ ) in a magnetotactic bacteria. Reprinted with permission from Nature Education Knowledge, "Bacteria That Synthesize Nano-sized Compasses to Navigate Using Earth's Geomagnetic Field". Chen, L., Bazylinski, D. A. & Lower, B. H., Copyright 2010.

If we view the leaf of a nelumbo, commonly called lotus, under an electron microscope, the surface is covered with small pinches, which are coated with wax (Figure 8). The superhydrophobic nature of the surface allows waterdrops to flow undamped over the leaf enclosing hydrophilic dirt and remove it from the surface. The advantage for the lotus is that microorganisms are not able to colonise and the surface stays free from dirt preventing photosynthesis.



**Figure 8:** Left: Superhydrophobic surfaces depicted with water droplets on a nelumbo leaf. Image by H. Zell from <https://commons.wikimedia.org/w/index.php?curid=10799164> (CC BY-SA 3.0). Right: SEM image of a lotus leaf, 3900x magnification. © eye of science, Meckes & Ottawa.

Despite their unawareness about the existence of nanomaterials, humans used them since hundreds of years. The ancient Egyptians used soot as pigments for black ink.<sup>[12]</sup> Potters used colloidal precious metals to produce astonishing colour effects. The best-known example for this phenomenon is the roman Lycurgus cup (Figure 9). Depicted on the cup is the fight between the king Lycurgus and Ambrosia transformed into a vine.



**Figure 9:** The Lycurgus cup from the 4<sup>th</sup> century. Left: If photographed without backlight, the cup remains green. Image by Johnbod from <https://commons.wikimedia.org/w/index.php?curid=11549754> (CC BY-SA 3.0.). Right: When light shines through the cup, it is red. Image by Johnbod from <https://commons.wikimedia.org/w/index.php?curid=11410907> (CC BY-SA 3.0.).

The use of silver and gold nanoparticles creates an interesting effect: If the cup is lighted from the outside, it appears green, but if the light is shining from the inside, it appears red. This observation can be attributed to the surface plasmon resonance effect.

Another historical example for human made nanoparticles is found in stained glass, which reached its summit in the Middle Ages. The glass was coloured by adding different metal salts or metals. Red church windows are often made with nanoscopic colloidal gold, a yellow colour can be achieved with silver particles (Figure 10).



**Figure 10:** A window from the Chartes Cathedral, 13<sup>th</sup> century. Image by Vassil from <https://commons.wikimedia.org/w/index.php?curid=6224078>.

Another instance for human made NMs, is found in construction materials. In the well known and much used Portland cement, nanotubes are forming.<sup>[13]</sup>

All these examples show, how humans already used nanomaterials to their benefit, even without knowing about their existence. The scientific approach for nanomaterials begun with the experiments of Michael Faraday, who reduced gold salts with white phosphorus leading to colloidal gold at the 1850s.<sup>[14]</sup>



## 1.2. Properties of Nanomaterials

NPs show interesting effects compared with the corresponding bulk material. The smaller a material gets, the bigger is the ratio of atoms on the surface. These energetically unfavoured positions raise the chemical reactivity of the corresponding particles, which is often used in catalysis. Additionally, the large surface leads to increased van der Waals forces. This is the reason why particles tend to agglomerate and 2D layers are physically bound to others, like in van der Waals heterostructures.<sup>[15]</sup> Noteworthy, the atoms on the surface have a smaller coordination number and are so lower bound than atoms in the middle. The melting point of gold nanoparticles nearly halves, if the colloids are beneath 2 nm in size, which is shown in Figure 11.<sup>[16]</sup>

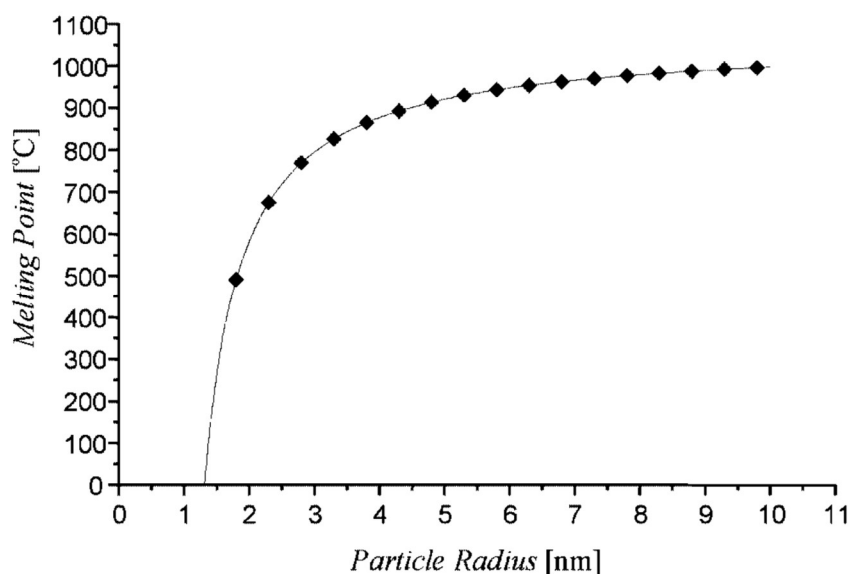


**Figure 11:** Correlation of particle size and melting point of gold NP. Reprinted by permission from John Wiley and Sons, *Nanoparticulated Gold: Syntheses, Structures, Electronics* by Benedetto Corain, Günter Schmid, Copyright 2003.

Another astonishing effect of NM is that the solubility of solutes in nanocrystals can be much higher than in the bulk material. As example, it was found that bismuth solutes about 10000 times better in nanocrystalline copper than in crystalline copper.<sup>[17]</sup> The explanation for this effect is that the chemical potential differs with its atomic structure.

Upconversion is the effect of converting photons of lower energy to photons with higher energy. Schietinger *et al.* demonstrated, that the upconversion of NaYF<sub>4</sub> nanocrystals vary radical with their size.<sup>[18]</sup> Another effect is called Fluorescence Enhancement, which occurs, when metals enhance the intensity of a fluorophore. Two important factors for fluorescence enhancement are the increase in the excitation rate and the quantum efficiency.<sup>[19]</sup>

In magnetism, microscopic small domains in crystals of a ferromagnetic compound are called magnetic domains. Each of these relatively rigid domains have their own magnetic orientation. Magnetic

nanoparticles in the size of these domains have only one magnetic orientation, but through thermal effects this orientation is changing so fast that these particles behave like paramagnets. This effect is called superparamagnetism. Stimulation with an external magnetic field magnetises the nanoparticles and as soon as the field is removed, the nanoparticles behave like paramagnets again.

Surface Plasmon Resonance is the phenomenon that occurs, when light waves hit metallic surfaces, resulting in collective oscillations of free electrons coupled to restricted modes of the conductor-dielectric barrier. With the excitation of these resonances, the nanoparticles absorb and scatter the light acute. This effect is shown in the already presented Lycurgus Cup (Chapter 1.1., p. 5).<sup>[20]</sup>

According to the particle-in-the-box model, charge carriers freely move within these potential walls, whereas the potential went infinite on the outside. By lowering the size of the particles, the movement is constrained, which leads to a change in the band gap and accordingly the absorptions maxima. Therefore, quantum dots of different size have divergent fluorescence wavelengths, exemplarily shown in Figure 12 for cadmium selenide quantum dots. This effect is known as quantum size confinement.

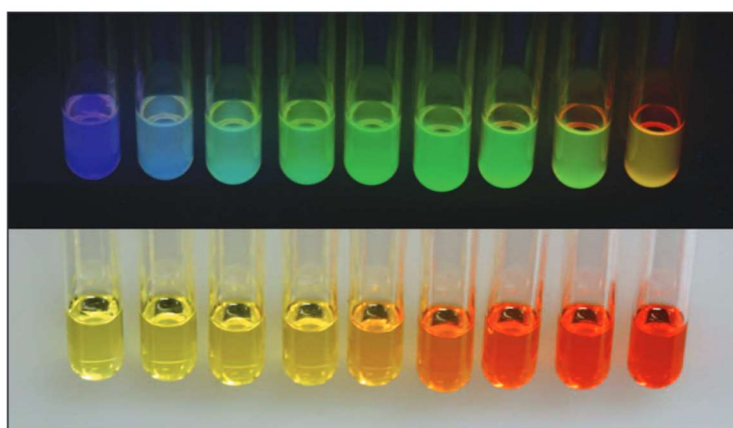


**Figure 12:** CdSe NPs with different sizes as suspension (~1.8 nm left to ~4.0 nm right.). Bottom: View under ambient illumination. Top: View under UV light. Reprinted with permission from K. J. Nordell, E. M. Boatman, G. C. Lisensky, J. Chem. Educ. 2005, 82, 1697, Copyright 2005, American Chemical Society.

### 1.3. Production of Nanomaterials

If we reconsider the three big natural sciences, biology, physics and chemistry, each of them has its own way to produce nanomaterials, with their own benefits and drawbacks. In the following chapter, just a small spectrum of examples the author considers as an important contribution will be described for each science. In the case of biology, plants, microbes, microorganisms and fungi are able to produce nanoparticles by the bottom up approach. An extract of the black tea leaf consists of a mixture of various compounds, like polyphenols, which are able to generate and stabilise silver and gold nanoparticles out of salt solutions.<sup>[21]</sup> Certainly, the pathway is set from chemical reactions, but this is chosen as biological example, because this natural product can synthesise NP without much workup. As another, pure biological example, several fungi can enzymatically reduce salts to nanoparticles. This technique is called myconanotechnology and is a rising field of interest, with non-hazardous methods and the ability to manufacture nanoparticles in large scales.<sup>[22]</sup>

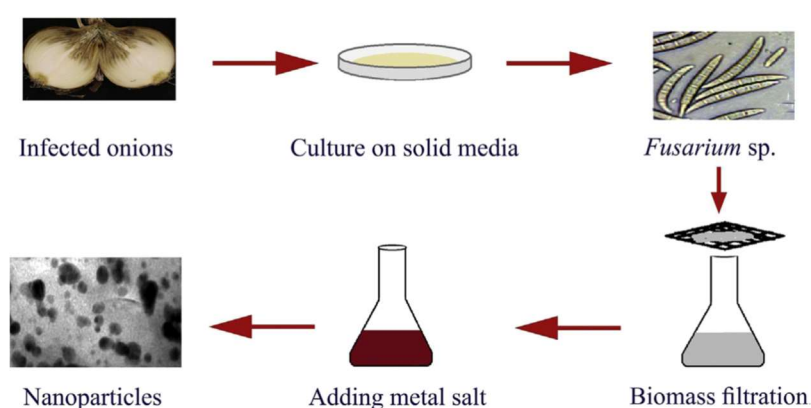


**Figure 13:** The process of biological nanoparticle synthesis, depicted with the onion isolated fungi *Fusarium sp.* Reprinted from F. Asghari, Z. Jahanshahi, M. Imani, M. Shams-Ghahfarokhi, M. Razzaghi-Abyaneh, in *Nanobiomaterials in Antimicrobial Therapy* (Ed.: A. M. Grumezescu), William Andrew Publishing, 2016, pp. 343-383 with permission from Elsevier.

In physics, there exist several different ways to produce NMs. The easiest way is to take the bulk material and grind it until the desired particle size. High temperature leading to edge melting of the particles accompanies this method. Consequently, this method is only suitable for hard compounds such as hcp and bcc metals or intermetallic compounds with CsCl structure.<sup>[23]</sup>

Metals in the gas phase can supersaturate after cooling down in the correct manner. After this step the atoms nucleate and form particles. The vaporisation of the metals can be achieved by different methods. The simplest one is to heat the metal until it vaporises. However, more feasible methods are laser ablation, spark discharge generation or ion sputtering. Once nucleation occurs, particle growth is preferred. In order to get small nanoparticles, the supersaturation has to be high to create a high nucleation density, followed by a sudden quenching of the system through removal of the reaction gas or slowing the kinetics. With these vapor phase methods particles are uncoated and agglomeration of

the latter is preferred. These agglomerates are sometimes bound to each other loosely enough to be separated without much effort.<sup>[24]</sup> If free atoms are deposited in a frozen solvent matrix, heating this solvent matrix results in formation of solvated NP. This method is called solvated metal atom dispersion (SMAD).<sup>[25]</sup>

Another physical approach is the electron-beam lithography, which is used to create nanostructures of desired geometry. An electron beam changes the solubility of certain areas of the resist, enabling solution of treated or non-treated areas in a solvent. This creates nanostructural masks which can cover a substrate, protecting the wanted areas from methods like etching or epitaxy.<sup>[26]</sup>

Finally, there is the chemical way to produce nanoparticles. In this approach, a chemical compound, the precursor, decomposes into fragments, which are thermodynamically unfavoured to form nuclei which further agglomerate to nanoparticles. Several compounds react with each other to form intermediates prior to nanoparticles after elimination and aggregation processes.

Another method for the chemical generation of NPs is to use liquid phase reactions. As already described above (Chapter 1.1., p. 6), Michael Faraday reduced aurate ions ( $[\text{AuCl}_4]^-$ ) with white phosphorus, creating gold particles, which agglomerate to colloidal gold.<sup>[14]</sup> Another liquid phase reaction for NP synthesis is used in the Tollens process, which is similar to the Tollens probe.<sup>[27]</sup> The detection of aldehydes with the Tollens probe with an ammoniac  $\text{AgNO}_3$  solution leading to a mirror of silver is part of the syllabus of the 10<sup>th</sup> class of secondary schools in Bavaria.<sup>[28]</sup> The only difference between Tollens process and Tollens probe is the usage of a sonication bath in the Tollens process.

As already mentioned for the synthesis of metal NPs in the gas phase, these particles are thermodynamically unfavoured, which leads to the agglomeration of uncoated nanoparticles to larger particles, if not hindered. To inhibit this agglomeration process, stabilisers are used to coat the surface of the nanoparticles. These stabilisers can be added independently, or in some cases, the reactants and the oxidation products can act as stabilisers. For example, in the strongly applied Turkevitch route,  $[\text{AuCl}_4]^-$  is reduced by sodium citrate to give gold colloids of the size of 15-20 nm.<sup>[29]</sup> Citrate and the oxidation products like acetonedicarboxylate act as protective groups. The stabilisers can influence the properties of the received nanoparticles, i.e. the solubility in different solvents,<sup>[30]</sup> the size<sup>[31]</sup> or the morphology.<sup>[32]</sup>

In contrast to the usage of a reducing agent, the reduction of metal salts can be induced by several physicochemical techniques. Pure metal NPs can be prepared via pulsed sonoelectrochemistry techniques,<sup>[33]</sup> by photoreduction<sup>[34]</sup> or electrochemistry.<sup>[35]</sup>

Another noteworthy preparation technique is the microemulsion technique, which is based on the areal division of two immiscible liquids. The interface affects the reactivity between the precursors and the reducing agents. Formed nanoparticles are stabilised in the microemulsions and are unable to further agglomerate. The outcome of the particles in matter of size, geometry and homogeneity are controlled by the reaction conditions.<sup>[36]</sup>

Important to mention are the different decomposition paths to create NPs. Chemical Vapour Deposition (CVD) is the deposition of elements out of the gas phase on certain substrates via reacting with the substrate or decomposition on hot surfaces, while volatile decomposition products leave the system. This is possible for single elements,<sup>[37]</sup> or for multielement layers.<sup>[38]</sup> In the latter case, one or more metalorganic precursors are utilised, so the name Metal Organic Chemical Vapour Deposition (MOCVD) has been established.

Analogue, for multielement nanoparticle synthesis in solution, a multi source precursor approach is possible. Several precursors are mixed in solution and the solution is heated through an oil bath or microwave. In case of the latter, it is possible to minimise heating inhomogeneity, which leads to a better control of the reaction conditions during the synthesis.<sup>[39]</sup> During the decomposition of the precursors, a reaction of the fragments takes place and nanoparticles are forming. Volatile byproducts can be easily removed afterwards. As an example, the reaction of Fe(III)-acetylacetonate ( $\text{Fe}(\text{acac})_3$ ) with tris(trimethylsilyl)phosphine  $\text{P}(\text{SiMe}_3)_3$  at temperatures of 240 - 280°C leads to FeP nanoparticles (Figure 14).<sup>40</sup>

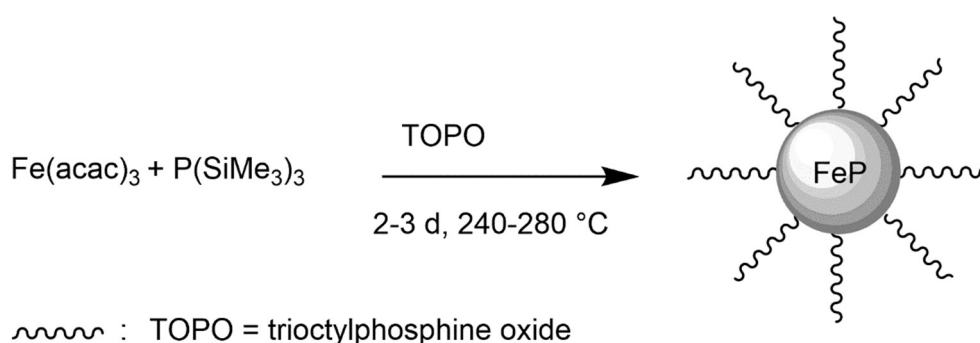


**Figure 14:** Multi source precursor synthesis of FeP NP stabilised with TOPO.

Similar to this reaction, a single-source precursor method can be operated. All components of the desired NP derive from one precursor. There is a plenty of advantages. For example, the stoichiometry of the elements in the precursor can be preserved. The final bonds between the elements are already preformed. Further, compared to multi source precursor methods, lower reaction temperatures can be used and homogeneity of the elements in the solution is given. The reactants of multi source precursor are often volatile and toxic gases. Single-source precursors are more easier to handle. Compared to the multi source precursors for FeP, the single-source precursor method of Scheer *et al.* unites all these advantages. The methodology describes the decomposition of  $[\{\text{Fe}(\text{CO})_4\}\text{PH}_3]$  at 150°C to form FeP nanoparticles (Figure 15).<sup>[41]</sup>

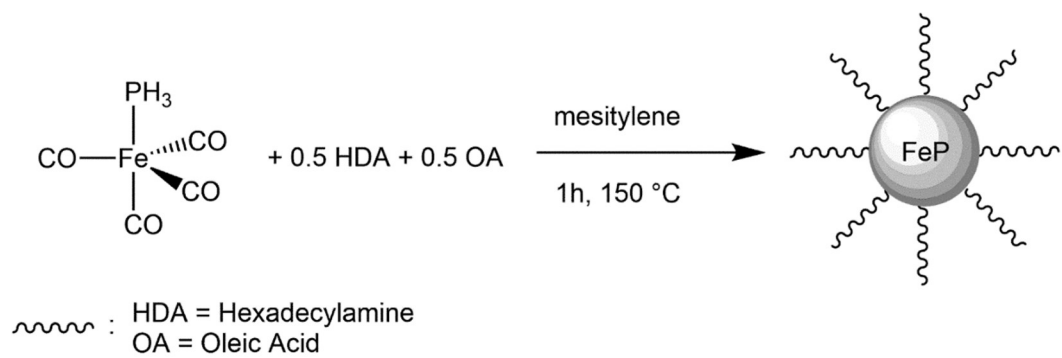


**Figure 15:** Single-source precursor synthesis of FeP NP stabilised with HDA and OA.

## 1.4. Applications and Dangers of Nanoparticles

The various synthetic procedures described above allows the access to nanoparticles of specific size, shape and composition coming along with fascinating properties. Hence, a huge amount of applications is conceivable. In the following chapter only a small selection of applications is given in order to get an overview of possible utilisations.

Nanoparticles can improve modern healthcare by various ways. Besides, the global mortality statistics is headed by heart attacks followed by cancer diseases. Common therapy is performed by irradiation, chemotherapy and/ or surgery. Through nanoparticles-based drug delivery systems, it is possible to selectively target tumour cells. This enables a maximum concentration of medicine at the target without harming the ambient healthy tissue.<sup>[42]</sup>

Another famous application is the use of gold nanoparticles in pregnancy tests. The gold nanoparticle are bound to antibodies complementary to the pregnancy hormone human chorionic gonadotropin (hCG). The following aggregation for a positive test creates a colour change to bright red, due to an plasmonic resonance effect.<sup>[43]</sup> This method could be expanded to a large field of detecting certain hormones. One further example of using nanoparticles in sensoric applications is the Roche Cardiac T test for myocardial infarction.<sup>[44]</sup>

The North American company NanoSphere Health is using nanosized products to overcome the barrier of the skin. Their transdermal products are used for targeted therapy with active components like cannabinoids.<sup>[45]</sup>

At a time, in which renewable energy is one of the most competitive research topics all over the world, solar cells display one very important part of this research. It was found that the use of nanoscopic two dimensional titanium-carbide in perovskite solar cells can push the power conversion efficiency by 26%.<sup>[46]</sup>

Since 1990, iron powder ( $\text{Fe}^0$ ) has been used in environmental treatments. Dangerous pollutions of trichloroethylene in drinking waters are reduced by  $\text{Fe}^0$ . Nanoscaled  $\text{Fe}^0$  has a bigger surface and thus, its reactivity is increased compared to normal iron powder.<sup>[47]</sup>

Nanomaterials are important for developing new materials. Carbon nanotubes reinforced in polymers exhibit more strength and toughness and additionally they are lighter than aluminium or carbon fibres reinforced in polymers. Thus, their application in aerospace technologies is promising,<sup>[48]</sup> the use in materials for bikes or rackets is also conceivable.

Endowing of fibres and clothes with silver nanoparticles act antimicrobial, which reduces skin diseases, odour production and prevents bleaching.<sup>[49]</sup>

Nanoparticles of titanium dioxide  $\text{TiO}_2$  are used in sunscreens. The small particle size ensures a better distribution on the skin and the whitening effect of usual sunscreens is also overcome.<sup>[50]</sup> In wall paints

nanoscale TiO<sub>2</sub> contributes to a self cleaning mechanism, which is attributed to the photocatalytic activity. However, it should be mentioned, that only micrometer sized TiO<sub>2</sub> is responsible for the clear white colour. Nanoparticles of silicon dioxide SiO<sub>2</sub> in paints increases the resistance to wear and weather,<sup>[51]</sup> whereas silver nanoparticles increases the resistance of interior paints against germs.<sup>[52]</sup>

*“There is no sun without shadow, and it is essential to know the night.”* This cite is from Albert Camus from *Le mythe de Sisyphe*.<sup>[53]</sup> Since possible applicational of nanoparticles have been described above (*vide supra*), the following lines deal with the dangers of nanoparticles, which also have to be taken into account.

TiO<sub>2</sub> is used as white pigment in medicine, cosmetics or as food additive E171. Rogler *et al.* found, that TiO<sub>2</sub> nanoparticles worsen gastric diseases like colitis ulcerosa. This is explained by the mechanism involving the sensor molecule NLRP3 inflammasome, which is usually involved for inflammation, but also has been activated by small inorganic particles. Additionally, an accumulation of TiO<sub>2</sub> in the blood of patients with colitis ulcerosa is observed.<sup>[54]</sup> An interesting fact is, that France prohibits the use of TiO<sub>2</sub> nanoparticles in food since January 2020.<sup>[55]</sup>

Tattoo pigments often contain particles which are smaller than 150nm, but their distribution underneath the skin is still not fully understood. Some of the pigments like Carbon Black are possibly carcinogenic for humans, stated by the International Agency for Research on Cancer (IARC). Apparently, it is dangerous to apply that inks without further knowing the degree of damage is caused by this nanoscopic pigments.<sup>[56]</sup>

Due to their structure, carbon nanotubes possess the ability for extensive functionalisation and loading for cargo, which make them desirable for therapeutic applications. Nevertheless, their use is dangerous because of their ability to cause pulmonary fibrosis and the worsening of lung diseases in rodents. A heavy functionalisation has to take place before using them for medical issues.<sup>[57]</sup>

The lipophilic and redox active fullerene was found to accumulate into lipid-rich regions like cell membranes. A study of Eva Oberdörster stated that these buckyballs can cause oxidative damage in the brain of fish.<sup>[58]</sup> New observations suggest that this damage was caused by a solvent contamination of the fullerene, namely tetrahydrofuran (thf). The use of novel synthetic routes make fullerenes nontoxic.<sup>[59]</sup>

In summary, these examples should not scare scientists and hamper the research of nanoparticles. Not all nanoparticles are alike, and the way, how humans or the environment are getting in contact with nanoparticles is important. The proper handling of nanoparticles can be learned likewise to every other chemical. Sure, if the bulk phase is toxic, the nanoparticles of this compound will likely be too. The same might apply for the nontoxicity, however this has to be investigated and not only assumed. Otherwise, possible dangers will be ignored. Therefore, it almost seems to be naive to put nanoparticles in food, just to improve unnecessary characteristics like colour. The dose, which gets into the organism, has



also to be considered, however its impact might once again be different from the bulk material. Silver nanoparticles are used for antimicrobial purposes, but it's shown that they don't affect the biological process of sewage treatment plants.<sup>[60]</sup> If a delivery system for tumour targeting is dangerous, it may still be less harmful than the classical chemotherapy itself. The pros and cons of the usage of nanoparticles have to be evaluated for each kind of NP separately.

## 1.5. References

- [1] M. H. Nayfeh, S. R. Habbal, S. Rao, *ApJ* **2005**, 621, L121-L124.
- [2] N. Dauphas, L. Remusat, J. H. Chen, M. Roskosz, D. A. Papanastassiou, J. Stodolna, Y. Guan, C. Ma, J. M. Eiler, *ApJ* **2010**, 720, 1577-1591.
- [3] L. Becker, T. E. Bunch, L. J. Allamandola, *Lunar Planet. Sci. Conf.* **1999**, 30, 1805.
- [4] C. Buzea, I. I. Pacheco, K. Robbie, *Biointerphases* **2007**, 2, MR17-MR71.
- [5] N. D. Greber, N. Dauphas, A. Bekker, M. P. Ptáček, I. N. Bindeman, A. Hofmann, *Science* **2017**, 357, 1271-1274.
- [6] J. Gim, N. Schnitzer, L. M. Otter, Y. Cui, S. Motreuil, F. Marin, S. E. Wolf, D. E. Jacob, A. Misra, R. Hovden, *Nat. Commun.* **2019**, 10, 4822.
- [7] C. W. Mason, *The Journal of Physical Chemistry* **1927**, 31, 321-354.
- [8] R. O. Prum, T. Quinn, R. H. Torres, *J. Exp. Biol.* **2006**, 209, 748-765.
- [9] Aristotle, *Historia Animalium*, trans. Thompson, D. A. W. (**1918**) (Clarendon, Oxford), [http://classics.mit.edu/Aristotle/history\\_anim.html](http://classics.mit.edu/Aristotle/history_anim.html), Book IX, Part 9, Accessed 30.01.2020
- [10] K. Autumn, M. Sitti, Y. A. Liang, A. M. Peattie, W. R. Hansen, S. Sponberg, T. W. Kenny, R. Fearing, J. N. Israelachvili, R. J. Full, *PNAS* **2002**, 99, 12252-12256.
- [11] L. Chen, D. A. Bazylinski, B. H. Lower, *Nat Educ Knowl* **2010**, 1.
- [12] T. Christiansen, M. Cotte, R. Loredó-Portales, P. E. Lindelof, K. Mortensen, K. Ryholt, S. Larsen, *Sci. Rep.* **2017**, 7, 15346.
- [13] S. S. S. Cardoso, J. H. E. Cartwright, O. Steinbock, D. A. Stone, N. L. Thomas, *Struct. Chem.* **2017**, 28, 33-37.
- [14] M. Faraday, *Philos. Trans. R. Soc. Lond.* **1857**, 147, 145-181.
- [15] A. K. Geim, I. V. Grigorieva, *Nature* **2013**, 499, 419-425.
- [16] G. Schmid, B. Corain, *Eur. J. Inorg. Chem.* **2003**, 2003, 3081-3098.
- [17] H. Gleiter, *Prog. Mater Sci.* **1989**, 33, 223-315.
- [18] S. Schietinger, L. d. S. Menezes, B. Lauritzen, O. Benson, *Nano Lett.* **2009**, 9, 2477-2481.
- [19] J. R. Lakowicz, *Anal. Biochem.* **2005**, 337, 171-194.
- [20] M. F. Ashby, P. J. Ferreira, D. L. Schodek, in *Nanomaterials, Nanotechnologies and Design* (Eds.: M. F. Ashby, P. J. Ferreira, D. L. Schodek), Butterworth-Heinemann, Boston, **2009**, pp. 17-39.
- [21] N. A. Begum, S. Mondal, S. Basu, R. A. Laskar, D. Mandal, *Colloids Surf. B* **2009**, 71, 113-118.
- [22] G. Subashini, S. Bhuvaneshwari, in *Fungi and their Role in Sustainable Development: Current Perspectives* (Eds.: P. Gehlot, J. Singh), Springer Singapore, Singapore, **2018**, pp. 753-779 and references therein.

- 
- [23] H. Gleiter, *Prog. Mater. Sci.* **1989**, *33*, 223-315 and references therein.
- [24] M. T. Swihart, *Curr. Opin. Colloid Interface Sci.* **2003**, *8*, 127-133 and references therein.
- [25] G. B. Sergeev, K. J. Klabunde, in *Nanochemistry (Second Edition)* (Eds.: G. B. Sergeev, K. J. Klabunde), Elsevier, Oxford, **2013**, pp. 55-73.
- [26] W. Zhang, A. Potts, D. M. Bagnall, B. R. Davidson, *Thin Solid Films* **2007**, *515*, 3714-3717.
- [27] Y. Yin, Z.-Y. Li, Z. Zhong, B. Gates, Y. Xia, S. Venkateswaran, *J. Mater. Chem.* **2002**, *12*, 522-527.
- [28] Staatsinstitut für Schulqualität und Bildungsforschung München, [http://www.isb-gym8-lehrplan.de/contentserv/3.1.neu/g8.de/id\\_26225.html](http://www.isb-gym8-lehrplan.de/contentserv/3.1.neu/g8.de/id_26225.html), Accessed 30.01.2020
- [29] J. Turkevich, P. C. Stevenson, J. Hillier, *Discuss Faraday Soc* **1951**, *11*, 55-75.
- [30] N. Yan, J.-g. Zhang, Y. Tong, S. Yao, C. Xiao, Z. Li, Y. Kou, *Chem. Commun.* **2009**, 4423-4425.
- [31] M. Pons, M. L. García, O. Valls, *Colloid. Polym. Sci.* **1991**, *269*, 855-858.
- [32] A. Ibrahim, H. Alzahrani, M. El-Latif, M. Selim, *Bulletin of the National Research Centre* **2019**, *43*.
- [33] V. Sáez, T. J. Mason, *Molecules* **2009**, *14*, 4284-4299.
- [34] R. Sato-Berrú, R. Redón, A. Vázquez-Olmos, J. M. Saniger, *J. Raman Spectrosc.* **2009**, *40*, 376-380.
- [35] C. Johans, J. Clohessy, S. Fantini, K. Kontturi, V. J. Cunnane, *Electrochem. Commun.* **2002**, *4*, 227-230.
- [36] M. A. Malik, M. Y. Wani, M. A. Hashim, *Arab. J. Chem.* **2012**, *5*, 397-417 and references therein.
- [37] O. Mitsutaka, T. Susumu, I. Masakazu, H. Masatake, *Chem. Lett.* **1998**, *27*, 315-316.
- [38] G. Haacke, S. P. Watkins, H. Burkhard, *Appl. Phys. Lett.* **1989**, *54*, 2029-2031.
- [39] M. N. Nadagouda, T. F. Speth, R. S. Varma, *Acc. Chem. Res.* **2011**, *44*, 469-478.
- [40] S. C. Perera, S. L. Brock, *MRS Proceedings* **2011**, *755*, DD5.9.
- [41] C. Hunger, W.-S. Ojo, S. Bauer, S. Xu, M. Zabel, B. Chaudret, L.-M. Lacroix, M. Scheer, C. Nayral, F. Delpech, *Chem. Commun.* **2013**, *49*, 11788-11790.
- [42] S. Sultana, M. R. Khan, M. Kumar, S. Kumar, M. Ali, *J. Drug Target.* **2013**, *21*, 107-125 and references therein.
- [43] Mark. I. Stockmann, *Physics Today* **2011**, *64*, *2*, 39
- [44] E. L. Lewandrowski, K. Lewandrowski, *Point of Care* **2002**, *1*, 78-83.
- [45] Nanosphere Health Sciences, <https://www.nanospherehealth.com/cannabis>, Accessed 30.01.2020
- [46] A. Agresti, A. Pazniak, S. Pescetelli, A. Di Vito, D. Rossi, A. Pecchia, M. Auf der Maur, A. Liedl, R. Larciprete, D. V. Kuznetsov, D. Saranin, A. Di Carlo, *Nature Materials* **2019**, *18*, 1228-1234.
- [47] P. G. Tratnyek, R. L. Johnson, *Nano Today* **2006**, *1*, 44-48.
- [48] R. Dahiya, R. Kapdi, B. Manohar, *IJRMET* **2016**, *6*, *2*, 100-104.
- [49] H. E. Emam, A. P. Manian, B. Široká, H. Duelli, B. Redl, A. Pipal, T. Bechtold, *J. Clean. Prod.* **2013**, *39*, 17-23.
- [50] J. Hoffbauer, *J. Verbrauch Lebensm.* **2008**, *3*, 290-293.
- [51] S. Zhou, L. Wu, J. Sun, W. Shen, *Prog. Org. Coat.* **2002**, *45*, 33-42.

- 
- [52] T. Künniger, A. C. Gerecke, A. Ulrich, A. Huch, R. Vonbank, M. Heeb, A. Wichser, R. Haag, P. Kunz, M. Faller, *Environ. Pollut.* **2014**, *184*, 464-471.
- [53] Albert Camus: *Der Mythos des Sisyphos*, deutsch von Vincent von Wroblewsky. Rowohlt, Reinbek 2000, ISBN 978-3-499-22765-3
- [54] P. A. Ruiz, B. Morón, H. M. Becker, S. Lang, K. Atrott, M. R. Spalinger, M. Scharl, K. A. Wojtal, A. Fischbeck-Terhalle, I. Frey-Wagner, M. Hausmann, T. Kraemer, G. Rogler, *Gut* **2017**, *66*, 1216-1224.
- [55] Ministère de la Transition écologique et solidaire, <https://www.ecologique-solidaire.gouv.fr/dioxyde-titane-ladditif-e171-sera-interdit-dans-denrees-alimentaires-partir-du-1er-janvier-2020>, Accessed 30.01.2020
- [56] T. Høgsberg, K. Loeschner, D. Löf, J. Serup, *Br. J. Dermatol.* **2011**, *165*, 1210-1218.
- [57] J. C. Bonner, *Expert Rev. Respir. Med.* **2011**, *5*, 779-787.
- [58] E. Oberdörster, *Environ. Health Perspect.* **2004**, *112*, 1058-1062.
- [59] X. R. Xia, N. A. Monteiro-Riviere, J. E. Riviere, *Toxicol. Lett.* **2010**, *197*, 128-134.
- [60] L. Li, G. Hartmann, M. Döblinger, M. Schuster, *Environ. Sci. Technol.* **2013**, *47*, 7317-7323, Verhalten von Nanopartikeln in Kläranlagen. Marina Maier, Marion Letzel und Martin Wegenke *Mitteilungen der Fachgruppe Umweltchemie und Ökotoxikologie* **2012**, *18* (3) 62.

## 2. Conceptual Formulation

As shown in the introduction, nanoparticles possess manifolded superior properties and applications compared to the corresponding bulk phase. Therefore, the investigation of new or improved routes for the synthesis of nanoparticles (known or unknown) is very desirable. The Scheer group is working in the field of molecular chemistry with the focus on elements of the 15<sup>th</sup> group and their future applications. The intersection of both fields is in the synthesis of new organometallic compounds containing P or As, which might be capable single-source precursors for nanoparticle synthesis.

The goal of this dissertation is:

- The synthesis and characterisation of new P- or As- containing compounds, which are capable single-source precursors for multielement nanoparticle synthesis.
- The examination of the reaction behaviour of these new compounds.
- The execution of preliminary tests to investigate the suitability of the compounds as single-source precursors for nanoparticle synthesis.

Capable single-source precursors for nanoparticle synthesis are:

- Metallorganic compounds with two or more non-volatile elements, in which one is phosphorus or arsenic, stabilised with volatile ligands like N<sub>2</sub>, NO, CO, H<sub>2</sub> or SiMe<sub>3</sub>, which can be easily removed from the system after decomposition.
- Indium-1,2,4-triphospholyles, which have already shown their possible usage as SSP in an initial study.

## 3. The Parent Diarsene HAs=AsH as Side-on Bound Ligand in an Iron Carbonyl Complex

### 3.1. Preface

The following chapter has already been published with open access. The article is reprinted with permission from Wiley-VCH.

International Edition: R. Rund, G. Balázs, M. Bodensteiner, M. Scheer, *Angew. Chem. Int. Ed.* **2019**, *58*, 16092-16096.

German Edition: R. Rund, G. Balázs, M. Bodensteiner, M. Scheer, *Angew. Chem.* **2019**, *131*, 16238-16242.

### 3.2. Author contribution

Reinhard Rund: Synthesis and characterisation of **3-1**, **3-1a**, **3-1b**, **3-1c**, **3-2**, **3-2D**, **3-3**, **3-3D**, **3-4**, **3-5**, **3-6** and  $[\{\text{Fe}(\text{CO})_4\}\text{Sb}(\text{SiMe}_3)_3]$

Gábor Balázs: DFT calculations

Michael Bodensteiner: Refinement of the solid state structure of **3-2**

Fabien Delpech: TEM images of **3-1a**, **3-1b**, **3-1c**

Manfred Scheer: Supervision of the research and revision of the manuscript

### 3.3. Abstract

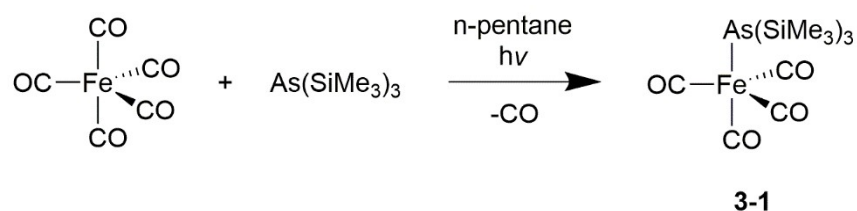
The terminal diarsene HAs=AsH ligand attracts special interest concerning its bonding relation in comparison to its isolable relative, ethene. Herein, by the methanolysis of  $[\{\text{Fe}(\text{CO})_4\}\text{As}(\text{SiMe}_3)_3]$  (**3-1**) the synthesis of  $[\{\text{Fe}(\text{CO})_4\}(\eta^2\text{-As}_2\text{H}_2)]$  (**3-2**) is reported, containing a parent diarsene as unprecedented side-on coordinated ligand. Following this synthetic route, also the D-labeled complex  $[\{\text{Fe}(\text{CO})_4\}(\eta^2\text{-As}_2\text{D}_2)]$  (**3-2D**) could be isolated. The electronic structure and bonding situation of **3-2** was elucidated by DFT calculations revealing that **3-2** is best described as an olefin-like complex. Moreover, the reactivity of **3-2** towards the Lewis acids  $[\{\text{M}(\text{CO})_5\}(\text{thf})]$  (M=Cr, W) was investigated, leading to the complexes  $[\text{Fe}(\text{CO})_4\text{AsHW}(\text{CO})_5]_2$  (**3**) and  $[\{\text{Fe}(\text{CO})_4\}_2\text{AsH}-\{\text{Cr}(\text{CO})_5\}]$  (**3-4**), respectively.

### 3.4. Introduction

The first ethylene complex  $K[PtCl_3(C_2H_4)]$ , reported by Zeise in 1827, represents the first organometallic transition metal compound ever synthesised.<sup>[1]</sup> Since then, this type of complexes has enormously gained in importance in chemistry as they are for example, intermediates in a broad range of industrial catalytic processes such as hydrogenation, dehydrogenation, or hydrosilylation.<sup>[2]</sup> Simultaneously, they represent fundamental examples of classic bonding modes. Concerning bonding relations,  $[Fe(CO)_4(\eta^2-C_2H_4)]$  is a classic prototype of an ethene complex, which, some decades ago, was synthesised by a high pressure synthesis<sup>[3a]</sup> or by matrix isolation techniques<sup>[3b]</sup> because of its instability at ambient conditions. Analyses showed that its bonding behavior was predominantly the Dewar–Chatt–Duncanson one.<sup>[3c,d]</sup> In view of the isolobal relationships, it is of principal interest to look at the parent non-carbon analogues of ethene, for example, the dipnictenes of the general formulae  $HE=EH$  ( $E=N, P, As, Sb, Bi$ ), with respect to their properties as ligands. The study of such parent  $HE=EH$  compounds can clarify the true reactivity and structural behavior of these systems without the distortions induced by sterically demanding substituents in  $RE=ER$ , which are usually required in order to stabilise the  $E=E$  double bonds.<sup>[4]</sup> The diazene  $HN=NH$ , which, to the best of our knowledge, is the only isolated hydrogen-substituted dipnictene known, is stable, though only at very low temperatures ( $<-165^\circ C$ ;  $\Delta H_f^{298}=212 \text{ kJmol}^{-1}$ ), but well accessible as a ligand in metal complexes such as for example,  $[\mu-N_2H_2\{Fe(NHS_4)\}_2]$  ( $NHS_4=2,2\text{-bis}(2\text{-mercaptophenylthio})\text{diethylamine}$ ).<sup>[4c]</sup> Complexes containing a diphosphene  $HP=PH$  ligand are very rare and only three complexes are known so far.<sup>[5]</sup> The parent diarsene  $HAs=AsH$  was first mentioned by Davy in 1810 as a product of the reaction of potassium and arsenic in a hydrogen atmosphere.<sup>[6]</sup> However, its existence could not be unequivocally proved until the synthesis and characterisation of  $[(Tren^{TIPS}U)_2(As_2H_2)]$  (**A**) ( $Tren^{TIPS}=N(CH_2CH_2NSiPr^i_3)_3$ ) was reported containing the diarsene  $HAs=AsH$  as bridging ligand between two bulky metal fragments of uranium.<sup>[7]</sup> However, the surroundings of the sterically demanding ligand have a pronounced influence on the properties and geometry of the diarsene ligand. Therefore, the search for synthetic pathways to achieve a simple and mononuclear complex of the diarsene free of any steric restrictions is still ongoing, also to shed light onto the bonding situation of this ethene-like ligand. Recently, we investigated the usage of single-source precursors for the synthesis of transition metal phosphide nanoparticles and could show that complexes containing only labile CO ligands and hydrogen substituents on phosphorus are suitable precursors for the synthesis of size- and stoichiometry- controlled nanoparticles.<sup>[8]</sup> This was demonstrated by the synthesis of FeP nanoparticles with a precise stoichiometry control by starting from the single-source precursor  $[Fe(CO)_4(PH_3)]$  or  $[Fe(CO)_3(\mu-PH_2)]_2$ .<sup>[8b, 9]</sup> Targeting the corresponding As-containing complexes, we realised that the synthetic pathway for this kind of compounds goes totally different ways and, to our surprise, we achieved the synthesis of the unprecedented diarsene iron carbonyl complex  $[Fe-(CO)_4(\eta^2-As_2H_2)]$  (**3-2**)—a complex without sterically demanding ligands—in which the diarsene ligand is only stabilised in the coordination sphere of one transition metal. Additionally, reactivity studies towards Lewis acids show that **3-2** can serve as a source of AsH units, resulting in novel complexes, such as  $[Fe(CO)_4]AsH\{W(CO)_5\}_2$  (**3-3**) and  $[Fe_2(CO)_8]AsH\{Cr(CO)_5\}$  (**3-4**).

### 3.5. Results and Discussion

Due to the high toxicity and difficulties in handling  $\text{AsH}_3$  gas, we chose a synthetic strategy in order to avoid the usage of  $\text{AsH}_3$  gas. The irradiation of  $\text{As}(\text{SiMe}_3)_3$  and  $\text{Fe}(\text{CO})_5$  in n-pentane affords  $[\{\text{Fe}(\text{CO})_4\}\text{As}(\text{SiMe}_3)_3]$  (**3-1**) in 81% yield (Scheme 1). Solid **3-1** is air-sensitive but can be stored at  $-30^\circ\text{C}$  under an inert atmosphere for several months, while, at room temperature, it decomposes to an unidentified brown solid.



**Scheme 1:** Synthesis of **3-1** from  $\text{Fe}(\text{CO})_5$  and  $\text{As}(\text{SiMe}_3)_3$ .

In the mass spectrum of **3-1**, the molecular ion peak was found. The  $^1\text{H}$  NMR spectrum of **3-1** shows a singlet at 0.30 ppm with the corresponding  $^{29}\text{Si}$  satellites ( $^2J_{\text{Si-H}}=6.67$  Hz). The infrared spectrum of **3-1** reveals three CO stretches at 2025, 1940 and  $1899\text{ cm}^{-1}$ , being in agreement with an axially coordinating  $\text{As}(\text{SiMe}_3)_3$  ligand. According to DFT calculations, the isomer of **3-1** with the  $\text{As}(\text{SiMe}_3)_3$  ligand, in equatorial position, is, with  $18.37\text{ kJ mol}^{-1}$ , less stable. Similarly,  $[\{\text{Fe}(\text{CO})_4\}\text{Sb}(\text{SiMe}_3)_3]$  shows three CO stretching modes in the IR spectrum.<sup>[10]</sup> In contrast, for  $[\{\text{Fe}(\text{CO})_4\}\text{P}(\text{SiMe}_3)_3]$ , four CO bands were reported and, therefore, an equatorially coordinating ligand was proposed,<sup>[11]</sup> although, in the solid state structure, the  $\text{P}(\text{SiMe}_3)_3$  ligand takes the axial position.<sup>[12]</sup> The molecular structure of **3-1** (Figure 16) shows a trigonal bipyramidally coordinated iron center with the  $\text{As}(\text{SiMe}_3)_3$  ligand in axial position as also found for the corresponding Sb compound  $[\{\text{Fe}(\text{CO})_4\}\text{Sb}(\text{SiMe}_3)_3]$ .<sup>[13]</sup>

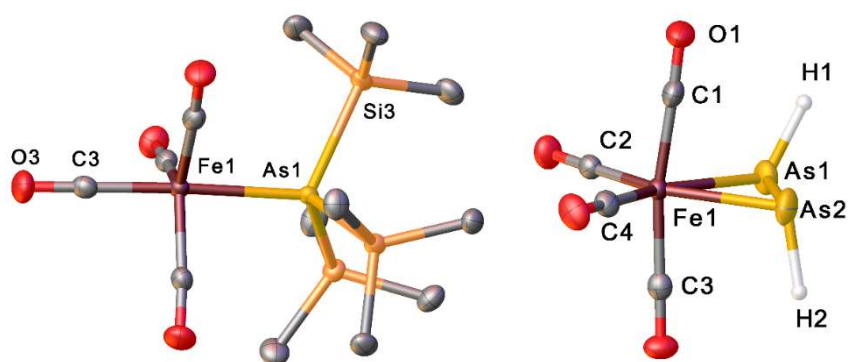
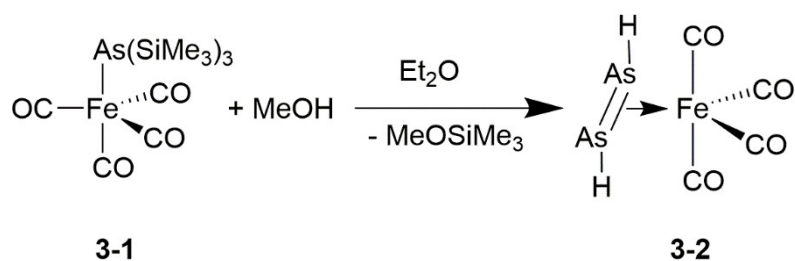


**Figure 16:** Molecular structure of **3-1** (left, hydrogen atoms are omitted for clarity) and **3-2** (right) with ellipsoids set at 50% probability. Selected distances [Å] and angles [°] of **3-1**: As1-Fe1 2.4406(8), As1-Si1 2.3823(11), As1-Si2 2.3717(12), As1-Si3 2.3780(12) and **3-2** (major part) [b]: As1-As2 2.3680(5), As1-Fe1 2.5004(5), As2-Fe1 2.4907(5); C2-Fe1-C4 104.71(12), As1-Fe1-As 2 56.645(14).

The methanolysis of **3-1** in diethylether at low temperatures results in the formation of yellow crystals of **3-2** in a very low yield, which are surrounded by a large amount of unidentified brown solid (Scheme 2). If the reaction is performed at  $-80^{\circ}\text{C}$  and all volatiles are removed in vacuo at a maximum temperature of  $-50^{\circ}\text{C}$ , and while warming up to room temperature, the residue is sublimated into a cooled Schlenk tube ( $-80^{\circ}\text{C}$ ) as a yellow solid of  $[\{\text{Fe}(\text{CO})_4\}\{\eta^2\text{-As}_2\text{H}_2\}]$  (**3-2**) obtained in 86% yield.<sup>[14]</sup> Compound **3-2** is extremely air- and moisture-sensitive and decomposes rapidly at temperatures above  $-20^{\circ}\text{C}$ . Interestingly, under similar reaction conditions, the methanolysis of  $[\{\text{Fe}(\text{CO})_4\}\text{P}(\text{SiMe}_3)_3]$  leads to  $[\{\text{Fe}(\text{CO})_4\}(\text{PH}_3)]$  in good yields. Thermolysis or photolysis of  $[\{\text{Fe}(\text{CO})_4\}(\text{PH}_3)]$  lead to the formation of the dinuclear complex  $[\{\text{Fe}(\text{CO})_3\}_2(\mu\text{-PH}_2)]_2$ ,<sup>[8b]</sup> indicating that the hypothetical complex  $[\text{Fe}(\text{CO})_4(\text{AsH}_3)]$  might form as an intermediate, which, however, is unstable and decomposes to **3-2** and other unidentified products.



**Scheme 2:** Synthesis of **3-2** by methanolysis of **3-1**.

Besides the bridging complex  $[\{\text{U}(\text{Tren}^{\text{TIPS}})\}_2(\mu\text{-}\eta^2\text{:}\eta^2\text{-As}_2\text{H}_2)]$  (**3-A**),<sup>[7]</sup> compound **3-2** is the only known complex containing a side-on coordinated parent diarsene ligand and here for the first time in a terminal fashion. Complexes containing substituted diarsene ligands such as phenyl groups in  $[\{\text{Fe}(\text{CO})_4\}\{\eta^2\text{-As}_2\text{Ph}_2\}]$  (**3-B**),<sup>[15]</sup> were reported.<sup>[16]</sup> In **3-A**, the diarsene ligand is stabilised between two bulky  $[\text{U}(\text{Tren}^{\text{TIPS}})]$  fragments. Due to the strong back donation of the  $[\text{U}(\text{Tren}^{\text{TIPS}})]$  fragments, the As-As distance in **3-A** is strongly elongated (As-As 2.4102(13) Å) and corresponds to an As-As single bond.<sup>[7]</sup> Hence, **3-2** is the first complex containing a  $\text{HAs}=\text{AsH}$  ligand stabilised by only one sterically not demanding organometallic fragment.

The solid state structure of **3-2** (Figure 16) shows a *trans*-diarsene  $\text{HAs}=\text{AsH}$  ligand, which coordinates to an  $\text{Fe}(\text{CO})_4$  fragment in equatorial position. The As-As distances in **3-2** (two independent molecules 2.3680(5), 2.3683(8) Å) is between an As-As single bond (2.42 Å) and an As=As double bond (2.28 Å) and can be considered as being an elongated double bond.<sup>[17]</sup> This slight elongation, which is due to the back bonding from the  $\text{Fe}(\text{CO})_4$  moiety,<sup>[4a]</sup> is much shorter than in the dinuclear U complex **3-A**. The positions of the hydrogen atoms bonded to arsenic were located from the difference Fourier map and subsequently refined with fixed coordinates.<sup>[18]</sup> According to this, the *trans* isomer of  $\text{As}_2\text{H}_2$  is present in the complex and only a minor amount of the *cis* isomer could be refined in the crystal structure of **3-2** (cf. Supporting Information). This is in line with the results of DFT calculations showing that the *trans* isomer of **3-2** is thermodynamically preferred by 7.60  $\text{kJ mol}^{-1}$  over the *cis* isomer.<sup>[19]</sup> Similarly, at the



same level of theory, the parent *trans*-diarsene HAs=AsH is with 11.25 kJmol<sup>-1</sup> more stable than the *cis*-isomer.<sup>[20]</sup>

The mass spectrum of **3-2** shows the molecular ion peak at  $m/z=319.77$  and fragments according to the subsequent loss of CO and/or H. According to DFT calculations, the symmetric and asymmetric As-H stretches in the IR spectra are situated at 2136 cm<sup>-1</sup> and 2149 cm<sup>-1</sup>, respectively, and hence are obscured by the CO absorption bands. In order to unambiguously attribute the As-H stretch in the IR spectrum of **3-2**, we prepared the deuterium-labeled derivative  $[\{\text{Fe}(\text{CO})_4\}\{\eta^2\text{-As}_2\text{D}_2\}]$  (**3-2D**) by the reaction of **3-1** with deuterated methanol. The infrared spectrum of **3-2D** shows four signals for the CO ligands at 1912, 1999, 2053, and 2124 cm<sup>-1</sup>, which are in agreement with the calculated values and, additionally, a new absorption at 1473 cm<sup>-1</sup>, which is attributed to the As-D vibration and in line with the expected shift due to the mass difference between hydrogen and deuterium ( $v_{\text{H}}/v_{\text{D}}=1.41$ ). This is also in agreement with the observations for **3-A**, in which the As-H stretches appear at 2030 cm<sup>-1</sup> and the As-D ones at 1410–1490 cm<sup>-1</sup>.<sup>[7]</sup>

Due to the high sensitivity of **3-2**, a partial decomposition takes place when it is dissolved in deuterated solvents and, in the <sup>1</sup>H NMR spectrum, among the signals corresponding to **3-2**, further signals for unidentified decomposition products are present. The partial decomposition of **3-2** when being dissolved in organic solvents cannot be suppressed even when being dissolved at low temperatures. <sup>2</sup>H NMR spectroscopic investigations of **3-2D** show a main resonance signal at  $\delta=1.33$  ppm, which is attributed to the As<sub>2</sub>D<sub>2</sub> unit. For **3-A**, no resonance signal for the hydrogen atoms attached to the arsenic atoms could be detected, due to the paramagnetic nature of the complex.

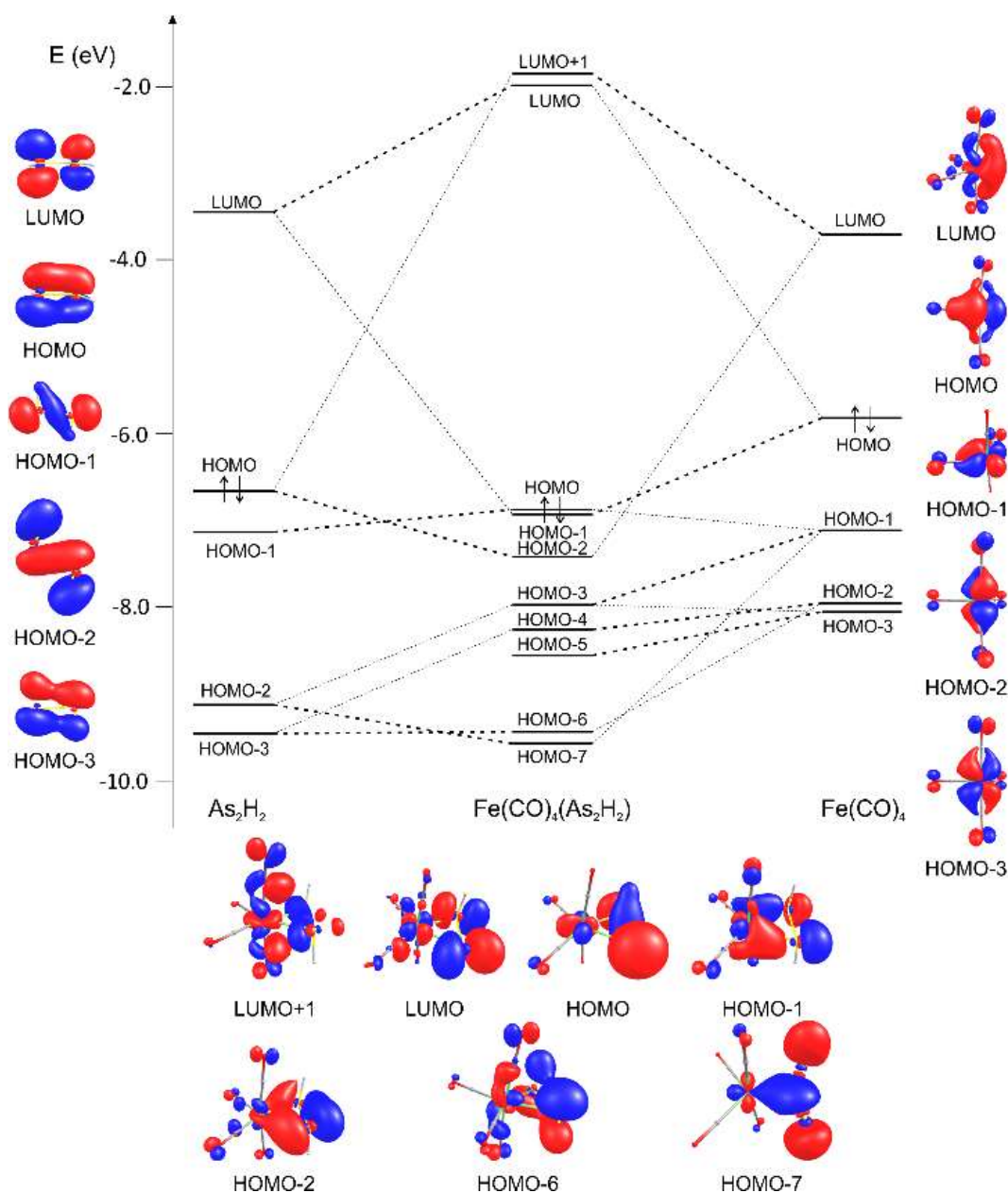


**Figure 17:** Orbital interaction diagram as well as molecular and fragment orbitals in **3-2**, calculated at the B3LYP/def2-TZVP level. The lines drawn in bold represent the main character of the corresponding molecular orbital.

In order to clarify the electronic structure of **3-2**, DFT calculations at the B3LYP/def2-TZVP level of theory were performed. The orbital interaction diagram (Figure 17) shows that the  $\pi$  orbitals of the  $\text{As}_2\text{H}_2$  ligand are stabilised while the As-As  $\sigma$  bond is slightly destabilised upon coordination. The overlap of the Highest Occupied Molecular Orbital (HOMO) of the  $\text{As}_2\text{H}_2$  ligand with the Lowest Unoccupied Molecular Orbital (LUMO) of the  $\text{Fe}(\text{CO})_4$  fragment represents the  $p$ donor coordination mode. The Fe-As backbonding becomes obvious by the overlap of the HOMO orbital of the  $\text{Fe}(\text{CO})_4$  fragment with the LUMO orbital (which is the As=As  $\pi^*$  orbital) of the  $\text{As}_2\text{H}_2$  ligand, which leads to the HOMO-1 orbital in **3-2**. Considering the main fragment contribution to the HOMO-1 and HOMO-2 orbitals, complex **3-2** can be best described as an olefin-like complex. The NBO analysis<sup>[21]</sup> shows NBO orbits corresponding to an As-As bond, which is realised by almost pure  $p$  orbitals ( $sp^{11}$  hybrid orbital) and two Fe-As bonds.

The occupancy of the latter two is 1.75e and polarised toward iron. The lone pair of the arsenic atoms are of high s character ( $sp^{0.3}$  hybrid orbitals). The Wiberg Bond Indices show an As-As bond order of 1.18, which indicates the multiple bond character and a bond order of 0.73 for the Fe-As bonds. For comparison, the WBI of the As-Fe bond in **3-1** is 0.58, while the WBI of the As-As bond in the free *trans*-As<sub>2</sub>H<sub>2</sub> is 2.05. Further, the electronic structure of **3-2** was investigated by the Bader's theory of atoms in molecules (AIM).<sup>[22]</sup> Bond Critical Points (BCPs) could be located corresponding to the As-As and two As-Fe bonds with electron densities of 0.090 ea.u.<sup>-3</sup> and 0.057 ea.u.<sup>-3</sup>, respectively. The Laplacian at the BCP corresponding to the As-As bond is negative ( $\nabla^2\rho = -0.046$  ea.u.<sup>-5</sup>), while the one at the BCPs corresponding to the As-Fe bond is positive ( $\nabla^2\rho = 0.046$  ea.u.<sup>-5</sup>). The positive Laplacian at the BCPs of the Fe-As bond and the negative energy density values (-0.273 hartree a.u.<sup>-3</sup>) indicate a moderately polar Fe-As bond. The pronounced ellipticity at these BCPs of 0.24 and 0.28 for the BCPs corresponding to the As-As as well as the As-Fe bonds, respectively, indicates the concentration of the electron density in the FeAs<sub>2</sub> plane. Based on the WBIs, complex **3-2** can be described as a diarsa-metallacyclopropane while, based on the fragment contribution to the molecular orbitals, complex **3-2** can be better described with a Dewar–Chatt–Duncanson model. The latter is also confirmed by the torsion angles of the As<sub>2</sub>H<sub>2</sub> unit being close to 90°.<sup>[3c,d, 18]</sup>

To investigate the reactivity of **3-2**, it was reacted with the Lewis acids [M(CO)<sub>5</sub>(thf)] (M=Cr, W) at -80°C in THF. From the reaction with [W(CO)<sub>5</sub>(thf)], [(Fe(CO)<sub>4</sub>)AsH{W(CO)<sub>5</sub>}]<sub>2</sub> (**3-3**) (Figure 18) was isolated in 43% yield. **3-3** represents the first compound with a planar As<sub>2</sub>Fe<sub>2</sub> ring that has been structurally characterised. A related substituted compound [(C<sub>5</sub>H<sub>5</sub>)Fe(CO)]{As(CH<sub>3</sub>)<sub>2</sub>]<sub>2</sub>, has only been characterised by spectroscopic methods (<sup>1</sup>H NMR and IR) and elemental analysis, but not by single crystal X-ray diffractions.<sup>[23]</sup> A compound with a butterfly-like structure, containing an Fe-Fe bond, was reported for [(Fe<sub>2</sub>(CO)<sub>6</sub>){μ-As(CH<sub>3</sub>)<sub>2</sub>}]<sub>2</sub>.<sup>[24]</sup>

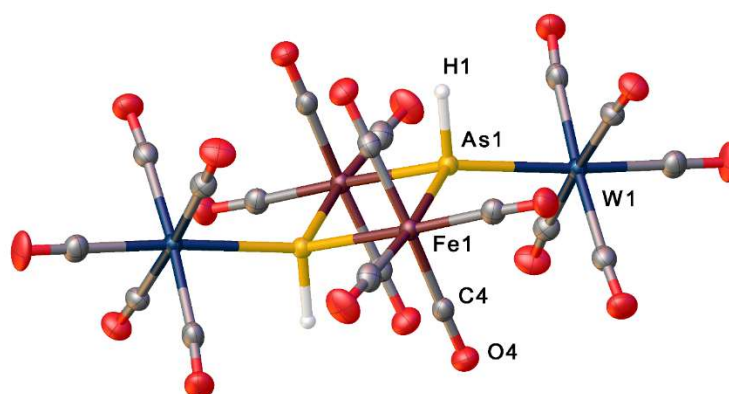


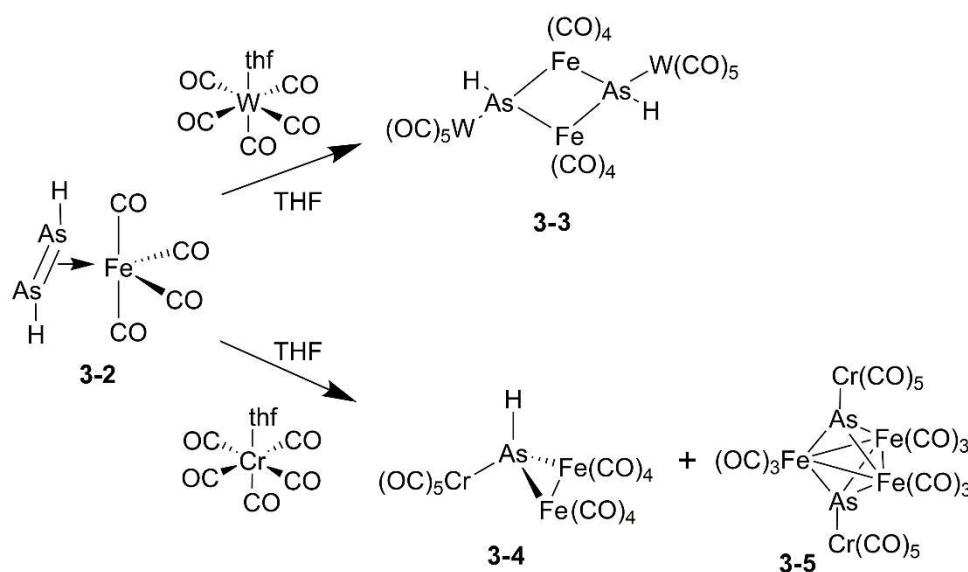
**Figure 18:** Molecular structure of **3-3**, with ellipsoids at 50% probability. Selected distances [Å]: As1-Fe1 2.4728(7), As1-Fe1' 2.4787(8), As1-W1 2.6380(5).

Performing the reaction of [W(CO)<sub>5</sub>(thf)] with **3-2D** leads to [(Fe(CO)<sub>4</sub>)AsD{W(CO)<sub>5</sub>}]<sub>2</sub> (**3-3D**). The <sup>2</sup>H NMR spectrum of **3-3D** shows a singlet at 3.05 ppm, corresponding to the As-D unit. In the <sup>1</sup>H NMR spectrum of **3-3**, the signal of the As-H unit appears at 3.12 ppm (note that the spectra were recorded

in different solvents). In the EI mass spectrum of **3-3D**, the molecular ion peak could not be detected, but several peaks corresponding to fragments such as  $\{W(CO)_5\}AsDFe_2(CO)_7^+$  and  $\{W(CO)_5\}AsDFe^+$ . The infrared spectra of **3-3** show four CO stretches at 1940, 2048, 2067 and 2095  $cm^{-1}$ . A single As-D stretch appears at 1422  $cm^{-1}$  for **3-3D**, whereas, in the IR spectrum of **3**, the As-H stretch is obscured by the CO absorption bands.

The molecular structure of **3-3** (Figure 18) shows a planar  $As_2Fe_2$  ring. A hydrogen atom is attached to each arsenic atom, which additionally coordinates to a  $W(CO)_5$  fragment. The  $W(CO)_5$  fragments are tilted by  $30^\circ$  out of the plane of the  $Fe_2As_2$  ring. The Fe-As distances in **3-3** (As1-Fe1 2.4728(7) and As1-Fe1' 2.4787(8) Å) are slightly shorter than the As-Fe distances in **3-2** (As1-Fe1 2.5004(5), As2-Fe1 2.4907(5) Å) but slightly longer than the Fe-As distance in **3-1** (2.4406(8) Å).

For the reaction of  $[Fe(CO)_4](\eta^2-As_2H_2)$  (**3-2**) with  $[Cr(CO)_5(thf)]$ , an isostructural compound to **3-3** was expected. Instead, however, the new compound  $[Fe_2(CO)_8]AsH[Cr(CO)_5]$  (**3-4**) (Scheme 3) is obtained in 20% yield after column chromatographic workup of the reaction mixture. Besides crystals of **3-4**, very few crystals of  $[Fe_3(CO)_9][\mu_3-AsCr(CO)_5]_2$  (**3-5**) were obtained and identified by single crystal X-ray diffractions and by mass spectrometry. The structure of the latter compound **3-5** was already reported.<sup>[25]</sup>



**Scheme 3:** Reactivity of **3-2** towards the Lewis acids  $[M(CO)_5thf]$  (M=Cr, W).

The infrared spectrum of **3-4** shows 5 stretches at 1940, 2034, 2054, 2065, and 2114  $cm^{-1}$  for the CO and As-H vibrations. In the  $^1H$  NMR spectrum of **3-4**, a singlet at 3.9 ppm can be attributed to the H atom of the AsH unit. In order to clearly attribute the As-H stretches and hence to prove the presence of the AsH unit, we performed the reaction of **3-2D** with  $[Cr(CO)_5(thf)]$ . To our surprise, the same reaction product **3-4** was isolated instead of the expected deuterated complex  $[Fe_2(CO)_8]AsD[Cr(CO)_5]$ .  $^2H$  NMR and IR spectroscopic investigations indicate that the H/D exchange occurs during the reaction and not during the column chromatographic workup, since the resonance signal corresponding to

$[\{\text{Fe}_2(\text{CO})_8\}\text{AsD}\{\text{Cr}(\text{CO})_5\}]$  is not present in the  $^2\text{H}$  NMR spectrum of the reaction mixture. In the EI mass spectrum of **3-4**, the molecular ion peak could be detected at  $m/z=603.68$  as well as peaks corresponding to the consecutive loss of all carbonyl groups, the hydrogen and the arsenic atom.

In the solid state structure of **3-4** (Figure 19), an AsH ligand coordinates to a  $\text{Cr}(\text{CO})_5$  and an  $\text{Fe}_2(\text{CO})_8$  fragment. The coordination geometry around the arsenic atom is tetrahedrally distorted. A phenyl-substituted complex  $[\{\text{Fe}_2(\text{CO})_8\}\text{AsPh}\{\text{Cr}(\text{CO})_5\}]$  (**3-C**) with a related structural motif was reported.<sup>[26]</sup> Moreover, in the literature, there are only a few complexes described containing AsH ligands in which the arsenic is tetrahedrally coordinated such as  $[\{\text{HOs}_2(\text{CO})_7\}\text{AsH}\{\text{HOs}(\text{CO})_4\}]$  or  $[\text{Et}_4\text{N}][\text{HAs}\{\text{Fe}_2(\text{CO})_6(\mu\text{-CO})(\mu\text{-H})\}\{\text{Fe}(\text{CO})_4\}]$ .<sup>[27]</sup>

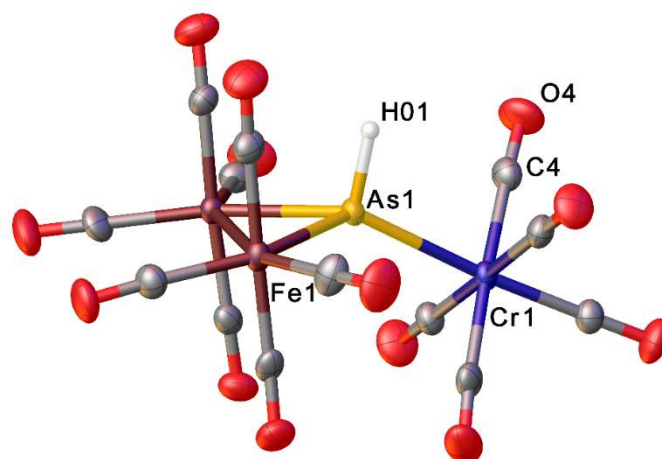


**Figure 19:** Molecular structure of **3-4** with ellipsoids set at 50% probability. Selected distances [Å]: As1-Fe1 2.3833(5), As1-Fe2 2.3873(5), As1-Cr1 2.4855(5).

### 3.6. Conclusion

In summary, we were able to isolate and characterise the very sensitive complex **3-2**, containing the unprecedented parent diarsene  $\text{HAS}=\text{AsH}$  as side-on coordinating ligand, which is stabilised in the coordination sphere of a mononuclear  $\text{Fe}(\text{CO})_4$  fragment without further stabilisation by bulky organic substituents. Although **3-2** is highly sensitive and only stable at low temperatures, it could be comprehensively characterised. DFT calculations show that **3-2** is best described as an olefin-like complex in which the  $\text{As}=\text{As}$  double bond character is preserved. Further, the initial reactivity of **3-2** towards Lewis acids was investigated leading to new products containing As-H ligands. Among others, complex **3-3** is the first structurally proved representative containing a planar  $\text{Fe}_2\text{As}_2$  unit.

## 3.7. Supporting Information

### 3.7.1. Synthesis and Characterisation

#### General remarks

All manipulations were carried out using Schlenk techniques under an atmosphere of dry nitrogen. Diethyl ether was dried over sodium, and freshly distilled before use. Dichloromethane, hexane, toluene and thf were dried using an MB SPS-800 solvent purifier and stored under nitrogen.  $\text{As}(\text{SiMe}_3)_3$  was prepared according to literature methods.<sup>[28]</sup>  $[\text{Fe}(\text{CO})_5]$  was obtained from commercial suppliers and freshly distilled. The mass spectra were recorded from the solid sample with a Jeol AccuTOF GCX instrument. For the irradiations a mercury immersion lamp TQ150Z1 has been used.

#### Synthesis of $[\{\text{Fe}(\text{CO})_4\}\text{As}(\text{SiMe}_3)_3]$ (3-1)

1 mL (7.2 mmol) of  $[\text{Fe}(\text{CO})_5]$  and 2 mL (7.2 mmol) of  $\text{As}(\text{SiMe}_3)_3$  was added to pentane at room temperature. This solution was irradiated with a mercury arc lamp for 30 minutes. The solvent was removed in vacuo, the remaining solid dissolved in pentane and filtered. The solution was concentrated until beginning of precipitation and cooled to  $-90\text{ }^\circ\text{C}$  for one hour. The supernatant was decanted and the precipitate washed with cold pentane. Drying in vacuo leads to a yellowish powder. It can be recrystallised from a concentrated pentane solution at  $-30\text{ }^\circ\text{C}$  as yellow plates.

Yield: 2.7 g, (5.8 mmol; 81 %)

**$^1\text{H}$  NMR** ( $\text{C}_6\text{D}_6$ , 300 MHz, 298 K):  $\delta$  [ppm] = 0.30 (s,  $^2J_{\text{Si-H}} = 6.67$  Hz; 27 H,  $\text{CH}_3$ )

**$^{13}\text{C}\{^1\text{H}\}$  NMR** ( $\text{CD}_2\text{Cl}_2$ , 101 MHz):  $\delta$  [ppm] = 2.51 (s,  $\text{CH}_3$ ), 215.97 (s, CO)

**IR** (KBr):  $\tilde{\nu}$  (CO) [ $\text{cm}^{-1}$ ] = 2025 (m), 1940 (w), 1899 (s, br)

**MS** (EI, solid): m/z (rel. int. %): 461.98 (1) [ $\text{M}^+$ ], 433.99 (1) [ $\text{M}^+ - \text{CO}$ ], 405.99 (1) [ $\text{M}^+ - 2\text{ CO}$ ], 379.00 (4) [ $\text{M}^+ - 3\text{ CO}$ ], 350.00 (5) [ $\text{M}^+ - 4\text{ CO}$ ], 294.06 (26) [ $\text{As}\{\text{Si}(\text{CH}_3)_3\}_3$ ], 73.05 (100) [ $\text{Si}(\text{CH}_3)_3$ ].

#### Synthesis of $[\{\text{Fe}(\text{CO})_4\}\text{Sb}(\text{SiMe}_3)_3]$ <sup>1</sup>

The whole synthesis was carried out in the dark. 0.5 mL (3.5 mmol) of  $[\text{Fe}(\text{CO})_5]$  and 1 mL (3.6 mmol) of  $\text{Sb}(\text{SiMe}_3)_3$  were added to pentane at room temperature. This solution was irradiated with a mercury lamp for 30 minutes. All volatiles were removed in vacuo, the remaining dark red solid dissolved again in pentane and filtered. The solution was concentrated in vacuo until beginning of precipitation and cooled to  $-90\text{ }^\circ\text{C}$  for one hour. The supernatant was decanted and the precipitate washed with cold pentane. Drying in vacuo leads to a yellowish powder. It can be recrystallised from a concentrated pentane solution at  $-30\text{ }^\circ\text{C}$  as brown plates.

---

<sup>1</sup> The reaction of  $\text{Sb}(\text{SiMe}_3)_3$  with  $[\text{Fe}_2(\text{CO})_9]$  in pentane for 12h leads to  $[\{\text{Fe}(\text{CO})_4\}\text{Sb}(\text{SiMe}_3)_3]$  in 30% yield (c.f. Breunig *et al.*<sup>[29]</sup>)

Yield: 820 mg (1.61 mmol, 46 %)

$^1\text{H NMR}$  ( $\text{C}_6\text{D}_6$ , 300 MHz, 298 K):  $\delta$  [ppm] = 0.305 (s, 27 H;  $\text{CH}_3$ )

$^{13}\text{C}\{^1\text{H}\}$  NMR ( $\text{C}_6\text{D}_6$ , 75 MHz, 298 K):  $\delta$  [ppm] = 0.20 (s,  $\text{CH}_3$ ), 213.5 (s, CO)

#### Synthesis of $[\{\text{Fe}(\text{CO})_4\}\{\eta^2\text{-As}_2\text{H}_2\}]$ (**3-2**)

To a solution of 500 mg (1.08 mmol)  $[\{\text{Fe}(\text{CO})_4\}\text{As}(\text{SiMe}_3)_3]$  in 40 mL diethyl ether at  $-80^\circ\text{C}$ , 0.3 mL of methanol was added and stirred at that temperature for one hour. All volatiles were removed in vacuo at  $-60^\circ\text{C}$ . Subsequently, the yellow-brown residue was condensed into a schlenk, which was kept at  $-80^\circ\text{C}$ , by slowly warming to room temperature. Compound **3-2** is formed as a yellow solid. It can be crystallised by dissolving the solid in cold diethyl ether and storage at  $-80^\circ\text{C}$ .

Yield: 150 mg (0.47 mmol, 86% based on  $[\{\text{Fe}(\text{CO})_4\}\text{As}(\text{SiMe}_3)_3]$ )

$^1\text{H NMR}$  ( $\text{CD}_2\text{Cl}_2$ , 400 MHz, 213 K):  $\delta$  [ppm] = 1.29 (s,  $\text{As}_2\text{H}_2$ )

IR (KBr):  $\tilde{\nu}_{\text{CO}}$  [ $\text{cm}^{-1}$ ] = 2076 (s), 2016 (s), 1963 (s)

MS (EI, 70 eV; solid):  $m/z$  (rel. int. %): 319.77 (29) [ $\text{M}^+$ ], 291.78 (9) [ $\text{M}^+ - \text{CO}$ ], 289.76 (36) [ $\text{M}^+ - \text{CO} - 2\text{H}$ ], 263.78 (4) [ $\text{M}^+ - 2 \text{CO}$ ], 261.77 (22) [ $\text{M}^+ - 2 \text{CO} - 2 \text{H}$ ], 235.78 (22) [ $\text{M}^+ - 3 \text{CO}$ ], 205.78 (66) [ $\text{M}^+ - 4 \text{CO} - 2 \text{H}$ ], 147.07 (100) [ $(\text{Me}_3\text{Si})_2\text{O} - \text{Me}$ ] $^+$ .

#### Synthesis of $[\{\text{Fe}(\text{CO})_4\}\{\eta^2\text{-As}_2\text{D}_2\}]$ (**3-2D**)

To a solution of 500 mg (1.08 mmol)  $[\{\text{Fe}(\text{CO})_4\}\text{As}(\text{SiMe}_3)_3]$  in 40 mL diethyl ether at  $-80^\circ\text{C}$ , 0.3 mL of deuterated methanol was added and stirred at that temperature for one hour. All volatiles were removed in vacuo at  $-60^\circ\text{C}$ . Subsequently, the yellow-brown residue was condensed into a schlenk, which was kept at  $-80^\circ\text{C}$ , by slowly warming to room temperature. Compound **3-2D** is formed as a yellow solid. It can be crystallised by dissolving the solid in cold diethyl ether and storage at  $-80^\circ\text{C}$ .

Yield: 135 mg (0.42 mmol, 77% based on  $[\{\text{Fe}(\text{CO})_4\}\text{As}(\text{SiMe}_3)_3]$ )

$^2\text{H NMR}$  ( $\text{Et}_2\text{O}/\text{C}_6\text{D}_6$ , 61 MHz, 213 K):  $\delta$  [ppm] = 1.33 (s,  $\text{As}_2\text{D}_2$ )

IR (KBr):  $\tilde{\nu}_{\text{CO}}$  [ $\text{cm}^{-1}$ ] = 2124 (w), 2053 (s), 1999 (s), 1912 (s);  $\tilde{\nu}_{\text{AsD}}$  [ $\text{cm}^{-1}$ ] = 1473 (w).

#### Synthesis of $[\{\text{Fe}(\text{CO})_4\}\text{AsH}\{\text{W}(\text{CO})_5\}]_2$ (**3-3**)

A solution of 120 mg (0.341 mmol)  $[\text{W}(\text{CO})_6]$  in THF was irradiated with a mercury lamp for 4 hours. The yellow solution of  $[\text{W}(\text{CO})_5(\text{thf})]$  was added to solid  $[\{\text{Fe}(\text{CO})_4\}\{\eta^2\text{-As}_2\text{H}_2\}]$  at  $-80^\circ\text{C}$  (obtained from 0.5 g, 1.08 mmol  $[\{\text{Fe}(\text{CO})_4\}\text{As}(\text{SiMe}_3)_3]$ ). The solution was slowly warmed to room temperature, while at approximately  $0^\circ\text{C}$  the color change from yellow to red. The solution was concentrated and stored at  $-30^\circ\text{C}$ , when **3-3** crystallises as red plates.

Crystalline yield: 0.132 g, (0.12 mmol, 43 % based on  $[\{\text{Fe}(\text{CO})_4\}\text{As}(\text{SiMe}_3)_3]$ )

$^1\text{H NMR}$  ( $\text{CD}_2\text{Cl}_2$ , 400 MHz, 298 K):  $\delta$  [ppm] = 3.12 (s, AsH).

$\text{IR}$  ( $\text{CH}_2\text{Cl}_2$ ):  $\tilde{\nu}_{\text{CO}}$  [ $\text{cm}^{-1}$ ] = 2095 (w), 2067 (s), 2048 (m), 1974 (m), 1940 (s).

#### Synthesis of $[\{\text{Fe}(\text{CO})_4\}\text{AsD}\{\text{W}(\text{CO})_5\}]_2$ (3-3D)

A solution of 120 mg (0.341 mmol)  $[\text{W}(\text{CO})_6]$  in THF was irradiated with a mercury lamp for 4 hours. The yellow solution of  $[\text{W}(\text{CO})_5(\text{thf})]$  was added to solid  $[\{\text{Fe}(\text{CO})_4\}\{\eta^2\text{-As}_2\text{D}_2\}]$  at  $-80^\circ\text{C}$  (obtained from 0.5 g, 1.08 mmol  $[\{\text{Fe}(\text{CO})_4\}\text{As}(\text{SiMe}_3)_3]$ ). The solution was slowly warmed to room temperature, while at approximately  $0^\circ\text{C}$  the color change from yellow to red. The solution was concentrated and stored at  $-30^\circ\text{C}$ , when **3-3D** crystallises as red plates.

Crystalline yield: 0.123 g, (0.11 mmol, 40 % based on  $[\{\text{Fe}(\text{CO})_4\}\text{As}(\text{SiMe}_3)_3]$ )

$^2\text{H NMR}$  (THF/ $\text{C}_6\text{D}_6$ , 61 MHz, 298 K):  $\delta$  [ppm] = 3.05 (s, AsD).

$\text{IR}$  ( $\text{CH}_2\text{Cl}_2$ ):  $\tilde{\nu}_{\text{CO}}$  [ $\text{cm}^{-1}$ ] = 2095 (w), 2067 (s), 2051 (m), 1975 (m), 1940 (s);  $\tilde{\nu}_{\text{AsD}}$  [ $\text{cm}^{-1}$ ] = 1422 (w)

**MS** (EI, 70 eV, solid):  $m/z$  (rel. int. %): 708.8 (70)  $[\text{M}^+ - \text{AsDW}(\text{CO})_5 - \text{CO}]$ , 680.8 (15)  $[\text{M}^+ - \text{AsDW}(\text{CO})_5 - 2 \text{CO}]$ , 652.8 (40)  $[\text{M}^+ - \text{AsDW}(\text{CO})_5 - 3 \text{CO}]$ , 624.8 (50)  $[\text{M}^+ - \text{AsDW}(\text{CO})_5 - 4 \text{CO}]$ , 596.8 (20)  $[\text{M}^+ - \text{AsDW}(\text{CO})_5 - 5 \text{CO}]$ , 568.8 (80)  $[\text{M}^+ - \text{AsDW}(\text{CO})_5 - \text{Fe}(\text{CO})_4]$ , 540.8 (100)  $[\text{M}^+ - \text{AsDW}(\text{CO})_5 - \text{Fe}(\text{CO})_4 - \text{CO}]$ , 512.79 (90)  $[\text{M}^+ - \text{AsDW}(\text{CO})_5 - \text{Fe}(\text{CO})_4 - 2 \text{CO}]$ , 484.8 (75)  $[\text{M}^+ - \text{AsDW}(\text{CO})_5 - \text{Fe}(\text{CO})_4 - 3 \text{CO}]$ , 456.8 (75)  $[\text{M}^+ - \text{AsDW}(\text{CO})_5 - \text{Fe}(\text{CO})_4 - 4 \text{CO}]$

#### Synthesis of $[\{\text{Fe}_2(\text{CO})_8\}\text{AsH}\{\text{Cr}(\text{CO})_5\}]$ (3-4)

A solution of 350 mg (1.59 mmol)  $[\text{Cr}(\text{CO})_6]$  in THF was irradiated with a mercury lamp for 4 hours, while a weak stream of nitrogen was blubbed through the solution. This orange solution of  $[\text{Cr}(\text{CO})_5(\text{thf})]$  was added to solid  $[\{\text{Fe}(\text{CO})_4\}\{\eta^2\text{-As}_2\text{H}_2\}]$  at  $-80^\circ\text{C}$  (obtained from 1g, 2.16 mmol  $[\{\text{Fe}(\text{CO})_4\}\text{As}(\text{SiMe}_3)_3]$ ). The solution was slowly warmed to room temperature, while at approximately  $0^\circ\text{C}$  the color change from yellow to red. The reaction mixture was purified by column chromatography on silica. With hexane/toluene: 1:1 a red fraction was eluted. Removing the solvent, compound 4 remains as red solid. It can be recrystallised by storing a concentrated dichloromethane solution at  $-30^\circ\text{C}$ .

Yield: 33 mg, (0.055 mmol, 20 % based on  $[\{\text{Fe}(\text{CO})_4\}\text{As}(\text{SiMe}_3)_3]$ )

$^1\text{H NMR}$  ( $\text{CD}_2\text{Cl}_2$ , 400 MHz, 298 K):  $\delta$  [ppm] = 3.87 (s, AsH)

$\text{IR}$  ( $\text{CH}_2\text{Cl}_2$ ):  $\tilde{\nu}_{\text{CO}}$  [ $\text{cm}^{-1}$ ] = 2113.9 (w), 2065.4 (s), 2054.0 (s), 2034.4 (m), 1939.5 (s)

**MS** (EI, 70 eV, solid):  $m/z$  (rel. int. %): 603.7 (12)  $[\text{M}^+]$ , 575.7 (25)  $[\text{M}^+ - \text{CO}]$ , 547.7 (18)  $[\text{M}^+ - 2\text{CO}]$ , 519.7 (4)  $[\text{M}^+ - 3\text{CO}]$ , 491.7 (21)  $[\text{M}^+ - 4\text{CO}]$ , 463.7 (17)  $[\text{M}^+ - 5\text{CO}]$ , 435.7 (36)  $[\text{M}^+ - 6\text{CO}]$ , 407.7 (100)  $[\text{M}^+ - 7\text{CO}]$ , 379.7 (59)  $[\text{M}^+ - 8\text{CO}]$ , 351.7 (53)  $[\text{M}^+ - 9\text{CO}]$ , 323.7 (61)  $[\text{M}^+ - 10\text{CO}]$ , 295.7 (50)  $[\text{M}^+ - 11\text{CO}]$ , 267.7 (43)  $[\text{M}^+ - 12\text{CO}]$ , 239.7 (100)  $[\text{M}^+ - 13\text{CO}]$ , 238.7 (51)  $[\text{M}^+ - 13\text{CO} - \text{H}]$ , 182.8 (28)  $[\text{M}^+ - 13\text{CO} - \text{H} - \text{As}]$ .



### 3.7.2. Crystallographic Details

#### General remarks:

Single crystal structure analyses were performed using different Rigaku Oxford Diffraction diffractometers. Data collection and reduction were performed with the CrysAlisPro<sup>[30]</sup> software package. Using the software Olex2<sup>[31]</sup> the structure solution and refinement was carried out using the programs ShelXT<sup>[32]</sup> and SHELXL<sup>[33]</sup>. Further details are given in Table 1.

The structure of **3-2** reveals two independent molecules in the asymmetric unit. One shows minor disorder at the As<sub>2</sub>H<sub>2</sub> and a CO ligand, respectively. There is no crystallographic indication for the presence of a *cis*-As<sub>2</sub>H<sub>2</sub> isomer at this site. In contrast, for the second molecule, hydrogen disorder can be located from the difference Fourier map and is attributed to a 50:50 ratio of the *cis* and *trans* isomer of As<sub>2</sub>H<sub>2</sub>. This results in an approximate ratio of 75:25 *trans*:*cis* for the crystal of **3-2**. Figure 20 shows the final model of the refinement.

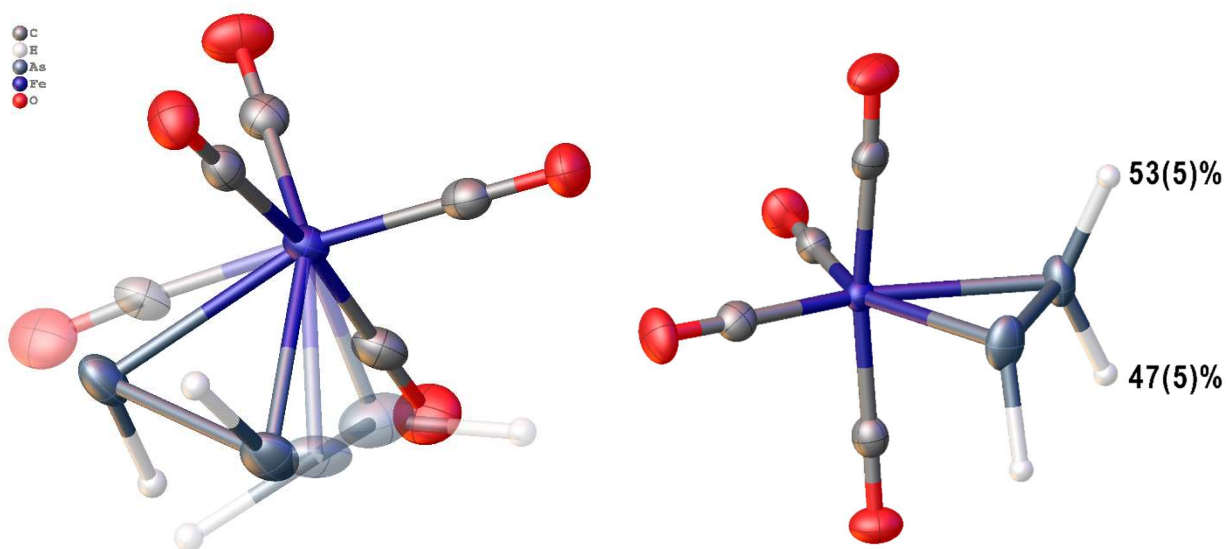


**Figure 20:** Disorder of the As<sub>2</sub>H<sub>2</sub>/CO site (left) and disordered hydrogen position in the other molecule of the asymmetric unit with the corresponding site occupancies.

Crystallographic data and details of the diffraction experiments are given in Table 1. CIF files with comprehensive information on the details of the diffraction experiments and full tables of bond lengths and angles are deposited in Cambridge Crystallographic Data Centre under the deposition codes CCDC 1943235-1943239.

**Table 1:** Experimental X-ray crystallographic details for **3-1**,  $[\{\text{Fe}(\text{CO})_4\}\text{Sb}(\text{SiMe}_3)_3]$ , **3-2**, **3-3** and **3-4**

Compound	<b>3-1</b>	$[\{\text{Fe}(\text{CO})_4\}\text{Sb}(\text{SiMe}_3)_3]$	<b>3-2</b>	<b>3-3</b>	<b>3-4</b>
CCDC number	1943235	1943238	1943236	1943239	1943237
Formula	$\text{C}_{13}\text{H}_{27}\text{AsFeO}_4\text{Si}_3$	$\text{C}_{13}\text{H}_{27}\text{SbFeO}_4\text{Si}_3$	$\text{C}_4\text{H}_2\text{As}_2\text{FeO}_4$	$\text{C}_{18}\text{H}_2\text{As}_2\text{Fe}_2\text{O}_{18}\text{W}_2$	$\text{C}_{13}\text{HAsCrFe}_2\text{O}_{13}$
$D_{\text{calc.}}/\text{g cm}^{-3}$	1.412	1.483	2.500	2.724	2.093
Device Type	Gemini Ultra, Atlas S2	SuperNova, Atlas	SuperNova, Atlas	GV50, Titan S2	GV50, Titan S2
$\mu/\text{mm}^{-1}$	8.937	16.099	22.674	26.619	19.140
Formula Weight	462.38	509.21	319.75	1135.44	603.753
Colour	clear orange	clear orange	yellow	red	red
Shape	block	block	block	block	needle
Size/ $\text{mm}^3$	0.19×0.08×0.04	0.16×0.13×0.07	0.10×0.07×0.06	0.12×0.10×0.05	0.45×0.10×0.05
T/K	123.00(14)	123.00(10)	123.00(10)	123.01(10)	123.00(16)
Crystal System	monoclinic	monoclinic	triclinic	triclinic	monoclinic
Flack Parameter	0.396(5)	-	-	-	-
Hooft Parameter	0.400(3)	-	-	-	-
Space Group	Cc	P2 <sub>1</sub> /n	P-1	P-1	P2 <sub>1</sub> /c
a/Å	9.5596(2)	9.7749(3)	6.13585(18)	8.6978(3)	9.1876(4)
b/Å	14.9087(3)	14.9134(4)	11.3123(3)	9.3306(3)	15.4769(5)
c/Å	15.4625(3)	15.8320(4)	12.3373(4)	9.6224(5)	14.0980(6)
$\alpha/^\circ$	90	90	91.344(2)	116.012(4)	90
$\beta/^\circ$	99.228(2)	98.727(3)	96.974(3)	98.358(4)	107.060(4)
$\gamma/^\circ$	90	90	91.093(2)	90.298(3)	90
V/Å <sup>3</sup>	2175.21(8)	2281.22(11)	849.56(4)	692.26(5)	1916.46(14)
Z	4	4	4	1	4
Z'	1	1	2	0.5	1
Absorption correction type	analytical	analytical	analytical	analytical	analytical
Wavelength/Å	1.54184	1.54184	1.54184	1.54184	1.54184

Radiation type	CuK $\alpha$	CuK $\alpha$	CuK $\alpha$	CuK $\alpha$	CuK $\alpha$
$\theta_{\min}/^\circ$	5.549	4.095	3.910	5.155	4.35
$\theta_{\max}/^\circ$	66.706	73.453	73.538	73.876	74.31
Measured Refl.	6930	25239	20822	13704	10760
Independent Refl.	3058	4535	3369	2767	3773
Reflections Used	3005	4001	3157	2740	3575
R <sub>int</sub>	0.0239	0.0384	0.0366	0.0575	0.0399
Parameters	209	208	227	194	275
Restraints	2	0	24	0	0
Largest Peak	0.371	0.852	0.612	0.865	0.5506
Deepest Hole	-0.247	-0.715	-0.701	-1.792	-0.8283
Goof	1.046	1.046	1.054	1.139	1.0355
wR <sub>2</sub> (all data)	0.0634	0.0624	0.0539	0.0693	0.0908
wR <sub>2</sub>	0.0629	0.0593	0.0530	0.0691	0.0888
R <sub>1</sub> (all data)	0.0263	0.0302	0.0250	0.0274	0.0340
R <sub>1</sub>	0.0257	0.0246	0.0230	0.0272	0.0322

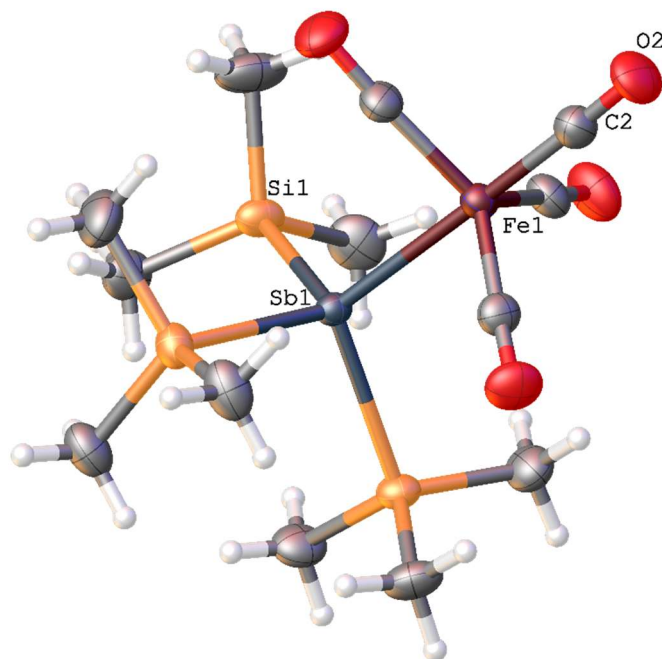
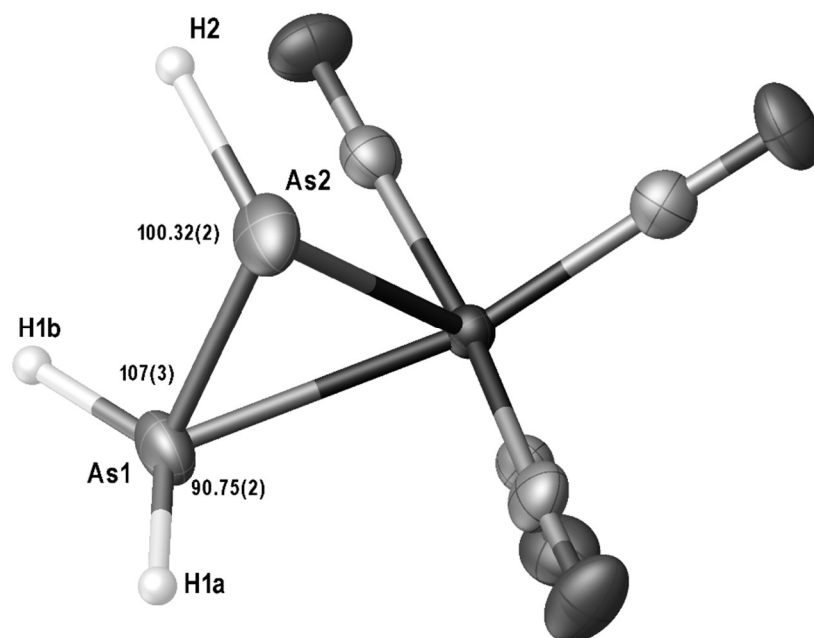


**Figure 21:** Molecular structure of  $\{\text{Fe}(\text{CO})_4\}\text{Sb}[\text{Si}(\text{CH}_3)_3]_3$  with ellipsoids set at 50% probability. Selected distances [Å]: Sb1-Fe1 2.5636(4), Sb1-Si1 2.5649(7), Sb1-Si2 2.5721(7), Sb1-Si3 2.5646(7)

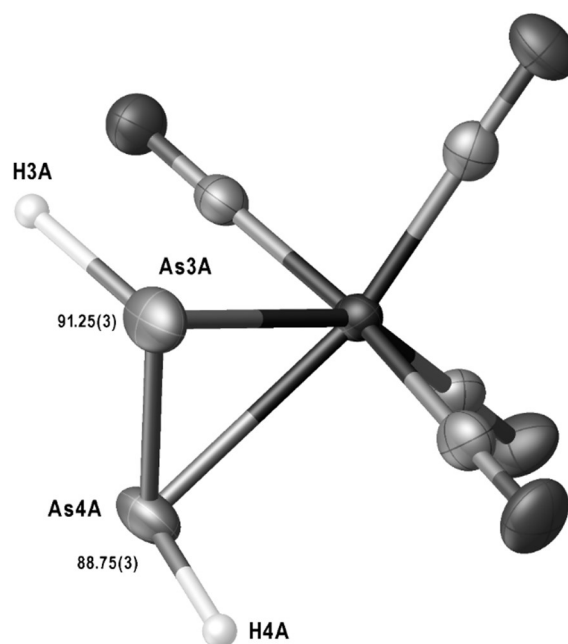
Inspection of the torsion angles of the As<sub>2</sub>H<sub>2</sub> unit in 3-2:

Moiety 1: fully occupied, only H1a/b disordered 53(3):47(3)%



Torsion angle: H1a-As1-As2-H2 -145.421(18), H1b-As1-As2-H2-9(4)

Moiety 2: major component (92%), no hydrogen disorder



Torsion angle: H3A-As3A-As4A 91.25(3), As3A-As4A-H4A 88.75(3)

### 3.7.3. NMR Spectroscopy

#### General remarks:

The NMR spectra were recorded on Bruker Avance 300 ( $^1\text{H}$ : 300.132 MHz,  $^{13}\text{C}$ : 75.468 MHz) and 400 ( $^1\text{H}$ : 400.130 MHz,  $^{13}\text{C}$ : 100.613 MHz); chemical shifts are in ppm and are relative to TMS.

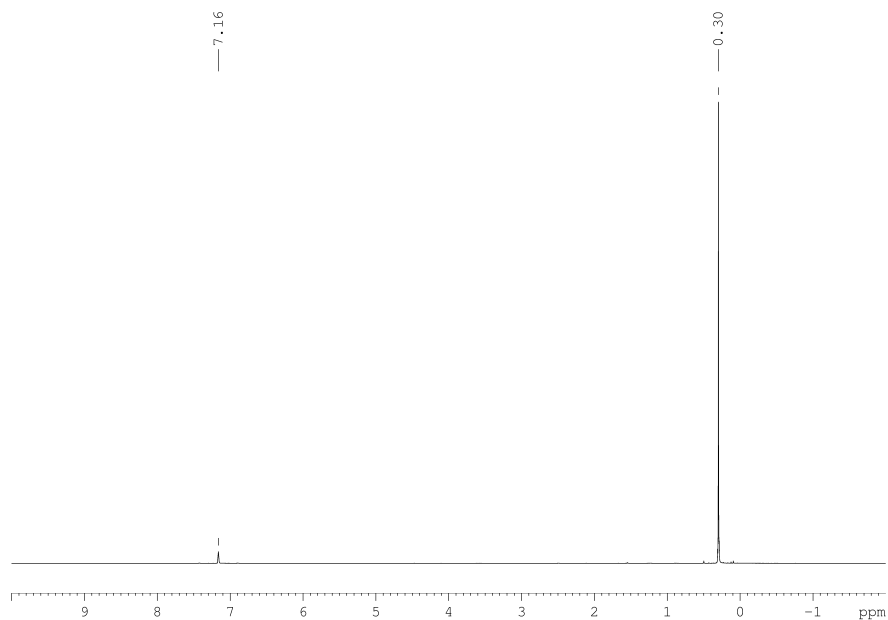


**Figure 22:**  $^1\text{H}$  NMR spectrum of **3-1** in  $\text{C}_6\text{D}_6$ .

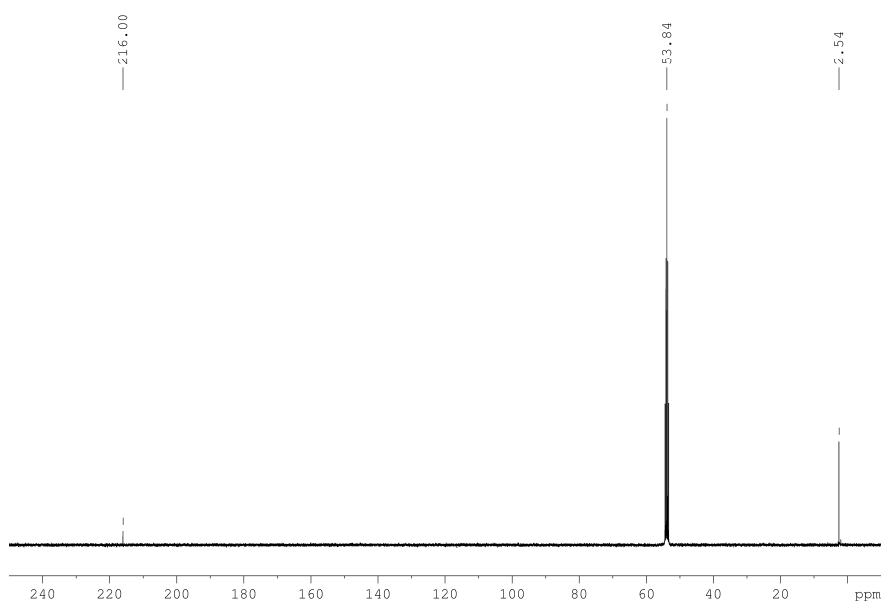


**Figure 23:**  $^{13}\text{C}\{^1\text{H}\}$  NMR spectrum of **3-1** in  $\text{CD}_2\text{Cl}_2$ .

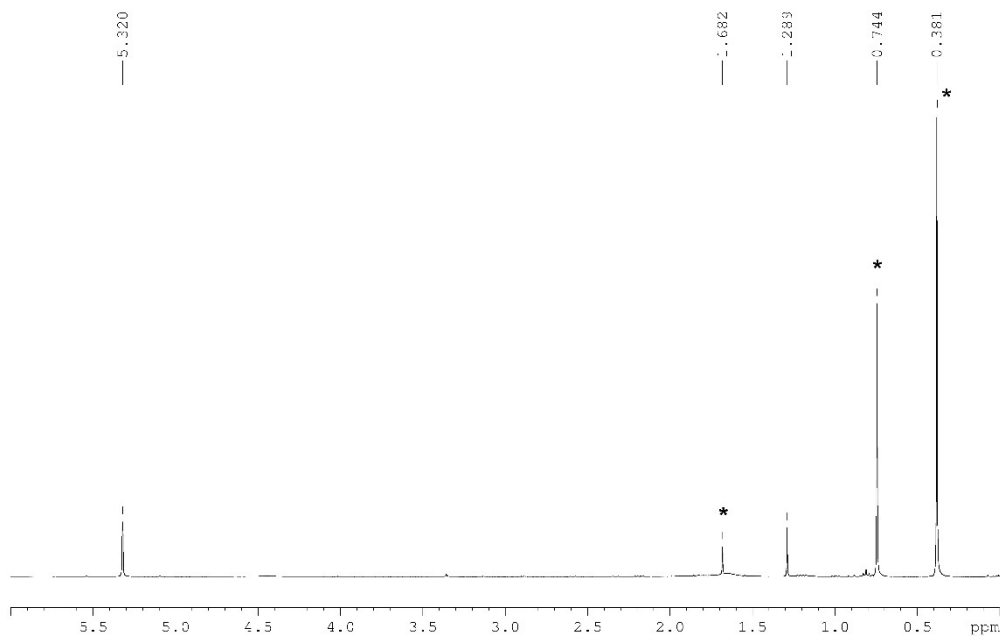


**Figure 24:**  $^1\text{H}$  NMR spectrum of **3-2** in  $\text{CD}_2\text{Cl}_2$  at 213 K. Signals marked with \* are unidentified byproducts, probably containing  $\text{OSiMe}_3$  groups.

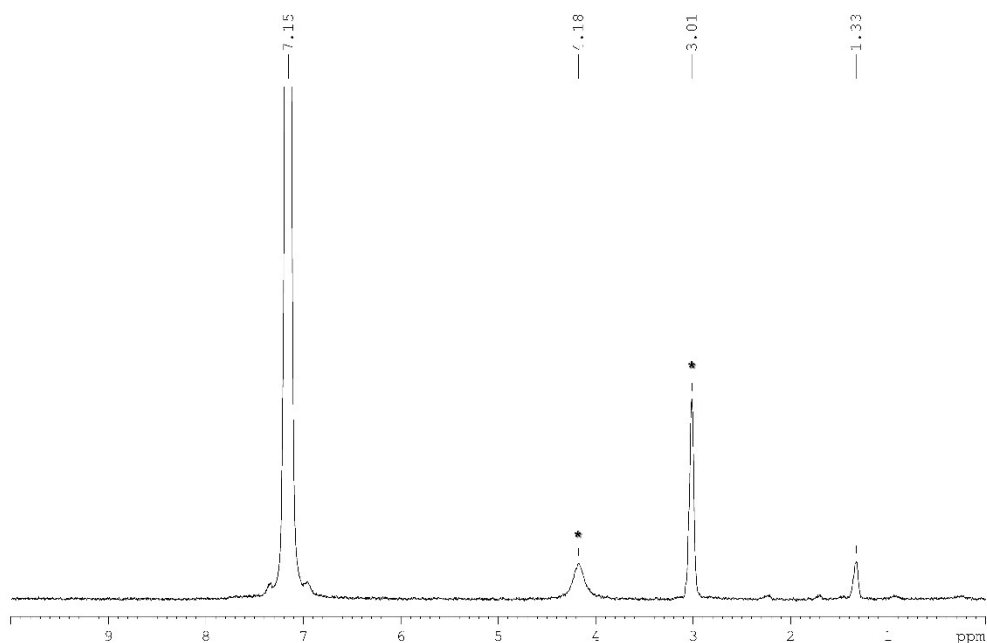


**Figure 25:**  $^2\text{H}$  NMR spectrum of **3-2D** in a mixture of  $\text{Et}_2\text{O}$  and  $\text{C}_6\text{D}_6$  at 213 K. Signals marked with \* corresponds to  $\text{CD}_3\text{OD}$ .

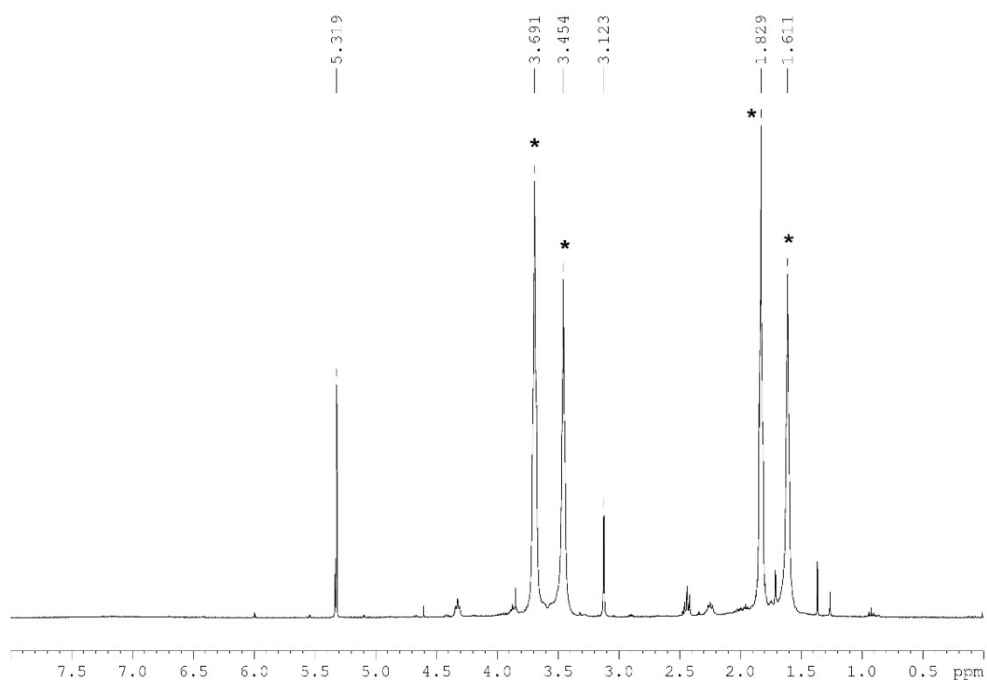


**Figure 26:** <sup>1</sup>H NMR spectrum of **3-3** in CD<sub>2</sub>Cl<sub>2</sub>. The signals marked with \* corresponds to THF and polyethers from the polymerisation of THF.

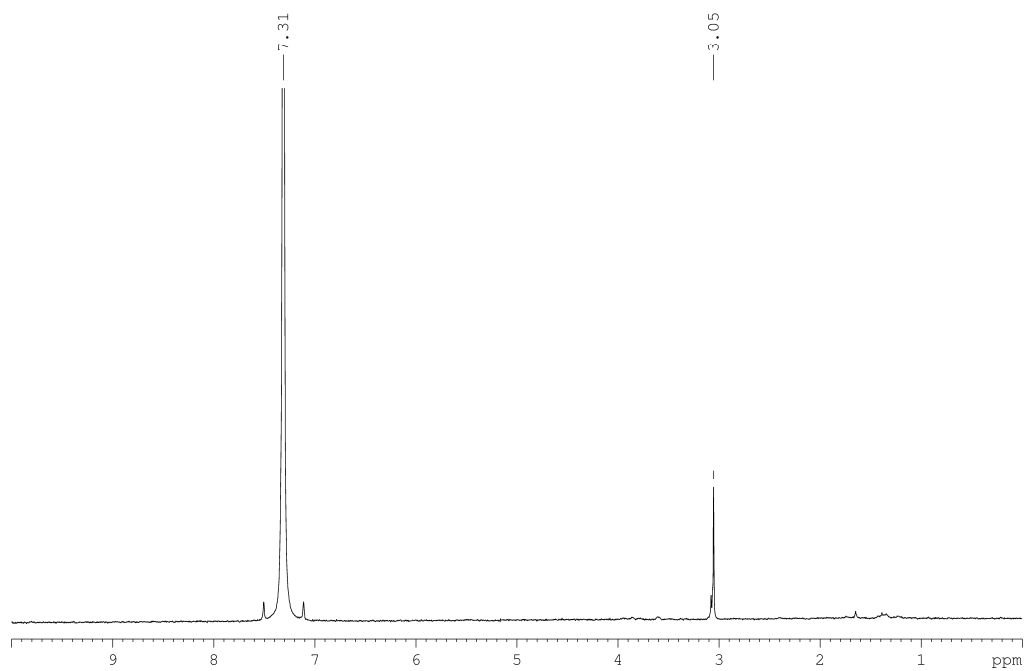


**Figure 27:** <sup>2</sup>H NMR spectrum of **3-3D** in a mixture of THF and C<sub>6</sub>D<sub>6</sub>.

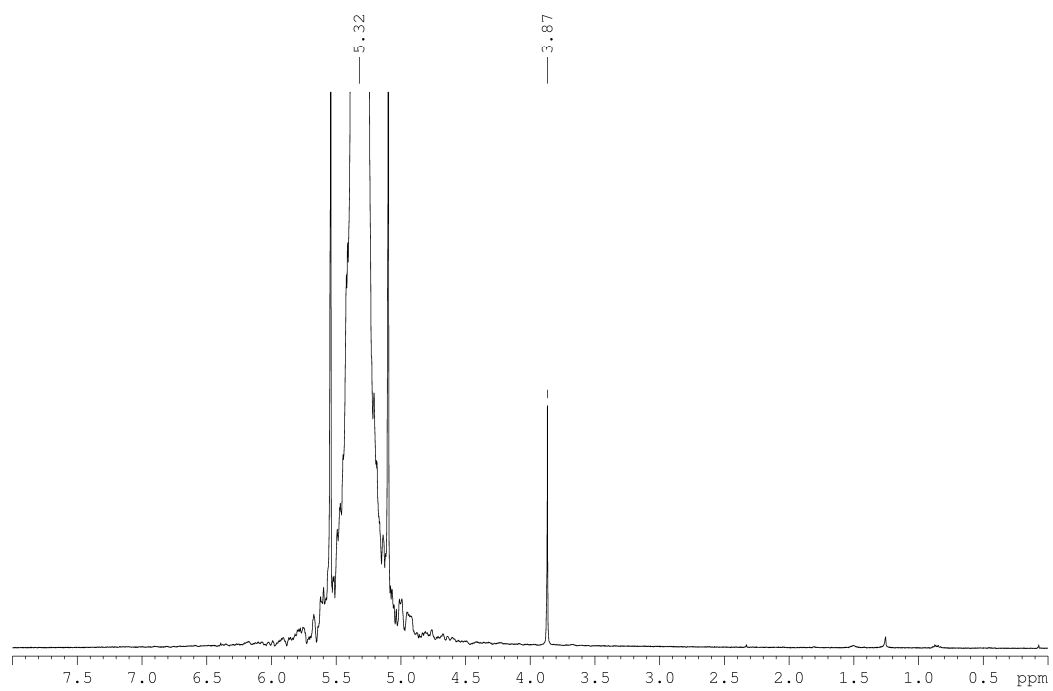


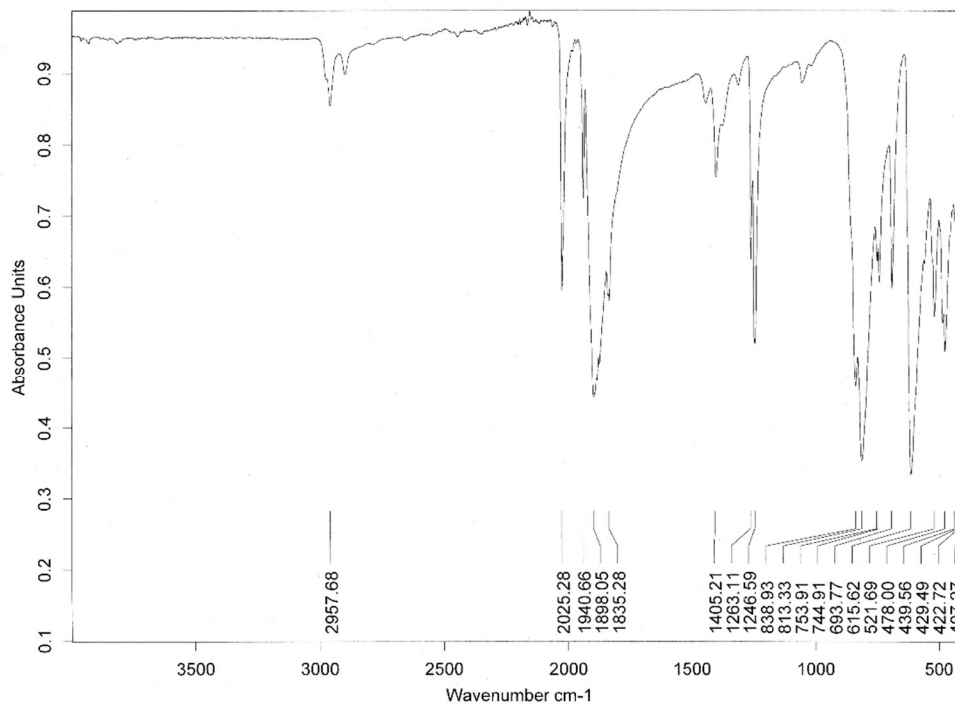
**Figure 28:** <sup>1</sup>H NMR spectrum of **3-4** in CD<sub>2</sub>Cl<sub>2</sub>.



### 3.7.4. IR spectroscopic data

#### General remarks:

The IR spectra of **3-1** and **3-2** were recorded on a Bruker Alpha Platinum ATR spectrometer, in a glove box. The IR spectra of **3-3** and **3-4** were recorded on a Thermo Fisher Scientific Nicolet iS5 spectrometer.



Page 1 of 1

**Figure 29:** ATR-IR spectrum of **3-1**

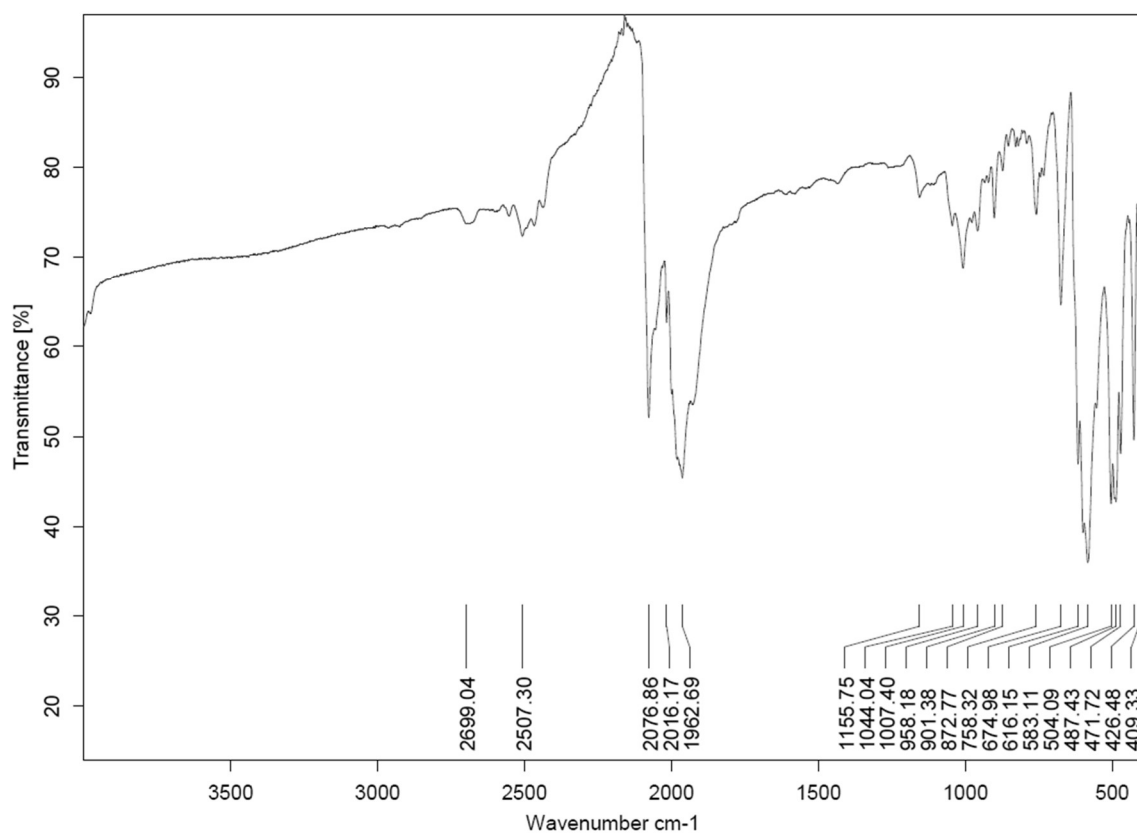


**Figure 30:** ATR-IR spectrum of  $[(\text{Fe}(\text{CO})_4)\{\eta^2\text{-As}_2\text{H}_2\}]$  (**3-2**).

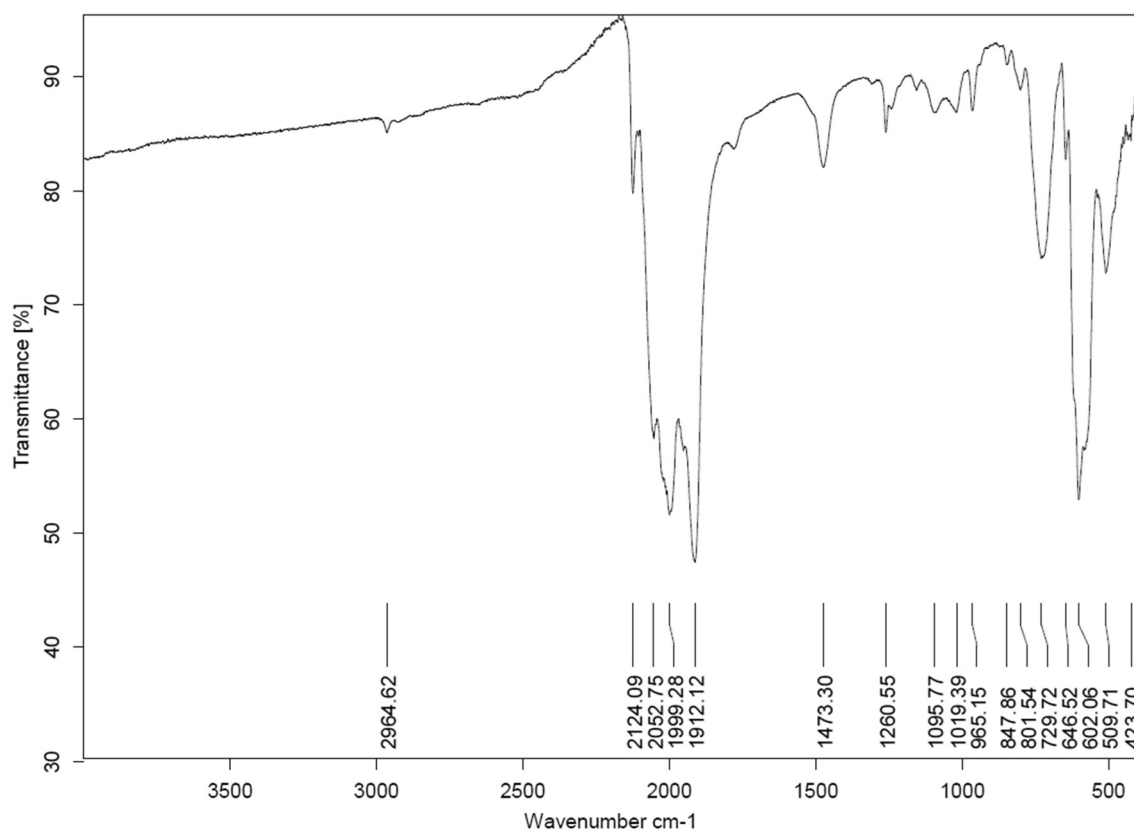


**Figure 31:** ATR-IR spectrum of  $[(\text{Fe}(\text{CO})_4)\{\eta^2\text{-As}_2\text{D}_2\}]$  (**3-2D**).  $\tilde{\nu}(\text{AsD}) = 1473 \text{ cm}^{-1}$ .

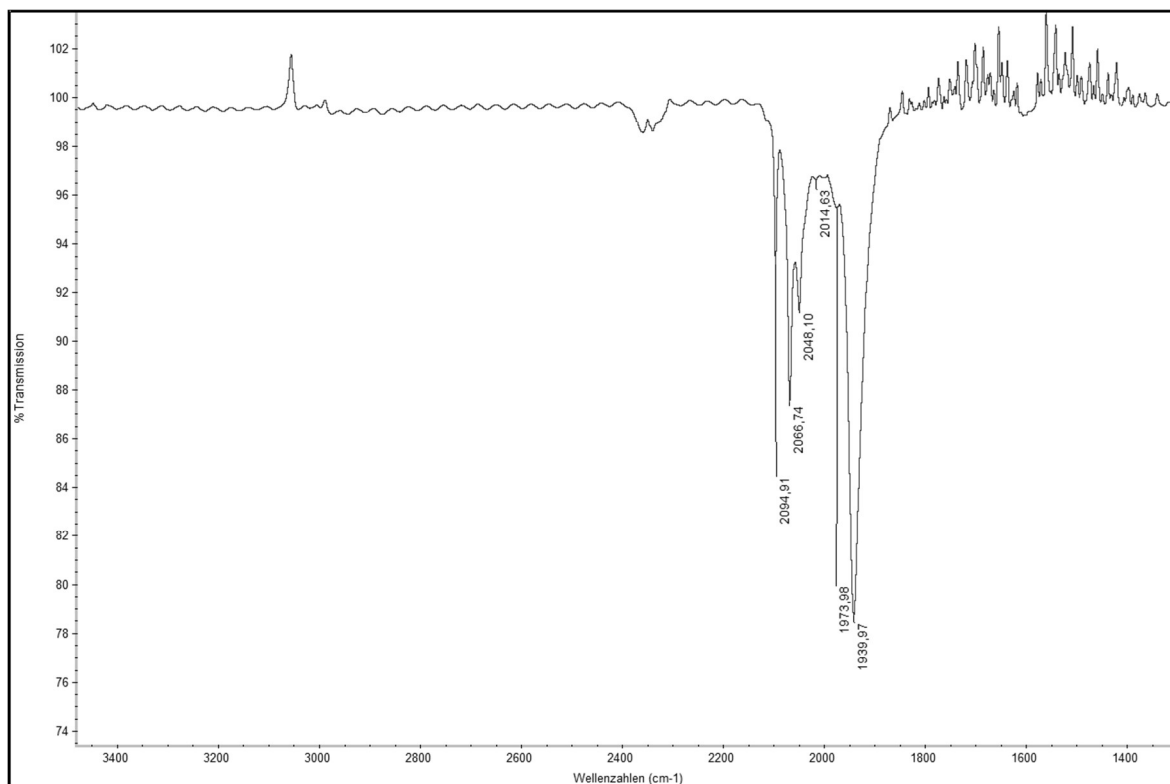


**Figure 32:** IR spectrum of **3-3**.

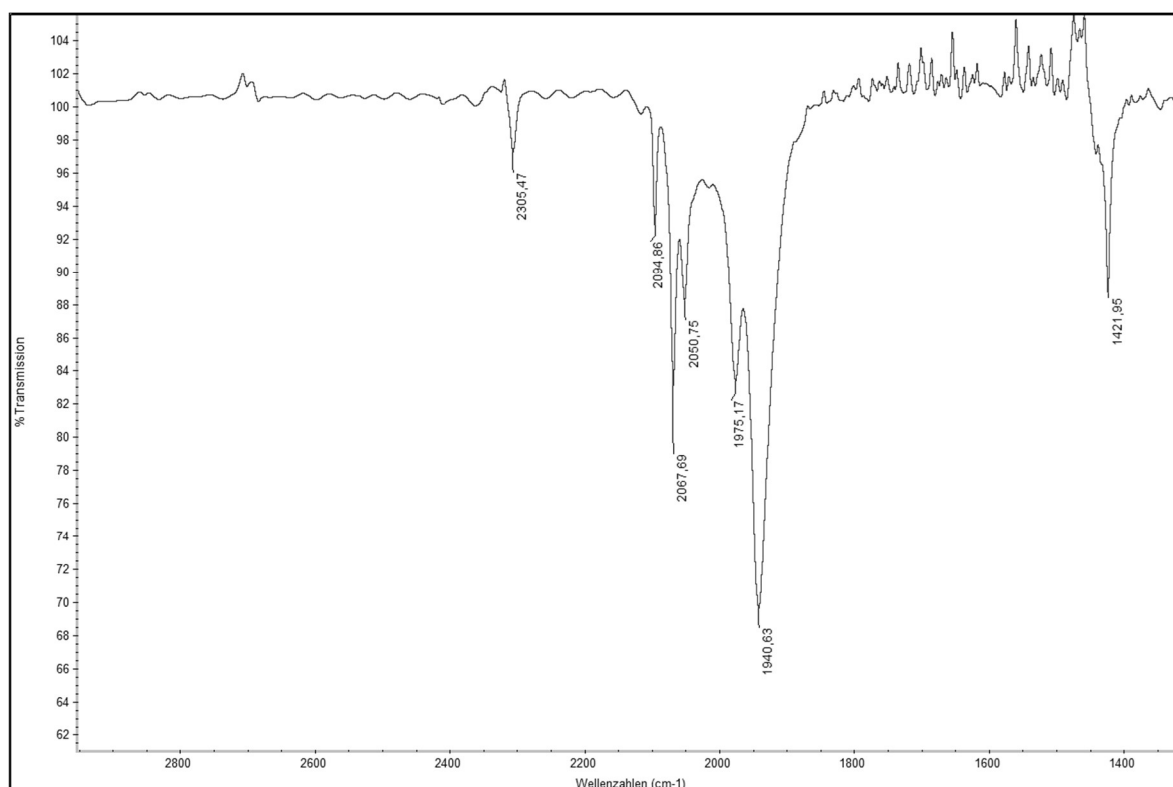


**Figure 33:** IR spectrum of **3-3D**. The absorption band at  $1975\text{ cm}^{-1}$  corresponds probably to  $[\text{W}(\text{CO})_6]$ .  $\tilde{\nu}(\text{AsD}) = 1422\text{ cm}^{-1}$ .

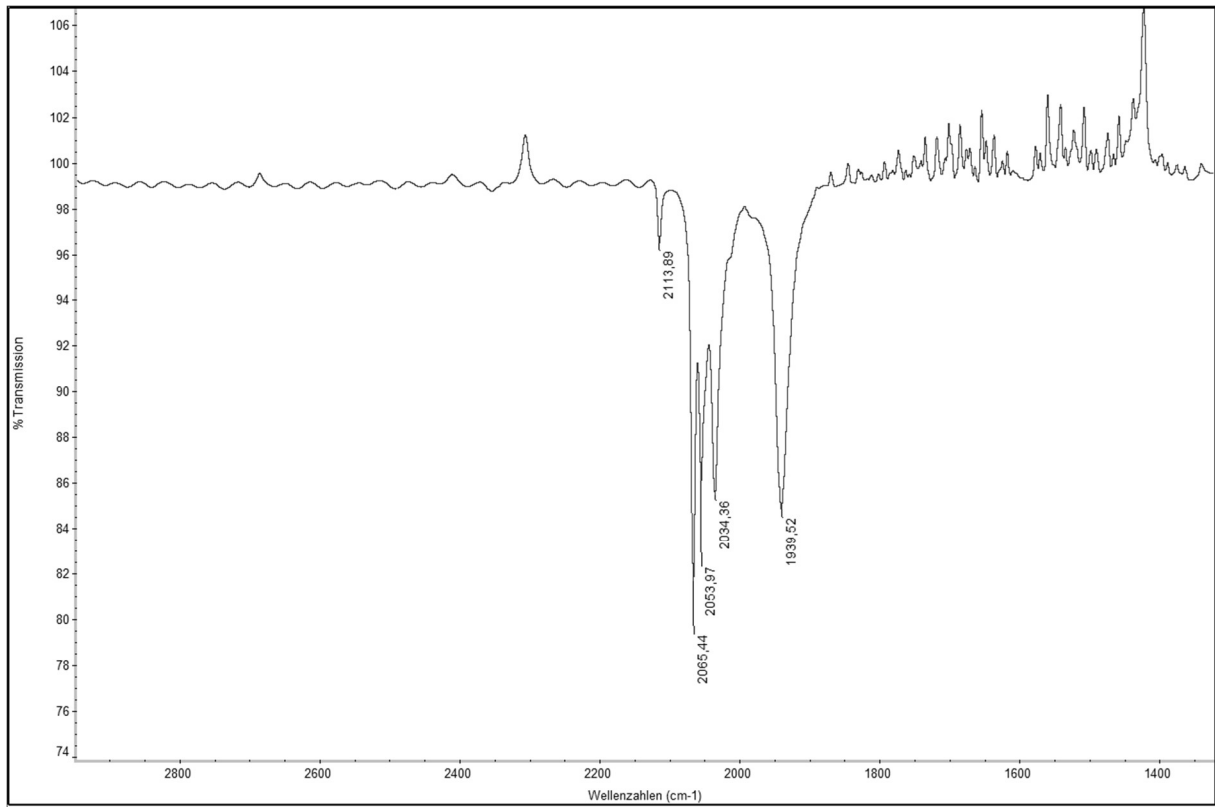
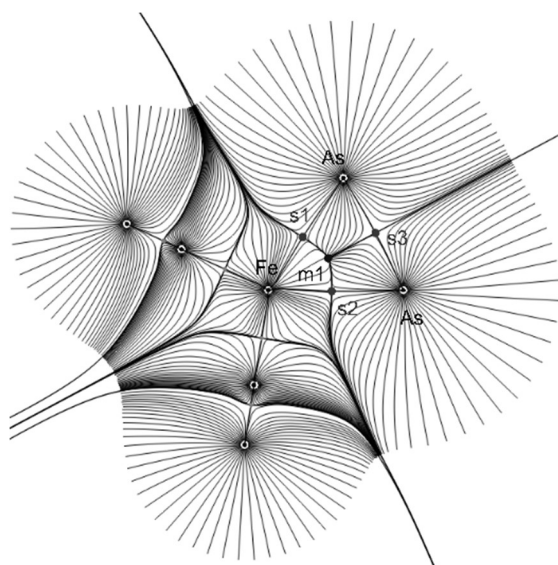


Figure 34: IR spectrum of 3-4.

### 3.7.5. Computational Details

#### DFT calculations

The geometry optimisations have been performed with the Gaussian 09 program<sup>[34]</sup> package at the B3LYP<sup>[35]</sup>/def2-TZVP<sup>[36]</sup> level of theory. The final energy of the molecules was corrected from the zero point vibrational energy. The AOMix program has been used for the construction of the orbital interaction diagram of **3-2**.<sup>[37]</sup> The NBO analysis has been performed with NBO6.<sup>[38]</sup> The topological QTAIM analysis has been performed using DGrid 5.0<sup>[39]</sup> and Figure 35 was created using AIM-UC.<sup>[40]</sup>



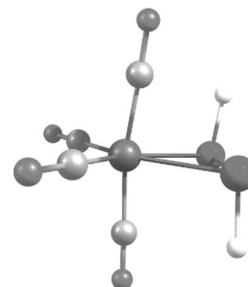
**Figure 35:** Selected Bond Critical points and Ring Critical point in **3-2**.

**Table 2:** . The electron density ( $\rho_{\text{BCP}}$  (e/au<sup>3</sup>)), the Laplacian of the electron density ( $\nabla^2\rho_{\text{BCP}}$  (e/au<sup>5</sup>)), the ellipticity ( $\epsilon$ ) and the total electron energy density ( $H_{\text{BCP}}$ ) of selected critical points in **3-2**.

Critical Point	$\rho_{\text{BCP}}$ (e/au <sup>3</sup> )	$\nabla^2\rho_{\text{BCP}}$ (e/au <sup>5</sup> )	$\epsilon$	H/ $\rho$
S1	0.0565	0.0460	0.24	-0.273
S2	0.0565	0.0460	0.24	-0.273
S3	0.0902	-0.0458	0.28	-0.444
m1	0.0482	0.0718	1.65	-0.183

**Table 3:** Cartesian coordinates of the optimised geometry of  $[\{\text{Fe}(\text{CO})_4\}(\eta^2\text{-As}_2\text{H}_2)]$  (**3-2**) at the B3LYP/def2-TZVP level of theory. E = -6190.41471123a.u.)

Atom	x	y	z
Fe	-0.004920000	0.008725000	0.029351000
As	-1.613099000	0.423280000	1.954368000
As	0.495310000	1.593222000	1.953643000
H	-0.123513000	2.848558000	1.303873000
H	-1.070983000	-0.693613000	2.870706000
O	-1.400871000	2.263700000	-1.288317000
O	2.450177000	0.404368000	-1.551555000
O	-1.573861000	-1.985803000	-1.468508000
O	1.282412000	-2.050309000	1.724343000
C	-0.854180000	1.398935000	-0.757839000



C	1.490468000	0.255323000	-0.928779000
C	-0.963836000	-1.205827000	-0.876384000
C	0.768061000	-1.243870000	1.081539000

**Table 4.** Cartesian coordinates of the optimised geometry of  $[[\text{Fe}(\text{CO})_4](\text{cis-As}_2\text{H}_2)]$  (**3-2**) at the B3LYP/def2-TZVP level of theory. E = -6190.41181716 a.u.)

Atom	x	y	z
Fe	-0.017240000	0.779538000	0.000000000
As	-0.022239000	-1.461885000	1.207336000
As	-0.022239000	-1.461885000	-1.207336000
H	1.489727000	-1.596646000	-1.389738000
H	1.489727000	-1.596646000	1.389738000
O	2.938697000	0.600121000	0.000000000
O	-0.020994000	2.545723000	-2.357068000
O	-0.020994000	2.545723000	2.357068000
O	-2.969141000	0.501422000	0.000000000
C	1.802292000	0.648024000	0.000000000
C	-0.022239000	1.858718000	-1.449508000
C	-0.022239000	1.858718000	1.449508000
C	-1.838482000	0.612176000	0.000000000

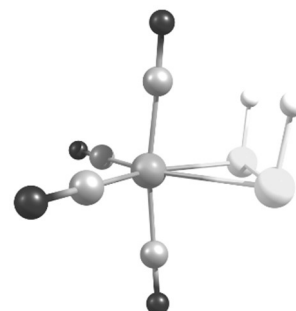
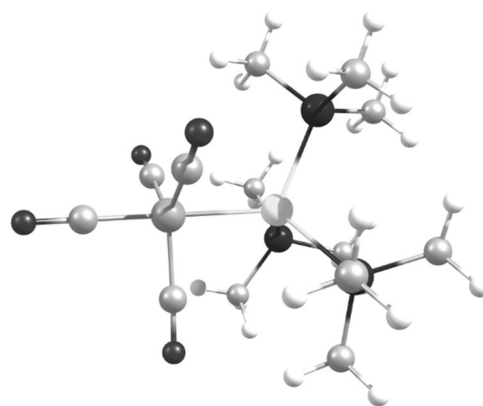


**Table 5.** Cartesian coordinates of the optimised geometry of  $[[\text{Fe}(\text{CO})_4]\text{As}(\text{SiMe}_3)_3]$  (**3-1**) at the B3LYP/def2-TZVP level of theory. E = -5181.35557029 a.u.)

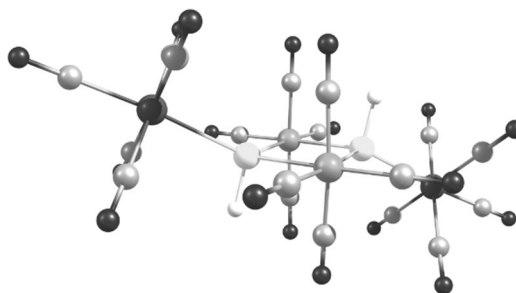
Atom	x	y	z
As	3.744602000	11.191662000	7.593617000
Fe	3.158192000	9.182898000	6.184076000
Si	6.083122000	11.240357000	8.225233000
Si	2.491324000	11.275336000	9.663782000
Si	3.314190000	13.289213000	6.461170000
O	0.486682000	10.316547000	5.660164000
O	3.583134000	7.418472000	8.507831000
O	5.397857000	9.793207000	4.365828000
O	2.478421000	6.854711000	4.555103000
C	6.373035000	12.405798000	9.678191000
H	6.072135000	13.430141000	9.455443000
H	7.442973000	12.419080000	9.907274000
H	5.851405000	12.086573000	10.581372000
C	1.534228000	9.897113000	5.881802000
C	7.115260000	11.822624000	6.764947000
H	6.990323000	11.184339000	5.890454000
H	8.171040000	11.791608000	7.051247000
H	6.886864000	12.848850000	6.473730000
C	3.425071000	8.128408000	7.617009000
C	2.535744000	13.002168000	10.418619000
H	3.551523000	13.337012000	10.632508000
H	1.989238000	12.983411000	11.366499000
H	2.057842000	13.748302000	9.782521000
C	4.246181000	14.705678000	7.283885000
H	4.003928000	15.635787000	6.760808000
H	5.327920000	14.576100000	7.234147000
H	3.966753000	14.834869000	8.330199000
C	1.472170000	13.663792000	6.510121000
H	1.104425000	13.820027000	7.525272000
H	0.877969000	12.874616000	6.049691000
H	1.290626000	14.586792000	5.950948000
C	0.717529000	10.795439000	9.285199000



H	0.247669000	11.468841000	8.567642000
H	0.132443000	10.828081000	10.209121000
H	0.655678000	9.783646000	8.883212000
C	2.744857000	7.766348000	5.192766000
C	4.530247000	9.578432000	5.089428000
C	6.594903000	9.498832000	8.701251000
H	6.022575000	9.109984000	9.544120000
H	7.651045000	9.503058000	8.987072000
H	6.475067000	8.805295000	7.868266000
C	3.873743000	13.112959000	4.678649000
H	3.680872000	14.050862000	4.149238000
H	3.329477000	12.319627000	4.165193000
H	4.938908000	12.894843000	4.594772000
C	3.227451000	10.057868000	10.893321000
H	3.225280000	9.036115000	10.514217000
H	2.622175000	10.076427000	11.804842000
H	4.249406000	10.315051000	11.175396000

**Table 6.** Cartesian coordinates of the optimised geometry of  $[[\text{Fe}(\text{CO})_4]\text{AsH}\{\text{W}(\text{CO})_5\}]_2$  (**3-3**) at the B3LYP/def2-TZVP level of theory. E = -9176.05598809 a.u.)

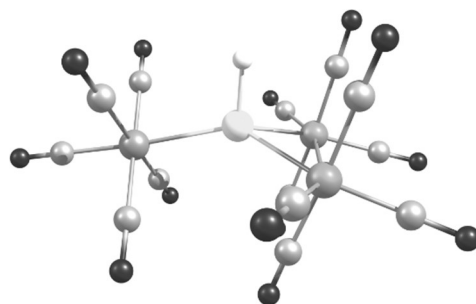
Atom	x	y	z
W	-4.249722000	-0.453932000	-0.012979000
As	-1.595235000	-0.055379000	-0.516246000
Fe	0.203268000	-1.865073000	-0.427779000
O	0.965810000	-0.863198000	-3.109929000
O	-0.630927000	-2.298512000	2.382513000
O	-4.382035000	-2.161480000	-2.732475000
O	-4.224042000	1.311157000	2.669591000
O	-1.686401000	-3.869954000	-1.516635000
O	-7.368211000	-0.858205000	0.325328000
O	-3.761227000	-3.146758000	1.667550000
O	-4.842977000	2.177159000	-1.760487000
O	2.514569000	-3.706572000	-0.220441000
C	-0.313518000	-2.120676000	1.308549000
C	-3.920901000	-2.179048000	1.076489000
C	-0.969120000	-3.097760000	-1.101845000
C	0.675216000	-1.235225000	-2.078927000
C	-4.321777000	-1.559679000	-1.761439000
C	-4.218556000	0.674455000	1.717723000
C	1.635287000	-2.996654000	-0.295865000
C	-4.619847000	1.247564000	-1.132190000
C	-6.236132000	-0.712434000	0.206297000
H	-1.506255000	0.293222000	-1.993544000
W	4.249722000	0.453932000	0.012979000
As	1.595235000	0.055379000	0.516246000
Fe	-0.203268000	1.865073000	0.427779000
O	-0.965810000	0.863198000	3.109929000
O	0.630927000	2.298512000	-2.382513000
O	4.382035000	2.161480000	2.732475000
O	4.224042000	-1.311157000	-2.669591000
O	1.686401000	3.869954000	1.516635000
O	7.368211000	0.858205000	-0.325328000
O	3.761227000	3.146758000	-1.667550000
O	4.842977000	-2.177159000	1.760487000
O	-2.514569000	3.706572000	0.220441000
C	0.313518000	2.120676000	-1.308549000
C	3.920901000	2.179048000	-1.076489000
C	0.969120000	3.097760000	1.101845000
C	-0.675216000	1.235225000	2.078927000



C	4.321777000	1.559679000	1.761439000
C	4.218556000	-0.674455000	-1.717723000
C	-1.635287000	2.996654000	0.295865000
C	4.619847000	-1.247564000	1.132190000
C	6.236132000	0.712434000	-0.206297000
H	1.506255000	-0.293222000	1.993544000

**Table 7.** Cartesian coordinates of the optimised geometry of  $[[\text{Fe}_2(\text{CO})_8]\text{AsH}[\text{Cr}(\text{CO})_5]]$  (**3-4**) at the B3LYP/def2-TZVP level of theory.  $E = -7282.70116203$  a.u.)

Atom	x	y	z
As	-0.338887000	11.083633000	9.161450000
Fe	1.903088000	10.313148000	8.566275000
Fe	-0.334251000	8.641582000	9.186135000
Cr	-1.922045000	12.834729000	8.181674000
H	-0.180386000	11.428633000	10.637633000
O	-1.248452000	8.586772000	6.366015000
O	3.919537000	8.177604000	8.208738000
O	1.014783000	6.027283000	8.868182000
O	-3.796606000	14.991594000	7.206764000
O	1.226776000	10.202934000	5.681988000
O	-0.157034000	14.965834000	9.481121000
O	-3.530296000	12.619152000	10.771471000
O	2.650960000	10.641466000	11.411051000
O	-3.090963000	8.040079000	9.986444000
O	0.348757000	8.735618000	12.063675000
O	-3.713732000	10.706387000	6.921057000
O	-0.302749000	13.097694000	5.605235000
O	3.285625000	12.845400000	8.038969000
C	-0.863189000	8.646981000	7.431807000
C	2.319783000	10.484781000	10.335423000
C	-3.085373000	14.172576000	7.575490000
C	-2.923896000	12.691661000	9.805293000
C	3.132478000	8.987392000	8.343702000
C	-0.904630000	12.981182000	6.570765000
C	-0.809514000	14.161635000	8.997190000
C	0.129003000	8.733892000	10.948592000
C	0.508121000	7.038915000	8.983279000
C	-3.031448000	11.496427000	7.388446000
C	1.430333000	10.226626000	6.798447000
C	-2.025353000	8.284176000	9.673399000
C	2.740159000	11.869214000	8.245592000





## 3.8. Miscellaneous and Outlook

### 3.8.1. $[\text{Fe}(\text{CO})_4(\eta^2\text{-As}_2\text{H}_2)]$ (**3-2**) and $\text{MnCp}(\text{CO})_2\text{thf}$

In order to further investigate the reactivity of **3-2**, it was also reacted with the Lewis acid  $\text{MnCp}(\text{CO})_2\text{thf}$  at  $-80^\circ\text{C}$  in THF. After column chromatographic workup, crystals of  $[\text{Fe}_3(\text{CO})_9\{\mu_3\text{-AsMnCp}(\text{CO})_2\}_2]$  (**3-6**) could be obtained. Compound **3-6** is isostructural to **3-5** and has already been reported by Schauer *et al.*<sup>[25]</sup> Nevertheless, this is a new synthetic route to the compound **3-6**. Additionally, to the violet band of **3-6** an additional green band could be isolated from the column. However, it was not possible to further characterise this compound so far.

#### Synthesis of $[\text{Fe}_3(\text{CO})_9\{\mu_3\text{-AsMnCp}(\text{CO})_2\}_2]$ (**3-6**)

A solution of 325 mg (1.6 mmol)  $\text{MnCp}(\text{CO})_3$  in THF was irradiated with a mercury lamp for 5 hours. The pink solution of  $\text{MnCp}(\text{CO})_2\text{thf}$  was added to solid  $[\{\text{Fe}(\text{CO})_4\}\{\eta^2\text{-As}_2\text{H}_2\}]$  at  $-80^\circ\text{C}$  (obtained from 1g, 2.16 mmol  $[\{\text{Fe}(\text{CO})_4\}\text{As}(\text{SiMe}_3)_3]$ ). The solution was slowly heated to room temperature, the color changed from red to brown after one day. The reaction mixture was separated by column chromatography on silica with a hexane: toluene mixture of 1:1. Only few crystals of **3-6** (<15mg) could be obtained.

### 3.8.2. Investigation of $[\{\text{Fe}(\text{CO})_4\}\text{As}(\text{SiMe}_3)_3]$ (**3-1**) as nanoparticle precursor

Because the main compound of this chapter,  $[\text{Fe}(\text{CO})_4(\eta^2\text{-As}_2\text{H}_2)]$  (**3-2**) is unstable at normal conditions, hard to handle and not accessible in huge amounts, its use as nanoparticle precursor is very limited and could not be investigated by us at this moment. The reaction products of the reaction of **3-2** with Lewis acids yielded compounds **3-4** and **3-5** having an interesting composition of three elements. Due to they are accessible in very little amounts the investigation of their use as potential nanoparticle precursors was not performed. Nevertheless, the precursor of **3-2**,  $[\{\text{Fe}(\text{CO})_4\}\text{As}(\text{SiMe}_3)_3]$  (**3-1**) could have the same potential to act as precursor for nanoparticles containing iron and arsenic. The  $\text{SiMe}_3$  groups can be easily removed by acids like oleic acid and the intermediate might decompose into  $\text{Fe}_2\text{As}$ ,  $\text{FeAs}$  or  $\text{FeAs}_2$ . To investigate the general decomposition path of compound **3-1** we performed a thermogravimetric analysis (Figure 36).

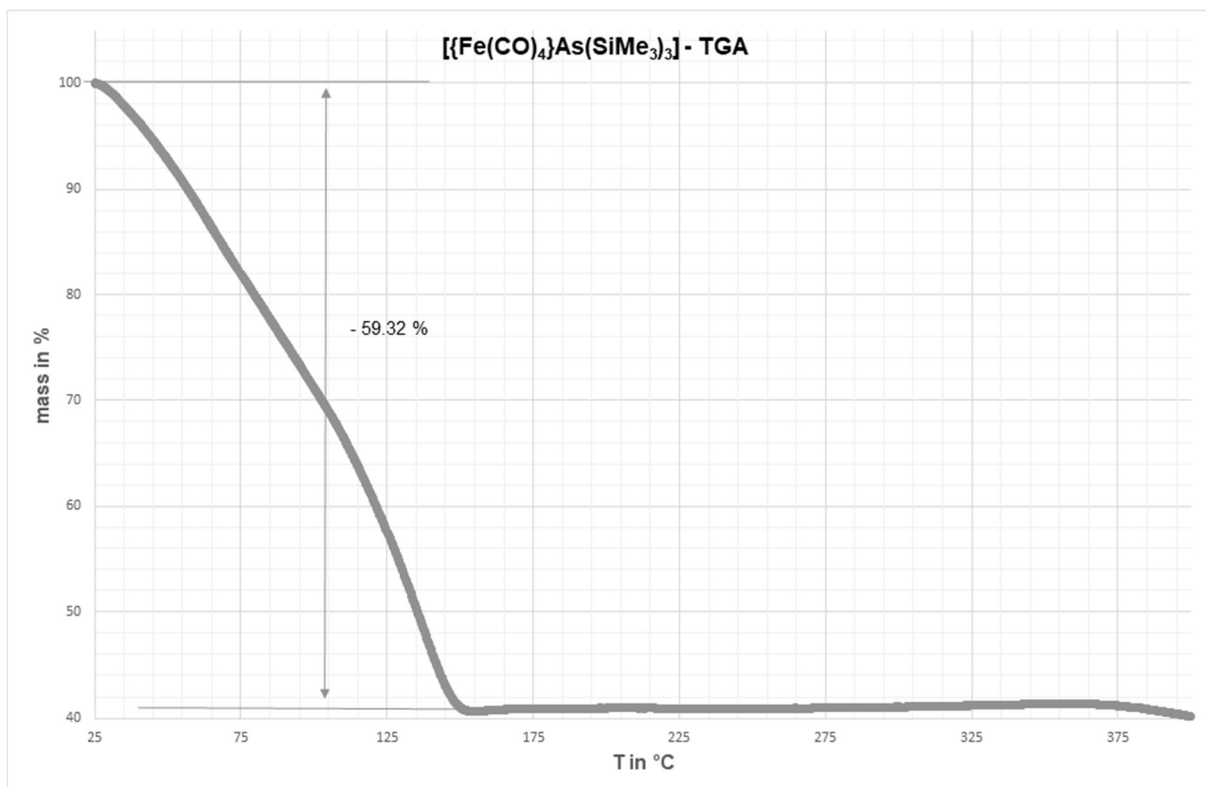


**Figure 36:** Thermogravimetric analysis of compound **3-1**

A one-step decomposition is observed for compound **3-1** starting at room temperature. After losing 59% of its mass, the residue might be a mixture of several compounds, but we were not able to further determine the composition of the residue. The infrared spectroscopy measurement of the residue of this TGA did not show any carbonyl signals, which confirms their elimination.

To investigate the decomposition of  $[\text{Fe}(\text{CO})_4]\text{As}(\text{SiMe}_3)_3$  (**3-1**) (100 mg, 1 eq) in solution, we performed provisional nanoparticle syntheses in mesitylene (5 mL) at 160°C for one hour with the pure compound  $[\text{Fe}(\text{CO})_4]\text{As}(\text{SiMe}_3)_3$  (**3-1a**),  $[\text{Fe}(\text{CO})_4]\text{As}(\text{SiMe}_3)_3$  and hexadecylamine (HDA) (53.1 mg, 1 eq) (**3-1b**) and  $[\text{Fe}(\text{CO})_4]\text{As}(\text{SiMe}_3)_3$  and oleic acid (OA) (62.1 mg, 1 eq) (**3-1c**).

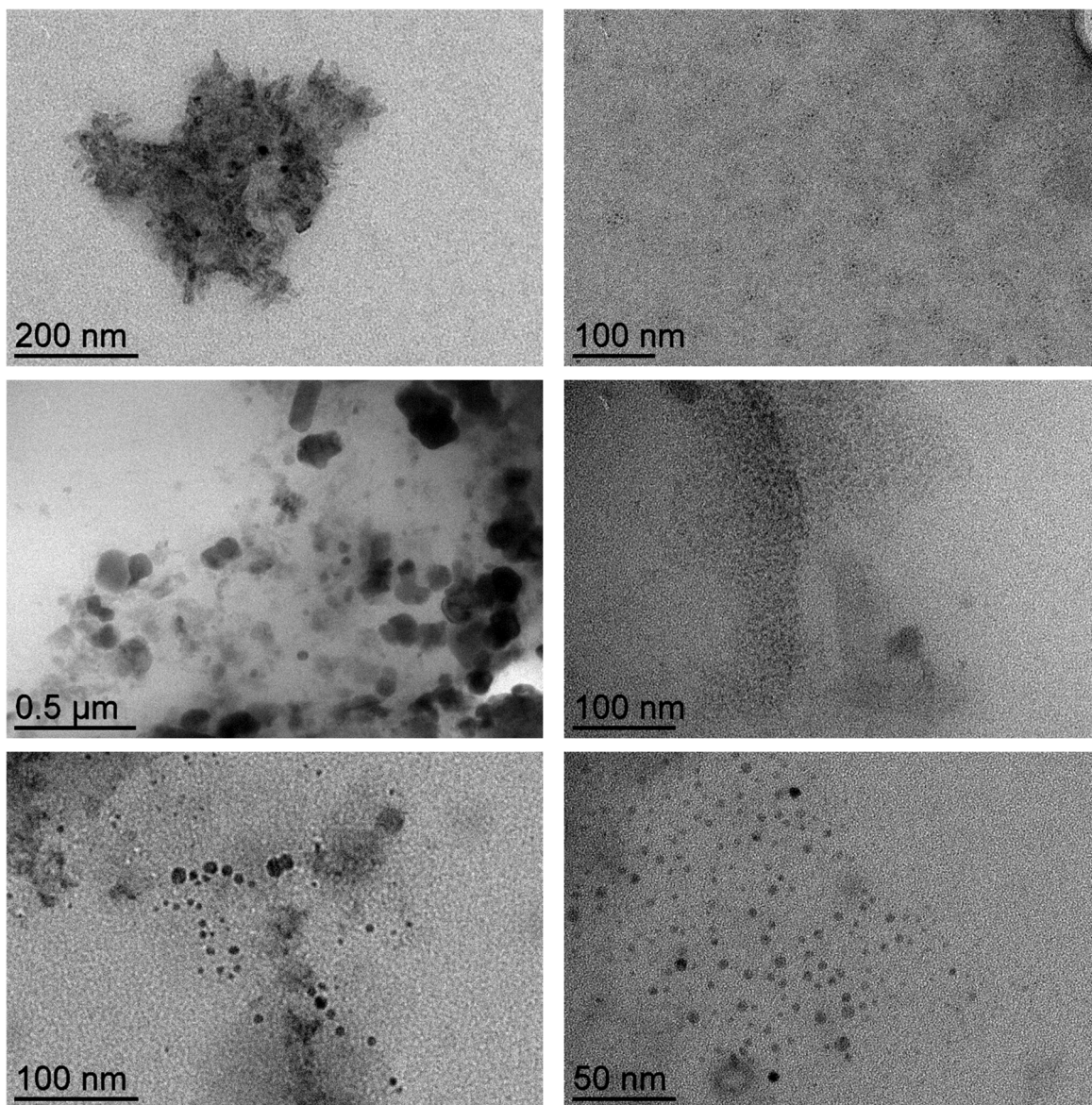


**Figure 37:** TEM images of the particles preserved from the decomposition of **3-1**. Upper Part: Particles of **3-1a**. Middle part: Particles of **3-1b**. Lower part: Particles of **3-1c**.

As shown in Figure 37, decomposition of **3-1** has occurred and nanoscale particles have formed. Unfortunately, these particles are wildly distributed in size or form. The composition of these particles could not be determined with the given method. Further investigations have not been performed yet. The investigation of the right conditions for the formation of homogenous nanoparticles from **3-1** could be the issue of further studies.

### 3.9. References

- [1] W. C. Zeise, *Ann. Phys.* **1831**, 97, 497-541.
- [2] a) N. Koga, C. Daniel, J. Han, X. Y. Fu, K. Morokuma, *J. Am. Chem. Soc.* **1987**, 109, 3455-3456; b) S. Niu, M. B. Hall, *J. Am. Chem. Soc.* **1999**, 121, 3992-3999; c) S. H. Bergens, P. Noheda, J. Whelan, B. Bosnich, *J. Am. Chem. Soc.* **1992**, 114, 2128-2135; d) K. Weissermel, H.-J. Arpe, *Industrial Organic Chemistry*, Vol. 3, VCH, Weinheim, **1997**.
- [3] a) H. D. Murdoch, E. Weiss, *Helv. Chim. Acta* **1963**, 46, 1588-1594; b) Y. Yamada, T. Tominaga, *J. Radioanal. Nucl. Chem.* **1988**, 126, 455-466; c) M. J. S. Dewar, *Bull. Soc. Chim. Fr.* **1951**, 18, C71-C79; d) J. Chatt, L. A. Duncanson, *J. Chem. Soc.* **1953**, 2939-2947.
- [4] a) J. D. Guo, D. J. Liptrot, S. Nagase, P. P. Power, *Chem. Sci.* **2015**, 6, 6235-6244; b) R. C. Fischer, P. P. Power, *Chem. Rev.* **2010**, 110, 3877-3923; c) P. P. Power, *Chem. Rev.* **1999**, 99, 3463-3504; d) L. Weber, *Chem. Rev.* **1992**, 92, 1839; e) K. Rosengren, G. C. Pimentel, *J. Chem. Phys.* **1965**, 43, 507-516; f) D. Sellmann, W. Soglowek, F. Knoch, M. Moll, *Angew. Chem. Int. Ed. Engl.* **1989**, 28, 1271-1272; *Angew. Chem.* **1989**, 101, 1244-1245.
- [5] a) N. Etkin, M. T. Benson, S. Courtenay, M. J. McGlinchey, A. D. Bain, D. W. Stephan, *Organometallics* **1997**, 16, 3504-3510; b) J. C. Green, M. L. H. Green, G. E. Morris, *J. Chem. Soc. Chem. Commun.* **1974**, 212-213; c) M. C. Fermin, J. Ho, D. W. 9 Stephan, *Organometallics* **1995**, 14, 4247-4256.
- [6] H. Davy, *Philos. Trans. R. Soc. London* **1810**, 100, 16-74.
- [7] B. M. Gardner, G. Balázs, M. Scheer, A. J. Wooles, F. Tuna, E. J. L. McInnes, J. McMaster, W. Lewis, A. J. Blake, S. T. Liddle, *Angew. Chem. Int. Ed.* **2015**, 54, 15250-15254; *Angew. Chem.* **2015**, 127, 15465-15469.
- [8] a) S. Bauer, C. Hunger, M. Bodensteiner, W.-S. Ojo, A. Cros- Gagneux, B. Chaudret, C. Nayral, F. Delpech, M. Scheer, *Inorg. Chem.* **2014**, 53, 11438-11446; b) C. Hunger, W.-S. Ojo, S. Bauer, S. Xu, M. Zabel, B. Chaudret, L.-M. Lacroix, M. Scheer, C. Nayral, F. Delpech, *Chem. Commun.* **2013**, 49, 11788-11790.
- [9] a) H. Sch-fer, W. Leske, *Z. Anorg. Allg. Chem.* **1987**, 552, 50-68; b) C. Dreher, M. Zabel, M. Bodensteiner, M. Scheer, *Organometallics* **2010**, 29, 5187-5191.
- [10] H. J. Breunig, *Polyhedron* **1984**, 3, 757-758.
- [11] H. Schumann, O. Stelzer, *J. Organomet. Chem.* **1968**, 13, 25-27.
- [12] A. R. Barron, A. H. Cowley, C. M. Nunn, *Acta Crystallogr. Sect. C* **1988**, 44, 750-751.
- [13] The synthesis was reported: see ref <sup>[10]</sup>. A new synthesis and the crystal structure analysis are reported in the Supporting Information.
- [14] Yield related to arsenic. Due to low stability and the formation of byproducts, this yield can vary between 50 and 86%.
- [15] M. Jacob, E. Weiss, *J. Organomet. Chem.* **1978**, 153, 31-38.
- [16] For selected examples see: a) D. Fenske, K. Merzweiler, *Angew. Chem. Int. Ed. Engl.* **1984**, 23, 635 –637; *Angew. Chem.* **1984**, 96, 600–602; b) J. Grobe, A. Karst, B. Krebs, M. L-ge, E.-U. Wgrthwein, *Z. Anorg. Allg. Chem.* **2006**, 632, 599-608.
- [17] a) P. Pyykkç, M. Atsumi, *Chem. Eur. J.* **2009**, 15, 186–197; b) P. Pyykkç, M. Atsumi, *Chem. Eur. J.* **2009**, 15, 12770-12779.
- [18] Crystallographic details, including details about the location of the hydrogen atoms and their refinement are given in the Supporting Information.

- [19] For details see Supporting Information.
- [20] According to calculations at different levels of theory, the *trans* isomer of the parent diarsene  $\text{HAs=AsH}$  is more stable than the *cis* isomer. See for example: a) W. W. Schçller, C. Begemann, U. Tubbesing, J. Strutwolf, *J. Chem. Soc. Faraday Trans.* **1997**, *93*, 2957; b) S. Nagase, S. Suzuki, T. Kurakake, *J. Chem. Soc. Chem. Commun.* **1990**, 1724-1726; c) C.-H. Lai, M.-D. Su, *J. Comput. Chem.* **2008**, *29*, 2487-2499.
- [21] NBO 6.0.: E. D. Glendening, J. K. Badenhoop, A. E. Reed, J. E. Carpenter, J. A. Bohmann, C. M. Morales, C. R. Landis, F. Weinhold (Theoretical Chemistry Institute, University of Wisconsin, Madison, WI, **2013**); <http://nbo6.chem.wisc.edu/>.
- [22] a) R. F. W. Bader, *Atoms in Molecules: A Quantum Theory*, Oxford, Clarendon Press, 1990; b) R. F. W. Bader, *Acc. Chem. Res.* **1985**, 18-19; c) R. F. W. Bader, *Chem. Rev.* **1991**, *91*, 893- 928.
- [23] R. G. Hayter, *J. Am. Chem. Soc.* **1963**, *85*, 3120-3124.
- [24] E. Keller, H. Vahrenkamp, *Chem. Ber.* **1977**, *110*, 430-440.
- [25] B. E. Collins, Y. Koide, C. K. Schauer, P. S. White, *Inorg. Chem.* **1997**, *36*, 6172-6183.
- [26] G. Huttner, G. Mohr, P. Friedrich, H. G. Schmid, *J. Organomet. Chem.* **1978**, *160*, 59-66.
- [27] a) K. Guldner, B. F. G. Johnson, J. Lewis, *J. Organomet. Chem.* **1988**, *355*, 419-425; b) D. E. Schipper, B. E. Young, K. H. Whitmire, *Organometallics* **2016**, *35*, 471-483.
- [28] G. Becker, H. Freudenblum, O. Mundt, M. Reti, M. Sachs, *Synthetic Methods of Organometallic and Inorganic Chemistry, Vol. 3*, Georg Thieme Verlag, **1996**
- [29] H. J. Breunig, *Polyhedron* **1984**, *3*, 757-758.
- [30] CrysAlisPro Software System, Agilent Technologies UK Ltd, Yarnton, Oxford, **2014**
- [31] O. V. Dolomanov, L. J. Bourhis, R. J. Gildea, J. A. K. Howard, H. Puschmann, *J. Appl. Crystallogr.* **2009**, *42*, 339-341
- [32] G. M. Sheldrick, *Acta Crystallographica Section A* **2015**, *71*, 3-8
- [33] G. Sheldrick, *Acta Crystallographica Section C* **2015**, *71*, 3-8
- [34] Gaussian 09, Revision E.01, M. J. Frisch, G. W. Trucks, H. B. Schlegel, G. E. Scuseria, M. A. Robb, J. R. Cheeseman, G. Scalmani, V. Barone, B. Mennucci, G. A. Petersson, H. Nakatsuji, M. Caricato, X. Li, H. P. Hratchian, A. F. Izmaylov, J. Bloino, G. Zheng, J. L. Sonnenberg, M. Hada, M. Ehara, K. Toyota, R. Fukuda, J. Hasegawa, M. Ishida, T. Nakajima, Y. Honda, O. Kitao, H. Nakai, T. Vreven, J. A. Montgomery, Jr., J. E. Peralta, F. Ogliaro, M. Bearpark, J. J. Heyd, E. Brothers, K. N. Kudin, V. N. Staroverov, T. Keith, R. Kobayashi, J. Normand, K. Raghavachari, A. Rendell, J. C. Burant, S. S. Iyengar, J. Tomasi, M. Cossi, N. Rega, J. M. Millam, M. Klene, J. E. Knox, J. B. Cross, V. Bakken, C. Adamo, J. Jaramillo, R. Gomperts, R. E. Stratmann, O. Yazyev, A. J. Austin, R. Cammi, C. Pomelli, J. W. Ochterski, R. L. Martin, K. Morokuma, V. G. Zakrzewski, G. A. Voth, P. Salvador, J. J. Dannenberg, S. Dapprich, A. D. Daniels, O. Farkas, J. B. Foresman, J. V. Ortiz, J. Cioslowski, and D. J. Fox, Gaussian, Inc., Wallingford CT, **2013**.
- [35] a) A. D. Becke, *J. Chem. Phys.* **1993**, *98*, 5648-5652, b) C. Lee, W. Yang, R. G. Parr, *Phys. Rev. B* **1988**, *37*, 785-789, c) A. D. Becke, *Phys. Rev. A* **1988**, *38*, 3098-3100, d) S. H. Vosko, L. Wilk, M. Nusair, *Can. J. Phys.* **1980**, *58*, 1200-1211, e) J. C. Slater, *Phys. Rev.* **1951**, *81*, 385-390, f) P. A. M. Dirac, *Proc. Royal Soc. A* **1929**, *123*, 714-733.
- [36] a) A. Schäfer, C. Huber, R. Ahlrichs, *J. Chem. Phys.* **1994**, *100*, 5829; b) K. Eichkorn, F. Weigend, O. Treutler, R. Ahlrichs, *Theor. Chem. Acc.* **1997**, *97*, 119.
- [37] a) S. I. Gorelsky, AOMix: Program for Molecular Orbital Analysis; version 6.90, **2017**, <http://www.sg-chem.net/>; b) S. I. Gorelsky, A. B. P. Lever, *J. Organomet. Chem.* **2001**, *635*, 187-196.

- [38] NBO 6.0. E. D. Glendening, J. K. Badenhoop, A. E. Reed, J. E. Carpenter, J. A. Bohmann, C. M. Morales, C. R. Landis, F. Weinhold (Theoretical Chemistry Institute, University of Wisconsin, Madison, WI, **2013**); <http://nbo6.chem.wisc.edu/>.
- [39] M. Kohout, DGrid, version 5.0, Dresden, **2017**.
- [40] D. M. Vega, AIM-UC Program for Electronic Charge Density Analysis, version v1.3, Laboratorio de Quimica Computacional Facyt, Universidad de Carabobo, Venezuela, **2013**

## 4. Examination of Indium Triphospholyls as Precursors for Nanoparticle Syntheses

### 4.1. Author contribution

Reinhard Rund: Synthesis and characterisation of **4-2**, **4-3**, **4-4**, **4-5**

Susanne Bauer: Synthesis and TGA of **4-1**, preparation of **4-6a**, **4-6b**, **4-6c** and evaluation of the corresponding analysis.

Andreas Stauber: Preliminary tests on the synthesis of **4-5**

Fabien Delpech, Wilfried-Solo Ojo: Performance of the TEM, HRTEM, EDX and XRD analyses of **4-6a**, **4-6b**, **4-6c**

Bruno Chaudret: Supervision of the research

Manfred Scheer: Supervision of the research and revision of the manuscript

### 4.2. Abstract

The synthesis and characterisation of the new compounds  $[K][P_3C_2R_2]$  ( $R = Ad$  (**4-2**),  $^sBu$  (**4-3**)) and  $[In][P_3C_2R_2]$  ( $R = Ad$  (**4-4**),  $Mes$  (**4-5**)) are described and the use of  $In(1,2,4-P_3C_2Mes_2)$  (**4-5**) as a promising precursor for InP nanoparticles (NP) was investigated by TGA, X-ray and mass spectroscopy. Further, we report the synthesis of nanoparticles consisting of indium and phosphorus via a single-source precursor approach using  $In(1,2,4-P_3C_2^tBu_2)$  (**4-1**) as precursor. The characterisation of the nanoparticles with TEM, HRTEM, EDX and XRD show that these particles consist only of a shell of InP around an In nucleus. The usage of a hot injection method changes the composition of the decomposition product, but no monodisperse nanoparticles are formed.

### 4.3. Introduction

Indium phosphide InP was first described in 1941 by Landelli after the cothermolysis of the elements.<sup>[1]</sup> Further, it was obtained in the reaction of trimethylindium with phosphine.<sup>[2]</sup> Additionally, it was synthesised by metalorganic vapor phase epitaxy (MOVPE).<sup>[3]</sup> By using MOVPE, it is also possible to obtain heterostructures of GaInAs/InP.<sup>[4]</sup> InP is a semiconductor with a band gap of about 1.35 eV,<sup>[5]</sup> which can be used in light-emitting diodes (LEDs). In 1983, Kinomura reported the formation of  $InP_3$  by a high pressure (3 GPa) and high temperature (1200 °C) synthesis. Although,  $InP_3$  was interpreted as a semiconductor, metallic behaviour was observed.<sup>[6]</sup>

Nanoparticles (NPs), often referred to as quantum dots, are small particles with a diameter of 1-100 nm. Their small size results in properties differing from those of the corresponding bulk material. Since this deviation makes new applications possible, investigating NPs has become an important research topic. InP is one of the best examined nanoscale materials.<sup>[7]</sup> There are several ways to produce InP NP,<sup>[8][9][10][11][12]</sup> usually stabilised by a shell of indium oxides.<sup>[13]</sup> The photoluminescence of such particles, a major feature for their applications, has a low quantum yield of only few percent.<sup>[14]</sup> The quantum yield can be increased through etching<sup>[15]</sup> or coating with a ZnS layer.<sup>[16][17]</sup> Thus, it was even possible to create InP/ZnS core-shell NPs in a facile one-pot synthesis emitting the full spectra of the visible light, thus representing white LEDs.<sup>[18]</sup> InP/ZnS NPs were used for tumour targeting, too.<sup>[19]</sup> The composition of the core, the shell and the interface of InP/ZnS NPs were determined by Delpech *et al.*<sup>[20]</sup>

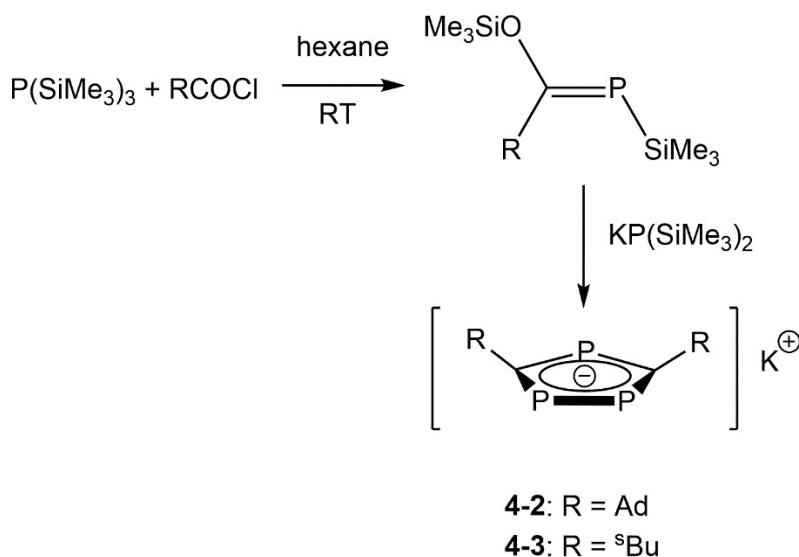
Recent calculations indicate that monolayered InP<sub>3</sub> shows exceptional electronic properties, such as a small indirect band gap (1.14 eV) or high electron mobility (1919 cm<sup>2</sup> V<sup>-1</sup> s<sup>-1</sup>) and it should be a promising compound for nanoscale electronics or photovoltaics.<sup>[21]</sup> The contact properties of these monolayered InP<sub>3</sub> was recently investigated.<sup>[22]</sup>

In all of these syntheses, a multisource precursor approach was applied, which includes the use of self-igniting and moisture-sensitive compounds such as P(SiMe<sub>3</sub>)<sub>3</sub> or its derivatives. On the other hand, single-source precursors are mostly easier to handle. The molar ratio of the elements in the product and also the bonds between the elements are preformed in the precursor. Only the right reaction condition has to be found to form eligible nanoparticles and the crystal growth needs to be controlled better sometimes, too.<sup>[23]</sup> Although a broad spectrum of organometallic precursors does exist<sup>[24]</sup> forming nanoparticles even in xerogel matrixes,<sup>[25]</sup> to date, only one precursor for indium phosphide has been reported. Nixon *et al.* proposed that [In][1,2,4-P<sub>3</sub>C<sub>2</sub><sup>t</sup>Bu<sub>2</sub>] (**4-1**) is a suitable precursor for crystalline indium phosphide.<sup>[26]</sup> However, no reactions or analytic results have yet been reported. Moreover, a broad variety of transition metal compounds containing triphospholyls are known,<sup>[27]</sup> but it remains to be seen if they are suitable precursors for the NP synthesis. Herein, we report the synthesis and characterisation of the novel triphospholyl In(I) compounds [In][1,2,4-P<sub>3</sub>C<sub>2</sub>R<sub>2</sub>] (R = Ad, Mes). Additionally, we present the results of using [In][1,2,4-P<sub>3</sub>C<sub>2</sub><sup>t</sup>Bu<sub>2</sub>] **4-1** as a single-source precursor, obtaining nanoparticles of In/InP. This is the first reported single-source approach to this type of compounds.

#### 4.4. Results and Discussion

Despite of changing the reaction parameters such as the reaction temperature or the stoichiometry of the stabilisers, the way to influence the composition and the shape of the obtained NPs still is the variation of the substituents at the ligand of the single-source precursor. So far, the 1,2,4-triphospholyl anions [1,2,4-P<sub>3</sub>C<sub>2</sub>R<sub>2</sub>]<sup>-</sup> with R = tert-butyl (<sup>t</sup>Bu),<sup>[28]</sup> isopropyl (<sup>i</sup>Pr),<sup>[29]</sup> mesityl (Mes),<sup>[30]</sup> trimethylsilyl<sup>[31]</sup> and phenyl (Ph)<sup>[32]</sup> were reported. We present the synthesis of the new 1,2,4-triphospholyl salts with sec-butyl (<sup>s</sup>Bu) and adamantyl (Ad) substituents. Further, it was our goal to synthesise a variety of novel triphospholyl In(I) compounds from these 1,2,4-triphospholyl anions, which should preliminary be tested for their suitability as single-source precursors for the generation of InP nanoparticles.





**Scheme 4:** General synthesis of potassium salts of triphospholyls

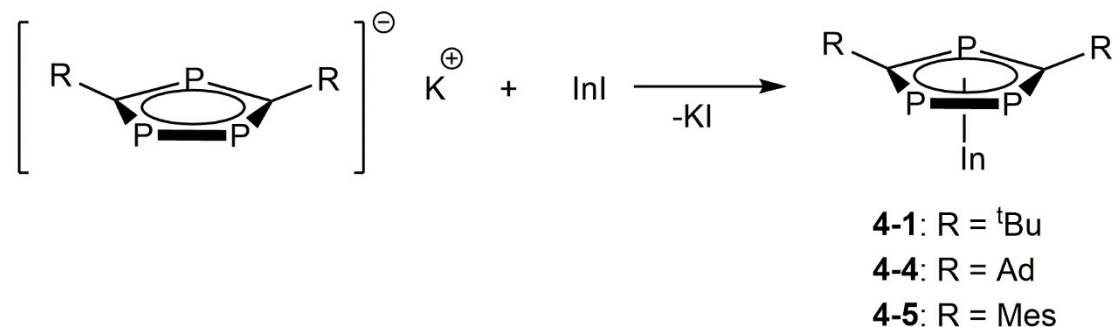
The potassium salts  $[K][1,2,4-P_3C_2R_2]$  (R = Ad (**4-2**), <sup>s</sup>Bu (**4-3**)) are synthesised by the reaction of potassium bis-(trimethylsilyl)phosphanide,  $[K][P(SiMe_3)_2]$ , with the corresponding phosphoalkene  $Me_3SiO(R)C=P(SiMe_3)_2$  (Scheme 4). In the  $^{31}P$  NMR spectrum of the isolated product **4-3**, two doublets of doublets at  $\delta = 249.6$  ppm and at  $\delta = 249.2$  ppm ( $^1J_{PP} = 21$  Hz,  $^2J_{PP} = 47$  Hz) and a doublet at  $\delta = 244.8$  ppm ( $^2J_{PP} = 48$  Hz) were observed for the phosphorus atoms, which can be explained by the chirality centers in the <sup>s</sup>Bu groups and the presence of the meso and the D/L isomers. In comparison, all previously reported derivatives  $[1,2,4-P_3C_2R_2]^-$  reveal a doublet and a triplet with similar coupling constants, except for  $[1,2,4-P_3C_2^iPr_2]^-$ , which shows a doublet of doublets and a pseudo doublet.<sup>[29]</sup> Yield and NMR chemical shifts are given in Table 8. The values of the new compounds are in the expected range.

**Table 8:**  $^{31}P$  NMR data and yields of various 1,2,4-triphospholyl salts.

$[M][1,2,4-P_3C_2R_2]$ ;	$^{31}P$ { $^1H$ } [ppm]		Yield [%]
R = <sup>t</sup> Bu, M = K <sup>[28]</sup>	256	248	47
R = SiMe <sub>3</sub> , M = Li <sup>[31]</sup>	327	316	
R = Mes, M = K <sup>[30]</sup>	266.4	261.7	44
R = <sup>i</sup> Pr, M = K <sup>[29]</sup>	247.6	244.7	48
R = Ph, M = Na <sup>[32]</sup>	274.7	253.9	76
R = Ad, M = K ( <b>4-2</b> )	248,7	241	57
R = <sup>s</sup> Bu, M = K ( <b>4-3</b> )	249.3, 249.4	244.8	29

Cloke, Nixon and coworkers described the metathesis reaction of InI and the potassium triphospholyl salt containing the <sup>t</sup>Bu substituent,<sup>[28]</sup> which we also follow in our approach. We discuss our results of the reactions of  $[K][1,2,4-P_3C_2R_2]$  (R = Mes, <sup>i</sup>Pr, <sup>s</sup>Bu (**4-3**), Ad (**4-2**)) with InI (Scheme 5). Unfortunately,

for the reaction of InI with  $[K][1,2,4-P_3C_2R_2]$  ( $R = {}^iPr$  or  ${}^sBu$  (**4-3**)) at various temperatures, no evaluable results were obtained due to non-reacting or decomposition, if higher reaction temperatures are used.



**Scheme 5:** Salt metathesis of 1,2,4-tri-phospholyls

For the reaction of the adamantyl derivative **4-2** with InI, a reaction temperature of 110 °C is needed to conduct the metathesis. The  ${}^{31}P\{^1H\}$  NMR spectrum of the crude reaction mixture shows a low-field shift to 249.5 ppm for the doublet and to 254.7 for the triplet in comparison to the starting material. In the Direct Insertion Probe – Mass Spectrometry (DIP-MS) (EI, 70 eV) of the reaction mixture, the molecular ion peak of  $[In][1,2,4-P_3C_2Ad_2]$  (**4-4**) is found at 502.0605 m/z. This is an indication, that the desired product **4-4** was formed, which could, however, unfortunately not be proven further. While and after the reaction, a white precipitate occurred. After filtration, a further precipitate is formed over time even at higher or lower temperatures. This white solid is insoluble in the usual polar or nonpolar solvents and the results of the elemental analysis do not match compound **4-4**. Therefore, we could not clearly confirm if this solid is a decomposition or an agglomeration product. A possible similar agglomerate for  $In(C_5H_5)$  was already described.<sup>[33]</sup>

Moreover, we targeted to synthesise  $[In][1,2,4-P_3C_2Mes_2]$  (**4-5**) by the reaction of  $[K][1,2,4-P_3C_2Mes_2]$  with InI. During the synthesis of  $[K][1,2,4-P_3C_2Mes_2]$  we realised that also  $[K][1,3-P_2C_3Mes_3]$  is formed as a byproduct in a ratio of about 20%. In the  ${}^{31}P\{^1H\}$  NMR spectra of the reaction mixture, a sharp singlet at 175.1 ppm was observed, which could be assigned to  $[K][1,3-P_2C_3Mes_3]$ . In comparison, the signal for  $[K][1,3-P_2C_3{}^iPr_3]$  appeared at 159.6 ppm.<sup>[29]</sup> Since it was not possible to separate both compounds, the mixture of the diphospholyl- and the triphospholyl salts was further reacted with InI. The suspension of both educts was refluxed in toluene for 5.5 hours and, after workup, a yellow powder remained. Yellow plate-like crystals of  $[In][1,2,4-P_3C_2Mes_2]$  (**4-5**) suitable for X-ray structure analysis and unidentifiable<sup>[34]</sup> yellow crystals could be isolated from a saturated dichloromethane solution at -30°C in a crystalline yield of 40%. Despite multiple attempts to separate the crystal mixture, analytically pure **4-5** could unfortunately not be obtained.

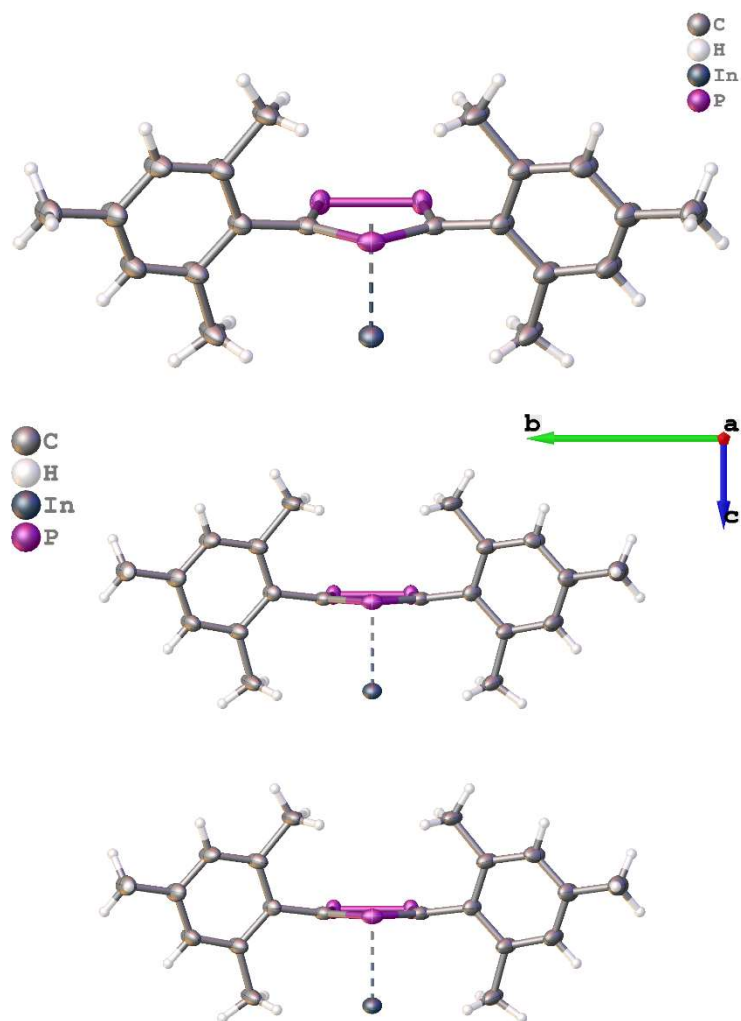


**Figure 38:** Upper part: Molecular structure of **4-5**. Ellipsoids are drawn at 50 % probability level. Selected bond lengths [Å]: P2-P21 2.1208 (13), P2-C1 1.755(2), P1-C1 1.748(3), In1-P1 3.0340(8), In1-P2 3.0268(6). Lower part: Crystal packing of **4-5**, view along the a-axis. Ellipsoids are drawn at the 50 % probability level.

The  $^{31}\text{P}\{^1\text{H}\}$  NMR spectrum of the crystal mixture in  $\text{thf-d}_8$  shows the expected  $\text{AB}_2$  pattern for **4-5** associated with an  $\eta^5$ -ligated, 1,2,4-substituted  $\text{P}_3\text{C}_2$  ring (triplet at 276.8 ppm and a doublet at 274.8 ppm,  $J_{\text{P-P}'} = 43.2$  Hz). The  $^1\text{H}$  NMR spectrum shows three singlets at 2.22 ppm, 2.25 ppm and 6.87 ppm for the protons of the Mes group. Additionally, the  $^{31}\text{P}\{^1\text{H}\}$  NMR spectrum displays a singlet at 184.7 ppm, indicating the formation of  $[\text{In}][1,3\text{-P}_2\text{C}_3\text{Mes}_3]$ , as expected owing to the impurities of  $[\text{K}][1,3\text{-P}_2\text{C}_3\text{Mes}_3]$  in the starting material of  $[\text{K}][1,2,4\text{-P}_3\text{C}_2\text{Mes}_2]$ . This compound could not be separated from **4-5**, due to similar solubility. The ratio of this side product ranges from 10 to 18%. The elemental analysis of the crystal mixture proves the presence of the diphospholyle in the same ratio as detected by  $^{31}\text{P}$  NMR.

The molecular structure of **4-5** is depicted in Figure 38. The indium atom is  $\eta^5$ -coordinated by the planar  $\text{P}_3\text{C}_2$  ring of the 1,2,4-triphospholyl ligand. In contrast to the related triphospholyl compound **4-1**, where the half-sandwich units are linked into chains by weak interactions between the indium centres and adjacent  $\text{P}_3\text{C}_2$  rings,<sup>[28]</sup> **4-5** represents a monomeric compound. In **4-5** the distance of the indium atom to the next ring is with 6.239 Å much longer than in **4-1** (3.526 Å).<sup>[28]</sup> This difference is attributed to the

larger steric bulk of the Mes units, which are tilted by 78.9° to the ring and could block significantly the intermolecular interactions (Figure 38). The bond lengths within the P<sub>3</sub>C<sub>2</sub> ring are with P1-C1 1.748 (3) Å, C1-P2 1.755 (2) Å, P2-P21 2.1208 (13) Å similar to [Cp\*Fe][1,2,4-P<sub>3</sub>C<sub>2</sub>Mes<sub>2</sub>] with P1-C1 1.761 (3) Å, C1-P2 1.777 (3) Å, P2-P21 2.118 (1) Å.<sup>[30]</sup> The indium centroid distance in **4-5** amounts to 2.563 Å, which is comparable to the value of 2.598 Å found for **4-1**.<sup>[28]</sup>

The Direct Exposure Probe–Mass Spectrometry (DEP-MS) (EI, 70 eV) clearly shows the molecular peak of **5** at 470.01572 m/z. Additionally, peaks for In<sup>+</sup> (114.90653 m/z) and InP<sub>2</sub>CMes<sup>+</sup> (307.94952 m/z) are found. This indicates that **4-5** decomposes under the conditions of the mass spectrometry into the phosphalkyne P≡CMes and InP<sub>2</sub>CMes. Further loss of P≡CMes could lead to the anticipated compound InP, which is quite promising for further nanoparticle synthesis.

Further, we intended to investigate the ability of **4-5** and **4-1** as single-source precursors for the generation of NPs. Therefore, we performed thermogravimetric analyses of **4-5** (Figure 39) and **4-1** (Figure 40). For **4-5**, starting at 290°C, a one-step decomposition is observed. It seems that all organic fragments are eliminated, leaving theoretically InP<sub>3</sub> with a weight loss of 55%. The remaining solid could be InP<sub>3</sub>, InP and P or In and P. It is of great interest to find out if this constitutes a pathway to generating InP<sub>3</sub> nanoparticles.

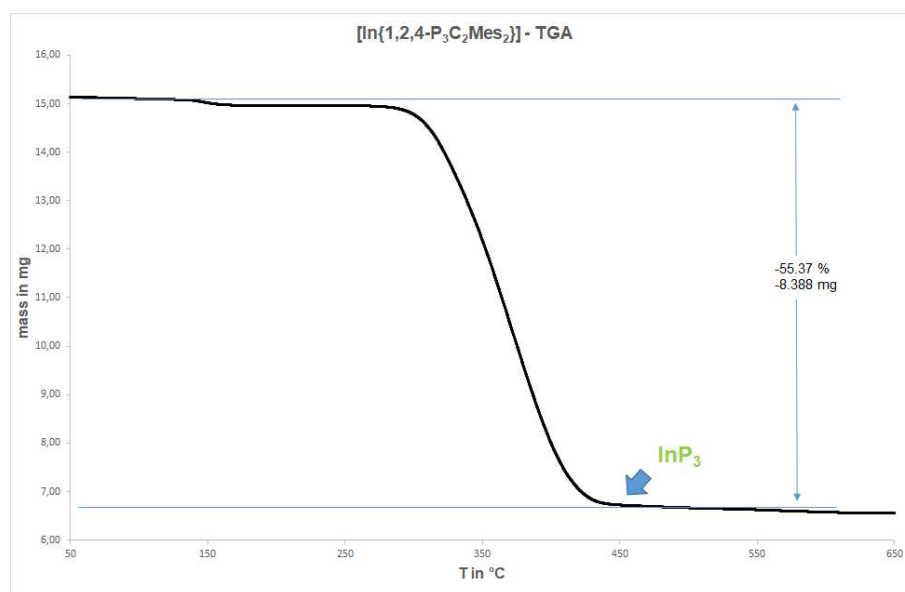


**Figure 39:** TGA of **4-5**.

For **4-1**, several steps of decomposition occur, starting at a temperature of 225 °C. The corresponding weight loss of 46% indicates a segregation of a <sup>t</sup>BuCP unit and an isobutene moiety, followed by an HCP elimination at higher temperatures. At 325 °C, the decomposition results formally in InP. However, a further P loss is observed at higher temperatures.

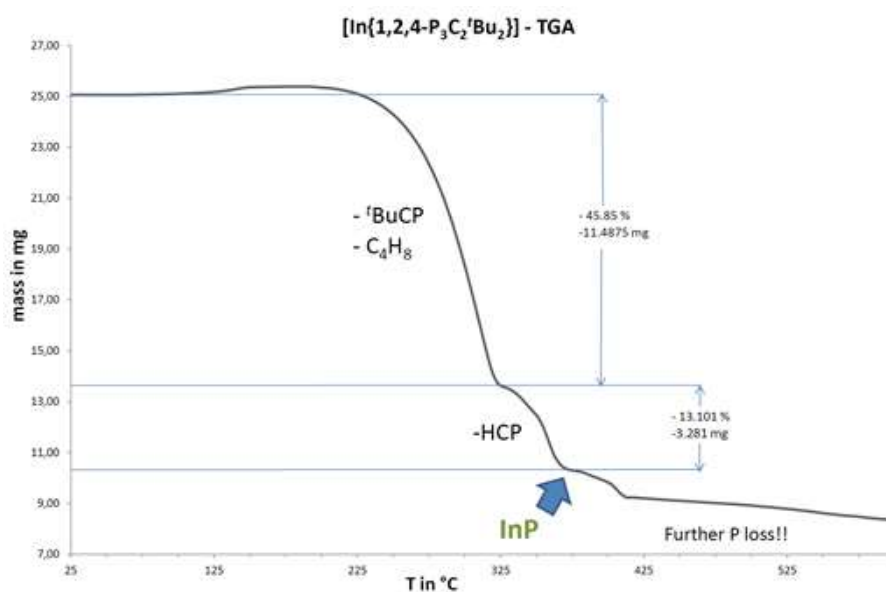


Figure 40: TGA of 4-1.

Both TGAs looked promising, but compound 4-5 could only be obtained with impurities. Therefore, we solely focused the investigation of the decomposition behaviour of the single-source precursor 4-1 in solution.

Compound 4-1 (1eq) was dissolved in mesitylene and transferred into a Fischer-Porter-Schlenk with hexadecylamine (HDA) (1eq) and oleic acid (OIA) (1eq). This solution was stirred at 290 °C for one hour. The yellow solution turns black and a fine, black powder evolves. The evolving particles (4-6a) are further investigated via Transmission Electron Microscopy (TEM), Energy-dispersive X-ray spectroscopy (EDX) and X-ray diffraction (XRD). Figure 41 shows the TEM images of the particles, which have an average size of 6.5 nm and are evenly distributed in size and form.

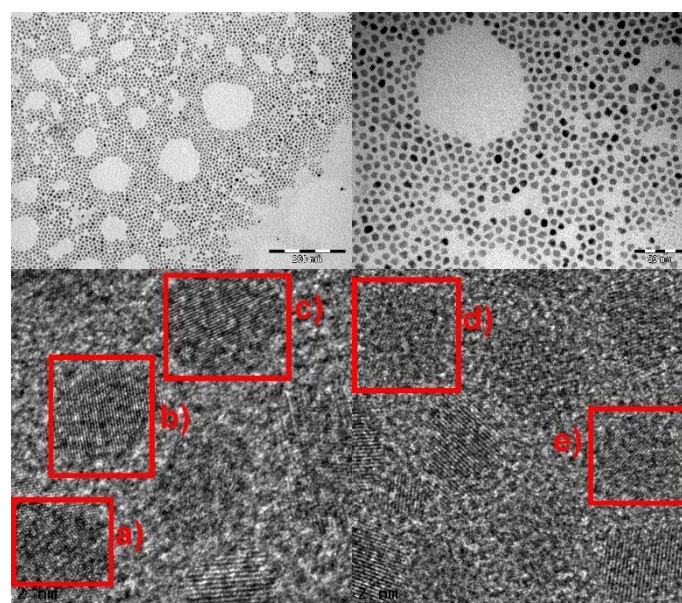
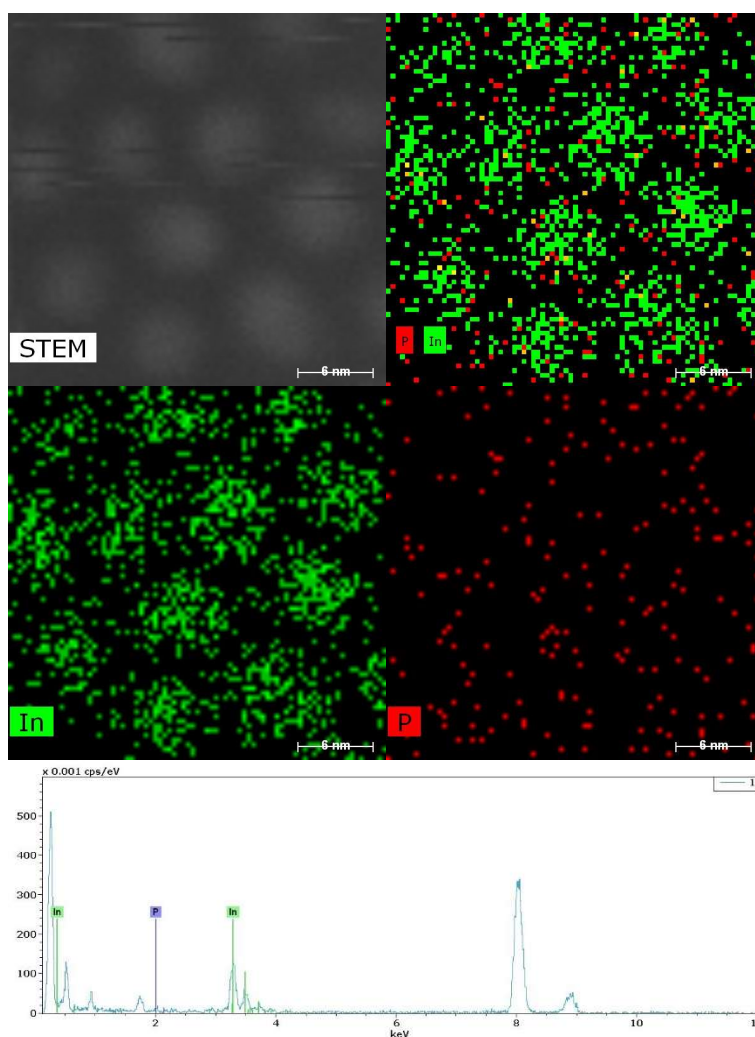


Figure 41: Upper part: TEM images of 4-6a. Lower part: HRTEM images of 4-6a (800k magnification left, 1000k right)

In Figure 41, the HRTEM images of various domains of different nanoparticles are shown. Particles a) and b) are neither In nor InP, but as the analysis does not give clear results, they could be  $\text{InP}_3$  or  $\text{In}_2\text{O}_3$ . Particle c) is most likely InP and d) and e) are beyond doubt InP.



**Figure 42:** Upper part: EDX illustration in HRTEM images of **4-6a**. Lower part: EDX spectra of **4-6a**.

Figure 42 shows the EDX analyses of the HRTEM measurements. Here, the distribution of the elements indium (green) and phosphorus (red) of selected particles is shown. The distribution is homogenous, but indium is clearly the dominating element. In the EDX images, characteristic peaks of the elements are detected (Figure 42). The quantitative analyses show that indium and phosphorus are distributed in a ratio of (7 to 10):1 (Figure 42). The XRD analysis of the purified and isolated residue **4-6a** shows that the decomposition product is a mixture of InP, In and the stabilisers (Figure 43).

The analysis of the decomposition products of **4-1**, stabilised with one equivalent of HDA and OIA at 290°C, shows a mixture of bulk InP, metallic In and some InP particles. The formation of elemental indium could be explained by the high temperature of 290°C used. This is confirmed by the work of Schaller *et al.*, who investigated the thermal stability of InP NPs between 300 and 800 K with photoluminescence spectroscopy and concluded that the stability decreases with higher temperatures.<sup>[35]</sup>



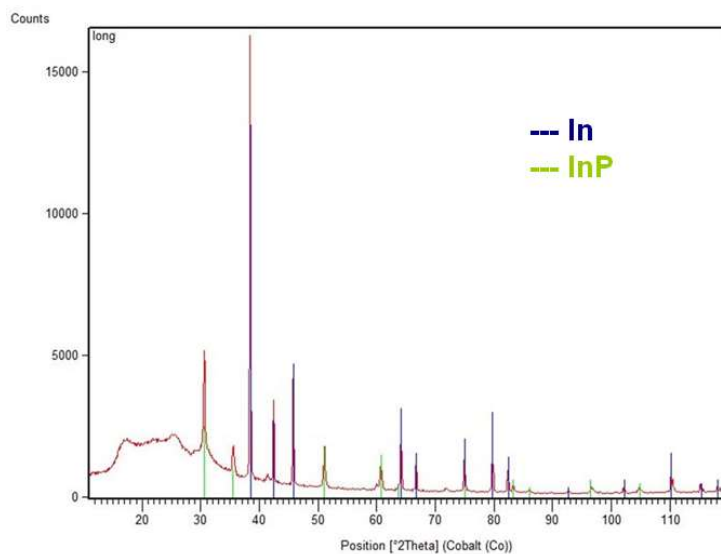


**Figure 43:** XRD spectra of **4-6a**. The XRD spectra of InP and In are included as comparison.

As the ratio between Indium and InP in the nanoparticles is too high, we tried to use a lower decomposition temperature. The precursor **4-1** ( 1 eq) was stirred at 150°C with the stabilisers HDA (1 eq) and OIA (1 eq) in mesitylene yielding **4-6b**. The XRD spectrum of **4-6b** again shows a mixture of indium phosphide and indium with an even lower ratio of the desired indium phosphide (Figure 44).

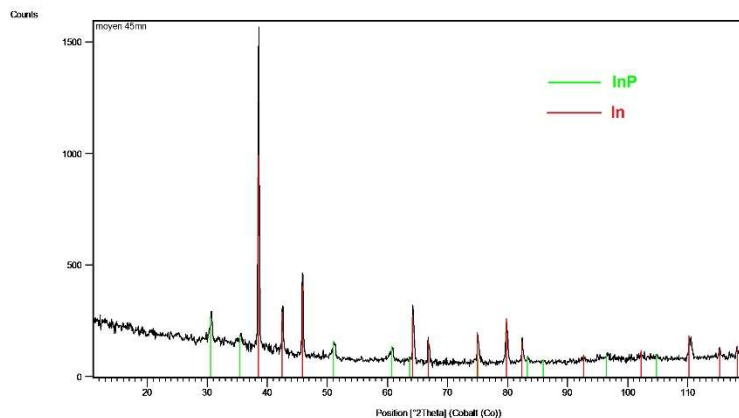


**Figure 44:** XRD spectra of **4-6b**. The XRD spectra of InP and In are included as comparison.

Another approach to obtain purer InP particles was the hot injection synthesis. Here, the stabilisers HDA (1eq) and OIA (1eq) were dissolved in mesitylene and heated to 185°C. A solution of the precursor **4-1** (1eq) dissolved in mesitylene was subsequently added and a sudden colour change to black was observed. The XRD spectra of the black precipitate **4-6c** is depicted in Figure 45.

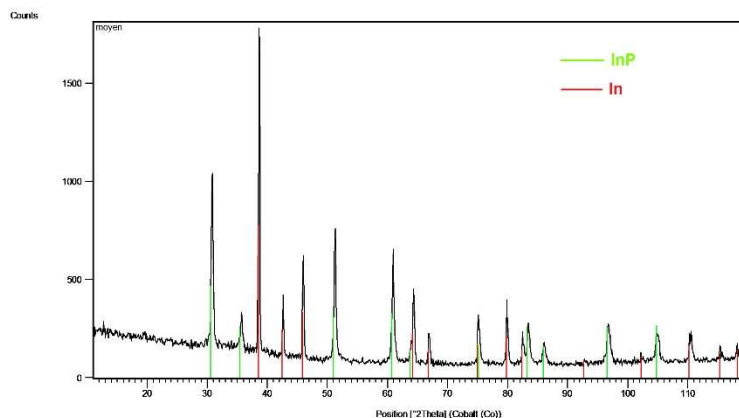


**Figure 45:** XRD spectra of **4-6c**. The XRD spectra of InP and In are included as comparison.

Despite the higher temperature of the hot injection method, the amount of evolving InP is higher compared to the other procedures. TEM images of this residue are shown in Figure 46. The resulting product does not represent, as in the other cases, monodisperse particles, but crystals with a rather long, needle-like corpus. As described earlier, since the reaction conditions can have a big impact on the product, their variation will be in the focus of further investigations.

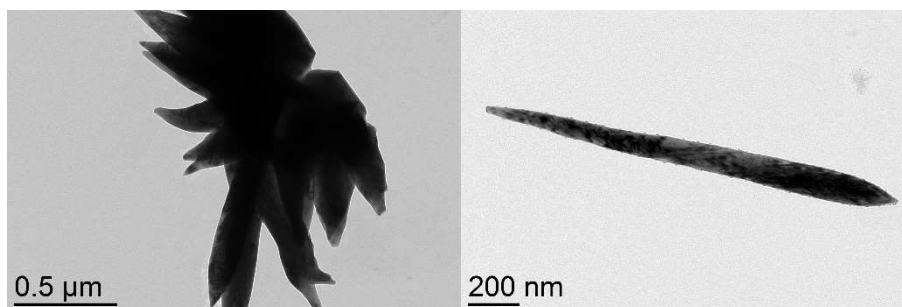


**Figure 46:** TEM images of **4-6c**.

## 4.5. Conclusion

In summary, we presented the synthesis and characterisation of new triphospholyl salts  $[K][1,2,4-P_3C_2R_2]$  ( $R = Ad, ^sBu$ ). By salt metathesis of these compounds and of  $[K][1,2,4-P_3C_2Mes_2]$  with InI, only for  $[K][1,2,4-P_3C_2R_2]$  ( $R = Ad, Mes$ ), the new compounds  $[In][1,2,4-P_3C_2R_2]$  ( $R = Ad, Mes$ ) could be obtained. First investigations indicate the good usability of  $[In][1,2,4-P_3C_2Mes_2]$  for nanoparticle synthesis. Further, we were able to obtain nanoparticles from  $[In][1,2,4-P_3C_2^tBu_2]$  (**4-1**). The decomposition of **4-1** at  $290^\circ$  leads to homogeneous particles of, predominantly, indium and, to a lesser extent, of indium phosphide. By using a hot injection method, a higher amount of InP is found in the product, but this method does not lead to monodisperse particles.



## 4.6. Supporting Information

### 4.6.1. Synthesis and Characterisation

#### General remarks

All manipulations were carried out using Schlenk techniques under an atmosphere of dry nitrogen. Dichloromethane, diethylether, pentane and toluene were dried using an MB SPS-800 solvent purifier and stored under nitrogen. Mesitylene was dried over sodium and freshly distilled prior to use. Hexadecylamine, oleic acid and indium-(I)-iodide were obtained from commercial suppliers.  $\text{KP}(\text{SiMe}_3)_2$ <sup>[36]</sup> and  $[\text{In}][1,2,4\text{-P}_3\text{C}_2^t\text{Bu}_2]$ <sup>[37]</sup> were synthesised according literature precedures.  $\text{Me}_3\text{SiO}(\text{Ad})\text{C}=\text{P}(\text{SiMe}_3)$  and  $\text{Me}_3\text{SiO}(^s\text{Bu})\text{C}=\text{P}(\text{SiMe}_3)$  were synthesised following the synthesis of  $\text{Me}_3\text{SiO}(^t\text{Bu})\text{C}=\text{P}(\text{SiMe}_3)$ .<sup>[38]</sup> The mass spectra were recorded with a Jeol AccuTOF GCX instrument.

#### Synthesis of $[\text{K}][1,2,4\text{-P}_3\text{C}_2\text{Ad}_2]$ (4-2)

0.843 g (3.89 mmol) of  $\text{KP}(\text{SiMe}_3)_2$  is dissolved in a mixture of toluene/ diethylether (ratio 2:1). 2.65 g (7.79 mmol) of  $\text{Me}_3\text{SiO}(\text{Ad})\text{C}=\text{P}(\text{SiMe}_3)$  is dissolved in toluene and cooled to  $-30^\circ\text{C}$ . The solution of  $\text{KP}(\text{SiMe}_3)_2$  is slowly added. This solution is refluxed for 20h at  $90^\circ\text{C}$  bath temperature. The colour of the orange solution changes to red and a red precipitate is formed. This precipitate is filtered, washed with toluene and n-pentane and dried in vacuo. Compound **4-2** was isolated as an orange powder.

Yield: 943 mg, (2.21 mmol; 56.8 %)

$^1\text{H NMR}$  (thf-d8, 300 MHz, 298 K):  $\delta$  [ppm] = 1.78 (6H, s,  $\delta\text{-CH}_2$ ), 2.03 (3H, s,  $\gamma\text{-CH}$ ), 2.29 (6H, s,  $\beta\text{-CH}_2$ )

$^{31}\text{P}\{^1\text{H}\}$  NMR (thf-d8, 121.5 MHz, 298 K):  $\delta$  [ppm] = 241.9 (2P, d,  $^2\text{J}_{\text{P-P}} = 48.66$  Hz), 248.6 (1P, t,  $^2\text{J}_{\text{P-P}} = 48.66$  Hz)

#### Synthesis of $[\text{K}][1,2,4\text{-P}_3\text{C}_2^s\text{Bu}_2]$ (4-3)

2.24 g (3.89 mmol) of  $\text{KP}(\text{SiMe}_3)_2$  is dissolved in a mixture of toluene/ diethylether (ratio 2:1). 5.40 g (20.6 mmol) of  $\text{Me}_3\text{SiO}(^s\text{Bu})\text{C}=\text{P}(\text{SiMe}_3)$  is dissolved in toluene. The phophaalkene solution is slowly added to the phosphide. This reaction mixture is refluxed for 16h at  $82^\circ\text{C}$  bath temperature. The colour of the orange solution changes to red and a yellow precipitate is formed. This precipitate is filtered, washed with toluene and n-pentane and dried in vacuo. Compound **4-3** was isolated as a yellow powder.

Yield: 817 mg, (3 mmol; 29 %)

$^1\text{H NMR}$  (thf-d8, 300 MHz, 298 K):  $\delta$  [ppm] = 0.92 (3H, d,  $^3\text{J}_{\text{H-H}} = 7.37$  Hz,  $\text{CH}_2\text{-CH}_3$ ), 1.44 (3H, d,  $^3\text{J}_{\text{H-H}} = 6.81$  Hz,  $\text{-CH-CH}_3$ ), 1.84 (2H, m,  $^3\text{J}_{\text{H-H}} = 6.11$  Hz,  $\text{-CH}_2\text{-}$ ), 3.51 (1H, m,  $^3\text{J}_{\text{H-H}} = 6.31$  Hz,  $\text{-CH-}$ )

$^{31}\text{P}\{^1\text{H}\}$  NMR (thf-d8, 121.5 MHz, 298 K):  $\delta$  [ppm] = 244.8 (2P, d,  $^2\text{J}_{\text{P-P}} = 48$  Hz), 249.15 (0.5 P, dd,  $^1\text{J}_{\text{P-P}} = 21$  Hz,  $^2\text{J}_{\text{P-P}} = 47$  Hz), 249.76 (0.5 P, dd,  $^1\text{J}_{\text{P-P}} = 21$  Hz,  $^2\text{J}_{\text{P-P}} = 47$  Hz)

#### Synthesis of [K][1,2,4-P<sub>3</sub>C<sub>2</sub>Ad<sub>2</sub>] and InI to form [In][1,2,4-P<sub>3</sub>C<sub>2</sub>Ad<sub>2</sub>] (4-4)

60 mg (0.24 mmol) of InI and 50 mg (0.12 mmol) of [K][1,2,4-P<sub>3</sub>C<sub>2</sub>Ad<sub>2</sub>] are suspended in toluene (30 mL) and heated to reflux for 5.25 h. The solution was filtrated through a hot frit, and the solvent was removed. The crude product consists of a mixture of various compounds and **4-4**. Unfortunately, we were not able to isolate **4-4** as pure compound.

**<sup>1</sup>H NMR** (thf-d<sub>8</sub>, 400 MHz, 298 K): δ [ppm] = not evaluable

**<sup>31</sup>P{<sup>1</sup>H} NMR of 4-4** (thf-d<sub>8</sub>, 162 MHz, 298 K): δ [ppm] = 246.1 (2P, d, <sup>2</sup>J<sub>P-P</sub> = 50.02 Hz), 253.6 (1P, t, <sup>2</sup>J<sub>P-P</sub> = 49.7 Hz)

**MS of 4** (DIP-EI, 70 eV): m/z (*rel. int.* %): 114.90 (100) [In<sup>+</sup>], 502.06 (40) [M<sup>+</sup>]

#### Synthesis of [In][1,2,4-P<sub>3</sub>C<sub>2</sub>Mes<sub>2</sub>] (4-5)

0.18 g (0.74 mmol) of InI and 0.150 g (0.38 mmol) of a mixture of 85% [K][1,2,4-P<sub>3</sub>C<sub>2</sub>Mes<sub>2</sub>] and 15% [K][1,3-P<sub>2</sub>C<sub>3</sub>Mes<sub>3</sub>] are suspended in toluene (30 mL) and heated to reflux for 5.5 h. The solution was filtrated through a hot frit, and the solvent was removed. The yellowish-orange oily solid was stirred in hot n-hexane (200 mL, about 50 °C), and filtered. The solvent was removed in vacuo giving a yellow powder. Yellow plate-like crystals of compound **4-5** suitable for X-ray analysis were obtained from a saturated dichloromethane solution at -30°C. The 15% (determined by NMR integrations) impurities of [In][1,3-P<sub>2</sub>C<sub>3</sub>Mes<sub>3</sub>] could not be separated.

Yield: 72.3 mg, (0.15 mmol, 40 %)

**<sup>1</sup>H NMR of 4-5** (thf-d<sub>8</sub>, 400 MHz, 298 K): δ [ppm] = 2.22 (12H, s, o-CH<sub>3</sub>), 2.25 (6H, s, m-CH), 6.87 (4H, s, p-CH<sub>3</sub>)

**<sup>31</sup>P{<sup>1</sup>H} NMR of 4-5** (thf-d<sub>8</sub>, 162 MHz, 298 K): δ [ppm] = 274.8 (2P, d, <sup>2</sup>J<sub>P-P</sub> = 43.20 Hz), 276.8 (1P, t, <sup>2</sup>J<sub>P-P</sub> = 43.20 Hz)

**MS of 4-5** (EI, solid): m/z (*rel. int.* %): 469.99 (11.29) [M<sup>+</sup>], 356.13 (2.05) [M<sup>+</sup>-In]

**EA** (InP<sub>3</sub>C<sub>20</sub>H<sub>22</sub>) calcd. (15% InP<sub>2</sub>C<sub>30</sub>H<sub>33</sub>): C, 53.27; H, 4.92. found: C, 53.26; H, 4.77.

#### Synthetic procedure for the Nanoparticles 4-6a

27.68 mg (0.08 mmol) of [In][1,2,4-P<sub>3</sub>C<sub>2</sub>tBu<sub>2</sub>] (**4-1**), 19.32 mg (0.08 mmol, 1 eq) of hexadecylamine (HDA) and 22.6 mg (0.08 mmol, 1 eq) of oleic acid (OIA) were dissolved in 2.5 mL mesitylen in a Fischer-Porter-Schlenk. The solution is warmed up with a metal bath to 290 °C. After 1h at 170°C the colour of the solution changed from yellow to into black. The solution was centrifuged for 30 min at 2000 rpm and decanted. The yield was about 1 mg.

#### Synthetic procedure for the Nanoparticles **4-6b**

27.68 mg (0.08 mmol) of **4-1**, 19.32 mg (0.08 mmol, 1eq) of HDA and 22.6 mg (0.08 mmol, 1eq) of OIA were dissolved in 2.5 mL mesitylen in a Fischer-Porter-Schlenk. The schlenk was given into a metal bath at 150°C and heated to 170°C. After 1h at 170°C the colour of the solution changed from yellow into dark green with black precipitate. The solution was centrifuged for 30 min at 2000 rpm and decanted. The yield was about 1 mg.

#### Synthetic procedure for the Nanoparticles **4-6c**

110.72 mg (0.32 mmol) of **4-1** is dissolved in 3 mL mesitylen. 72.28 mg (0.32 mmol, 1eq) of HDA and 90.4 mg (0.32 mmol, 1eq) of OIA were dissolved in 7.5 mL mesitylen in a round bottom flask with new septum. This flask was heated to 185°C and the solution of **4-1** injected at once. The colour of the solution turns from yellow into greenish, greyish and finally black. This solution was refluxed at 185°C for 2h. The solution was centrifuged for 30 min at 2000 rpm, decanted and washed with toluene. The yield was about 3mg.

#### 4.6.2. Crystallographic Details

##### General remarks

Single crystal structure analyses were performed using Agilent Technologies diffractometer Gemini Ultra, Atlas diffractometer (1). Frames integration and data reduction were performed with the CrysAlisPro<sup>[39]</sup> software package. Using the software Olex2<sup>[40]</sup> (Dolomanov *et al.*, 2009), the structure solution was carried out using the programs ShelXT<sup>[41]</sup> (Sheldrick, 2015). Least squares refinements on  $F_o^2$  were performed using SHELXL-2014<sup>[42]</sup> (Sheldrick, 2015). Further details are given in Table 9.

Single crystals of [In][1,2,4-P<sub>3</sub>C<sub>2</sub>Mes<sub>2</sub>] suitable for X-ray diffractions could be obtained as yellow blocks by cooling a saturated solution to -28°C. Crystallographic data and details of the diffraction experiments are given in Table 9.

**Table 9:** Experimental X-ray crystallographic details for [In][1,2,4-P<sub>3</sub>C<sub>2</sub>Mes<sub>2</sub>]

Compound	[In][1,2,4-P <sub>3</sub> C <sub>2</sub> Mes <sub>2</sub> ]
Formula	C <sub>20</sub> H <sub>22</sub> InP <sub>3</sub>
D <sub>calc.</sub> / g cm <sup>-3</sup>	1.586
Device Type	Xcalibur, Atlas S2, Gemini
μ/mm-1	11.872
Formula	470.10
Colour	clear colourless
Shape	needle
Size/mm <sup>3</sup>	0.08×0.05×0.03
T/K	123(1)
Crystal	monoclinic
Space	C2/m
a/Å	9.84870(10)
b/Å	23.2166(4)
c/Å	8.77950(10)
α/°	90
β/°	101.1830(10)
γ/°	90
V/Å <sup>3</sup>	1969.35(5)
Z	4
Z'	0.5
Absorption	analytical
Wavelength/	1.54184
Radiation	CuK <sub>α</sub>
θ <sub>min</sub> /°	3.808
θ <sub>max</sub> /°	72.920
Measured	4558
Independent	1946
Reflections	1828

R <sub>int</sub>	0.0205
Parameters	115
Restraints	0
Largest	0.418
Deepest	-0.301
GooF	1.047
wR <sub>2</sub> (all)	0.0565
wR <sub>2</sub>	0.0555
R <sub>1</sub> (all data)	0.0258
R <sub>1</sub>	0.0234

### 4.6.3. NMR Spectroscopy

#### General remarks:

The NMR spectra were recorded on Bruker Avance 300 ( $^1\text{H}$ : 300.13 MHz,  $^{13}\text{C}$ : 75.47 MHz,  $^{31}\text{P}$ : 121.50 MHz) and 400 ( $^1\text{H}$ : 400.13 MHz,  $^{13}\text{C}$ : 100.61 MHz,  $^{31}\text{P}$ : 162.04 MHz); chemical shifts are given in ppm and are relative to TMS.

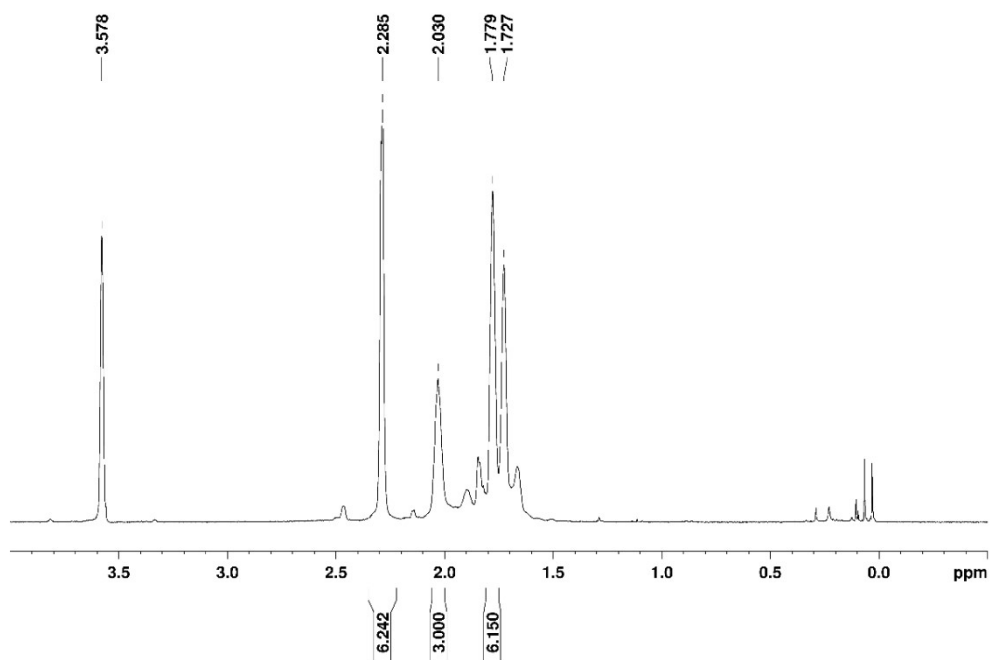


**Figure 47:**  $^1\text{H}$  NMR spectrum of **4-2** in thf- $d_8$ .

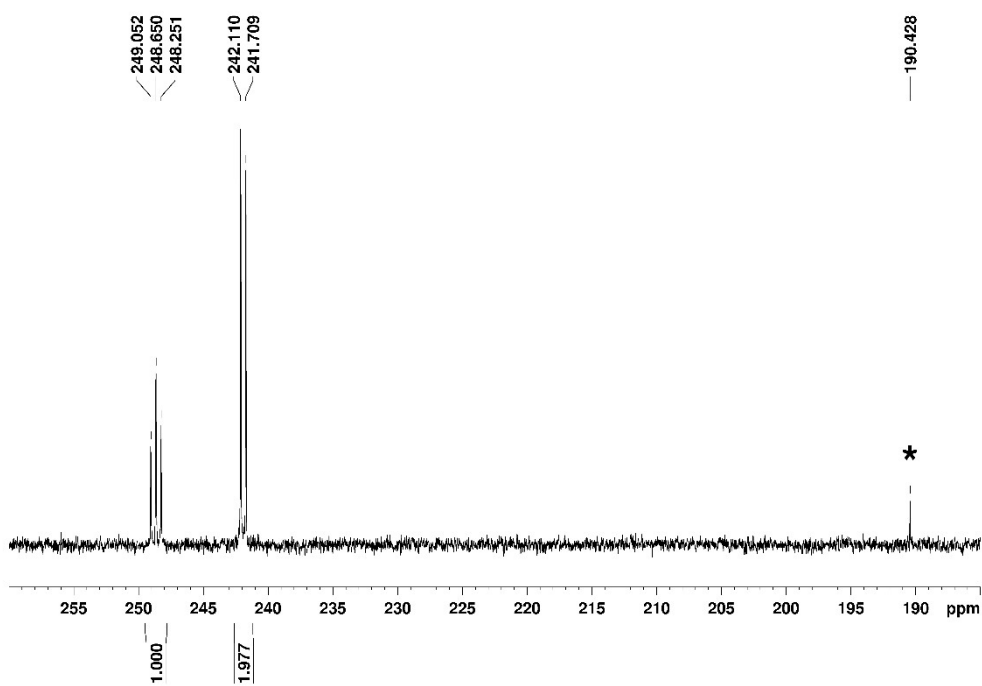


**Figure 48:**  $^{31}\text{P}\{^1\text{H}\}$  NMR of **4-2** in  $\text{thf-d}_8$ . The signal marked with \* is attributed to an unidentified byproduct, possibly  $[\text{K}][1,3\text{-P}_2\text{C}_3\text{Ad}_3]$ .

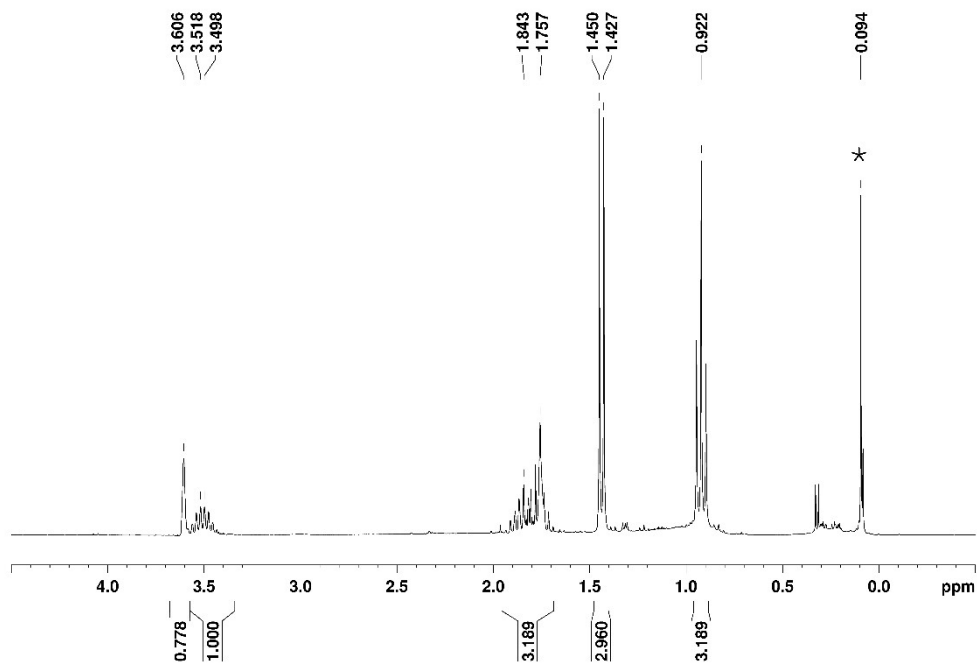


**Figure 49:**  $^1\text{H}$  NMR of **4-3** in  $\text{thf-d}_8$ .

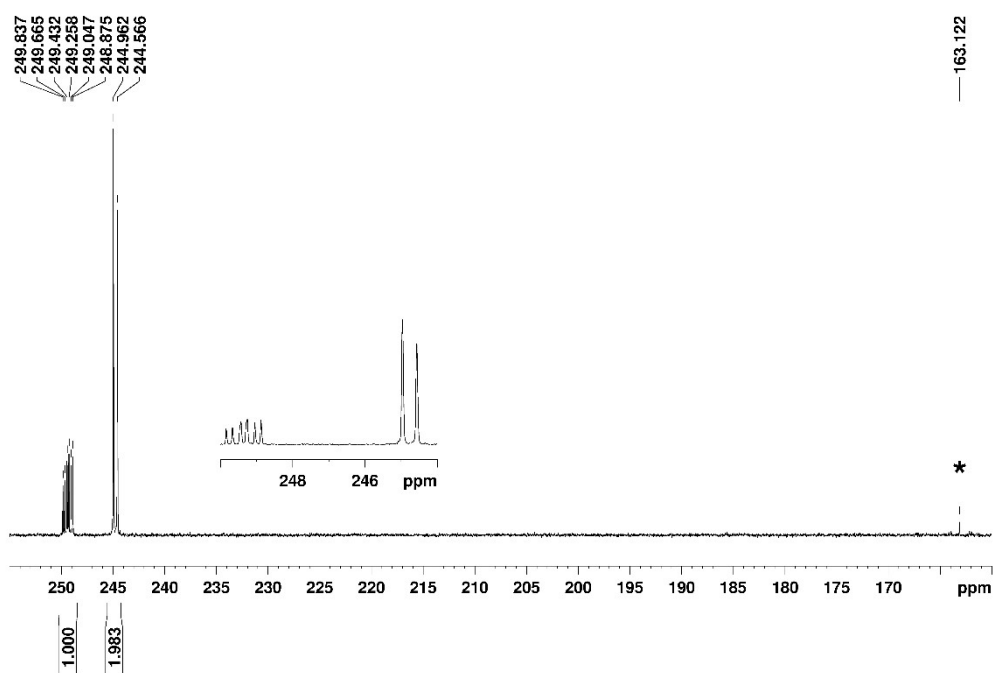


**Figure 50:**  $^{31}\text{P}\{^1\text{H}\}$  NMR of **4-3** in  $\text{thf-d}_8$ . The signal marked with \* is presumed to be the byproduct  $[\text{K}][1,3\text{-P}_2\text{C}_3^{\text{sBu}_3}]$ .

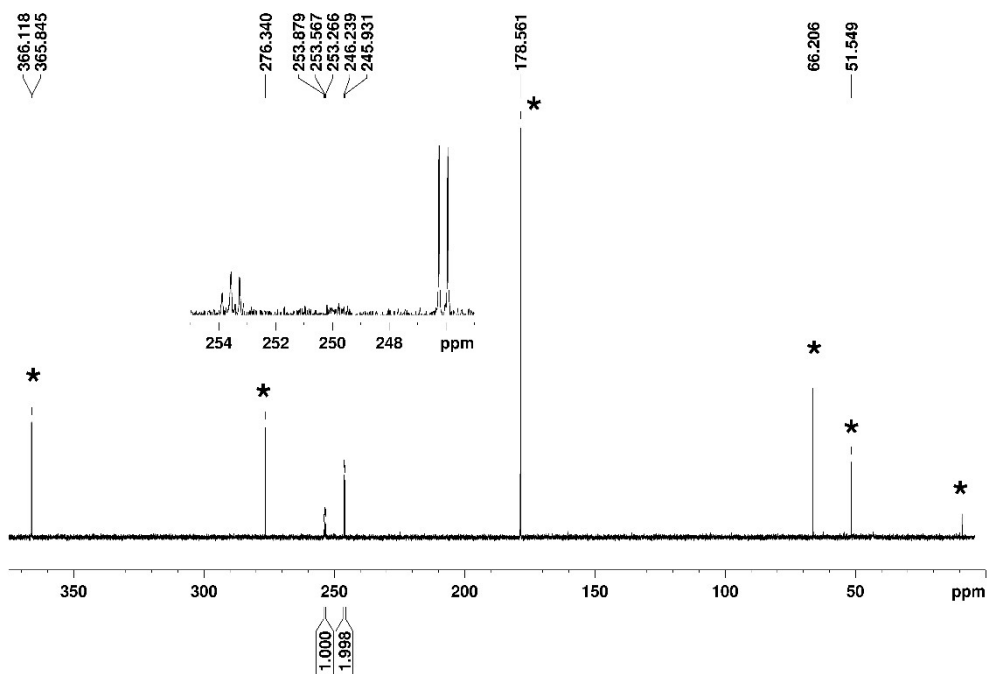


**Figure 51:**  $^{31}\text{P}\{^1\text{H}\}$  NMR of the reaction mixture of  $[\text{K}][1,2,4\text{-P}_3\text{C}_2\text{Ad}_2]$  with  $\text{InI}$  in  $\text{thf-d}_8$ . The signals marked with \* are from unidentified byproducts, the unmarked from  $[\text{In}][1,2,4\text{-P}_3\text{C}_2\text{Ad}_2]$ .



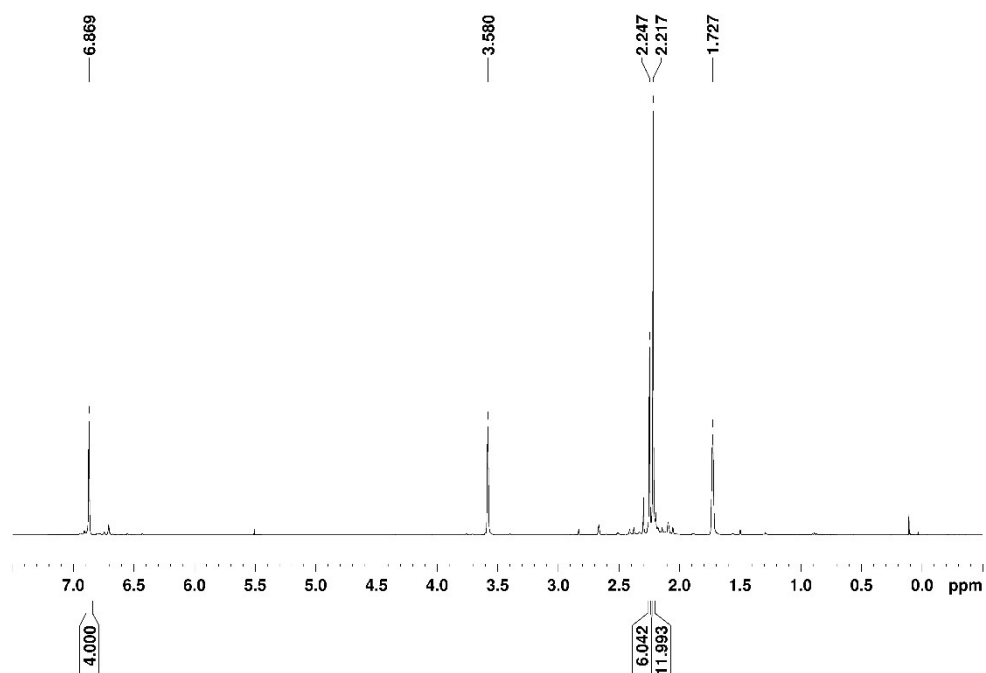


Figure 52:  $^1\text{H}$  NMR of 4-5 in  $\text{thf-d}_8$ .

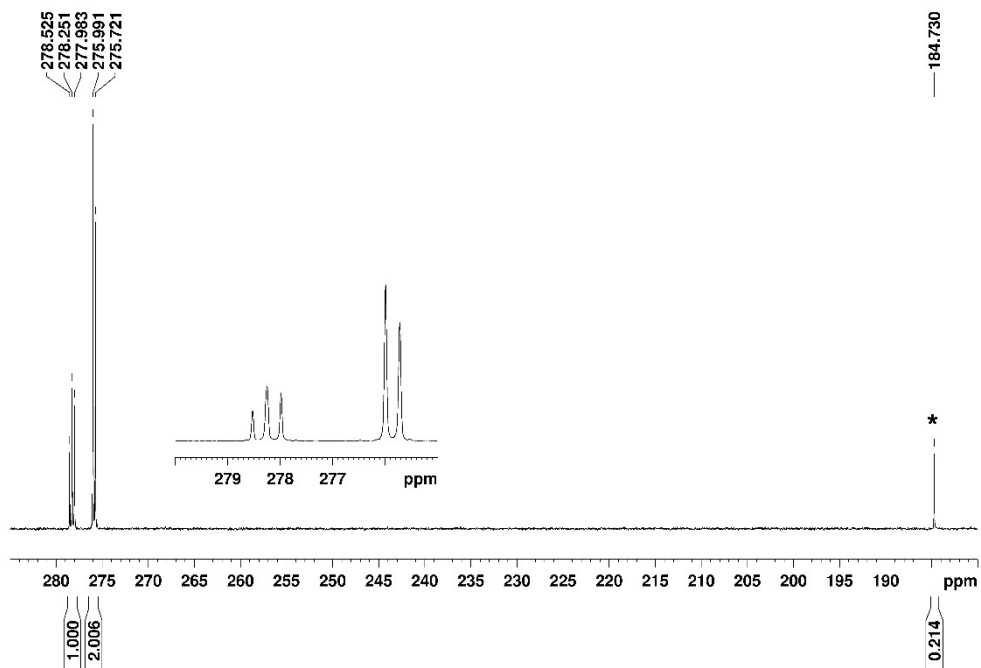
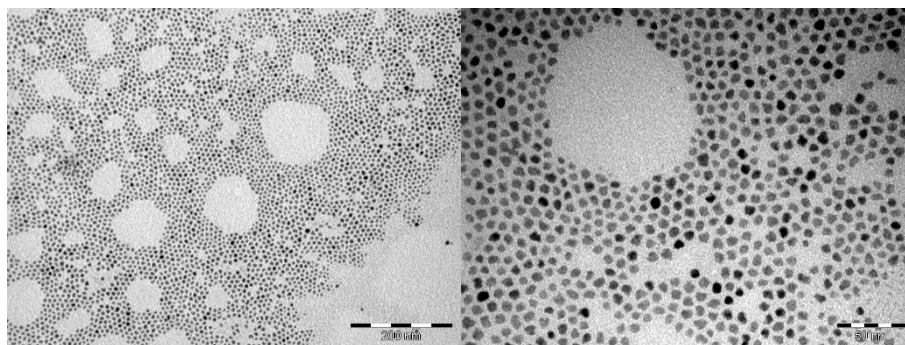


Figure 53:  $^{31}\text{P}\{^1\text{H}\}$  NMR of 4-5 in  $\text{thf-d}_8$ . The signal marked with \* is assigned to the byproduct  $[\text{In}][1,3\text{-P}_2\text{C}_3\text{Mes}_3]$ .

#### 4.6.4. Characterisation of Nanoparticles

The TEM and HRTEM images were performed on the university of Toulouse at the Laboratoire de Physique et Chimie de Nano-Objets from Prof. Dr. Fabien Delpech and Dr. Celine Navral. Therefore copper grids with Formvar/cole coating with 400 mesh grid size were used, on which a drop of diluted colloidal solution of the particles was applied. The size of the particles was determined by the program *ImageJ*.<sup>[43]</sup>



**Figure 54:** TEM images of 4-6a.

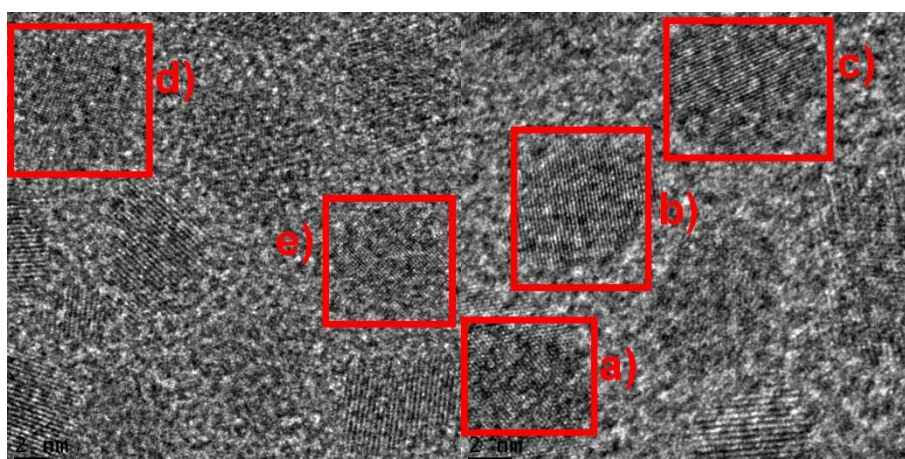


**Figure 55:** HRTEM images of 4-6a (800k magnification left, 1000k right).

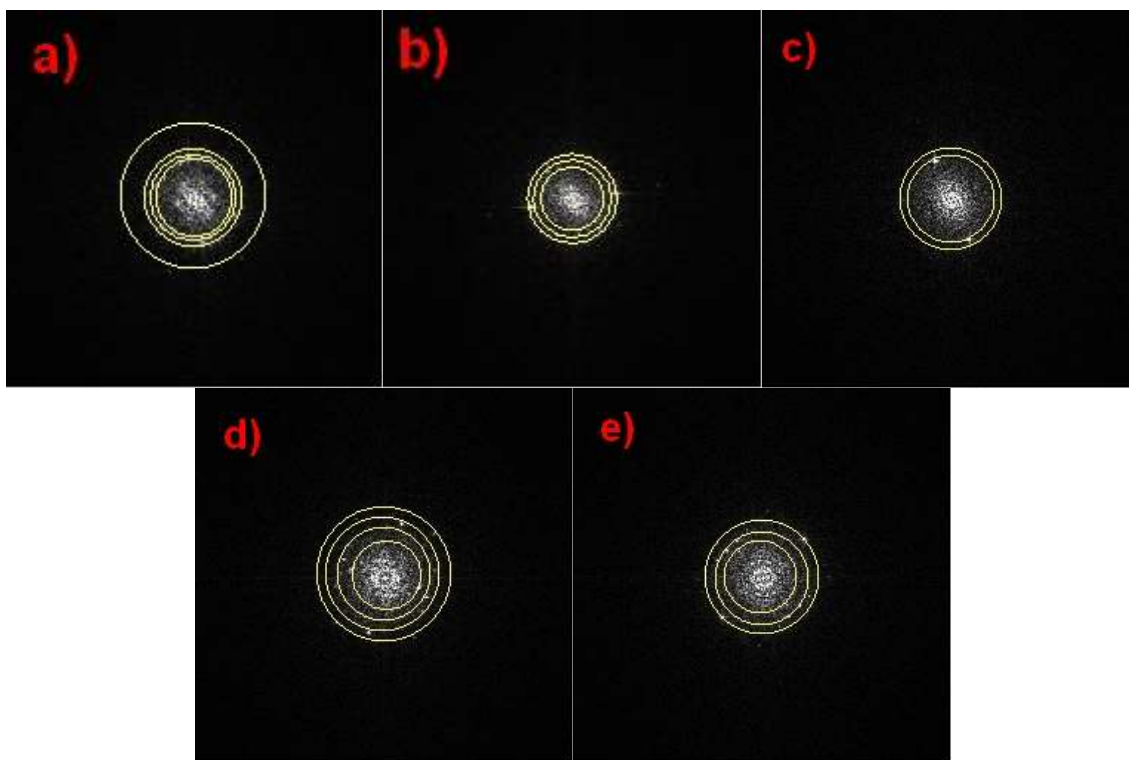


**Figure 56:** HRTEM images overlaid with fast fourier transformation patterns of 4-6a.

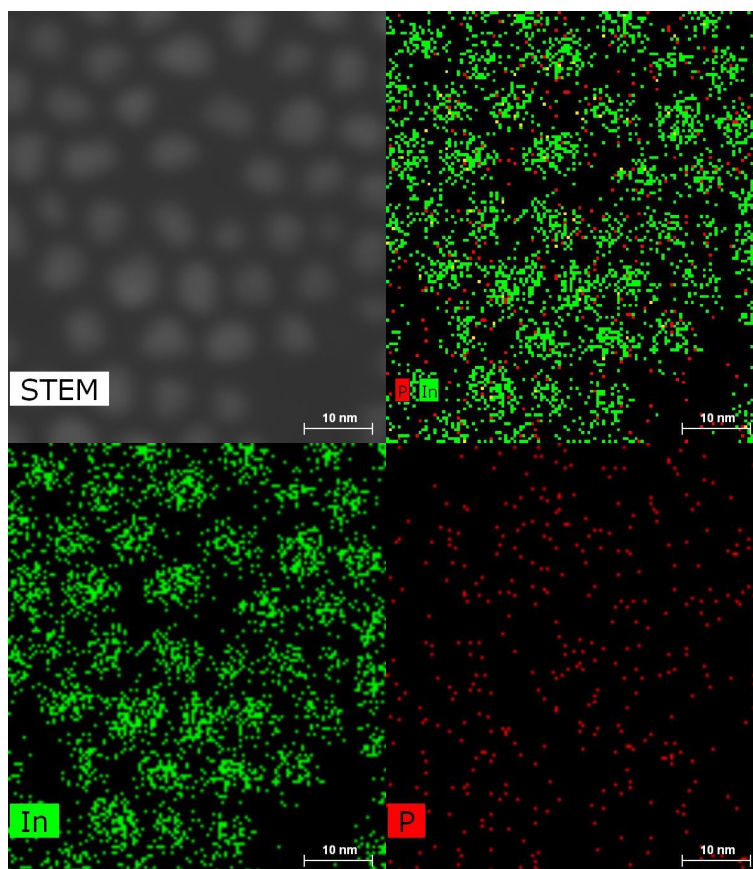


**Figure 57:** EDX illustration in HRTEM images of 4-6a.

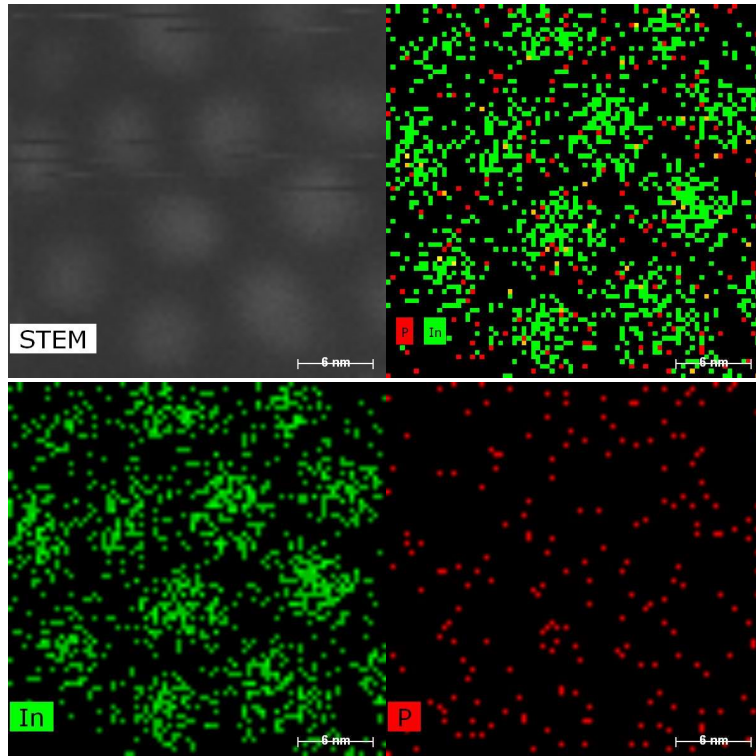


Figure 58: EDX illustration in HRTEM images of 4-6a.

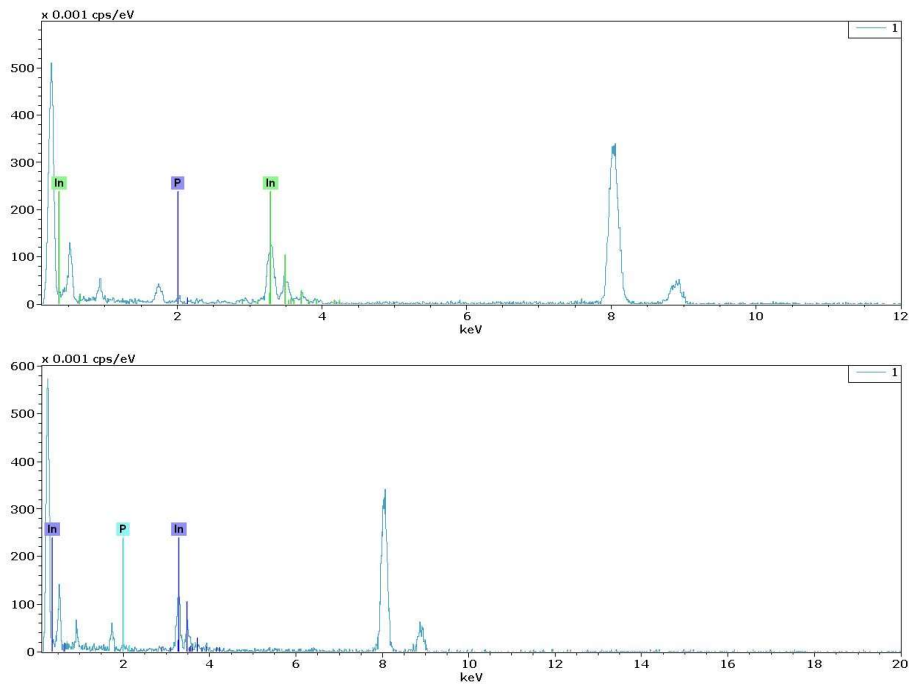
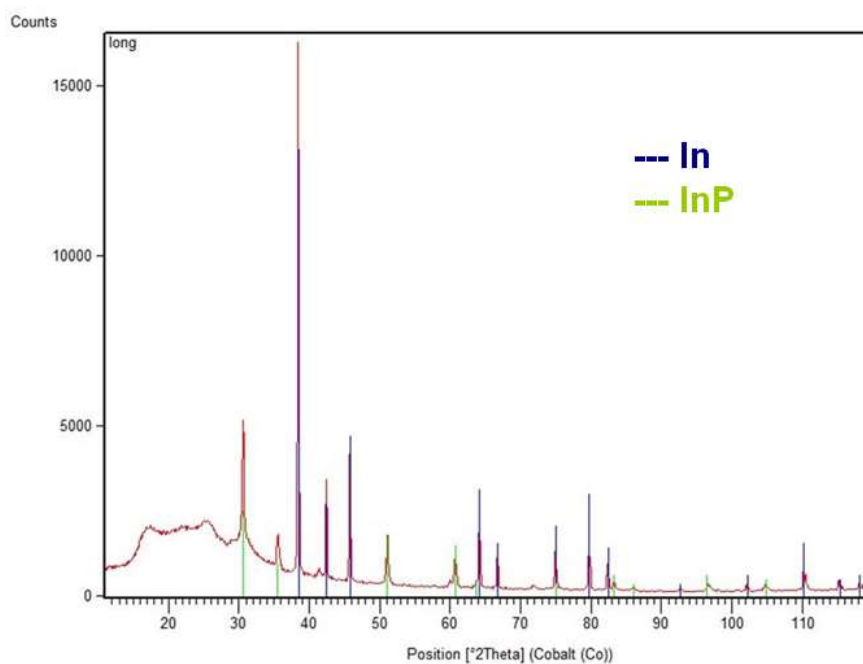
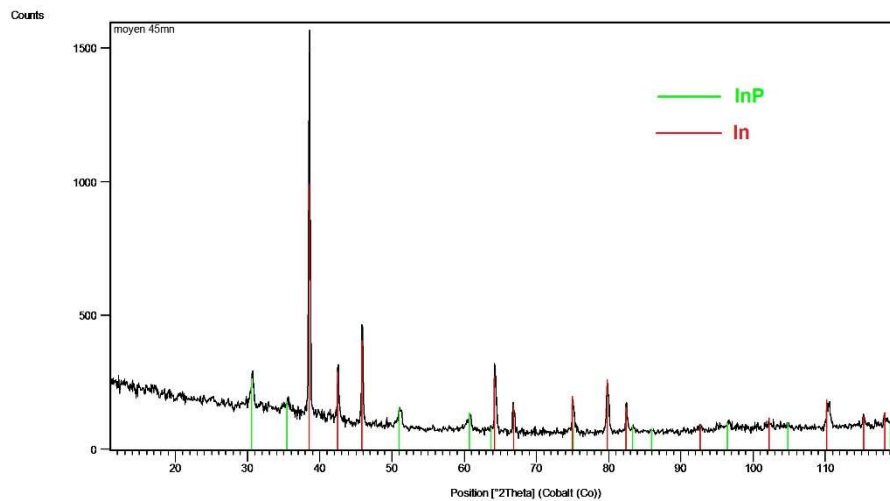


Figure 59: EDX spectra of 4-6a.



**Figure 60:** XRD spectra of **4-6a**. The XRD spectra of InP and In are included as comparison.



**Figure 61:** XRD spectra of **4-6b**. The XRD spectra of InP and In are included as comparison.

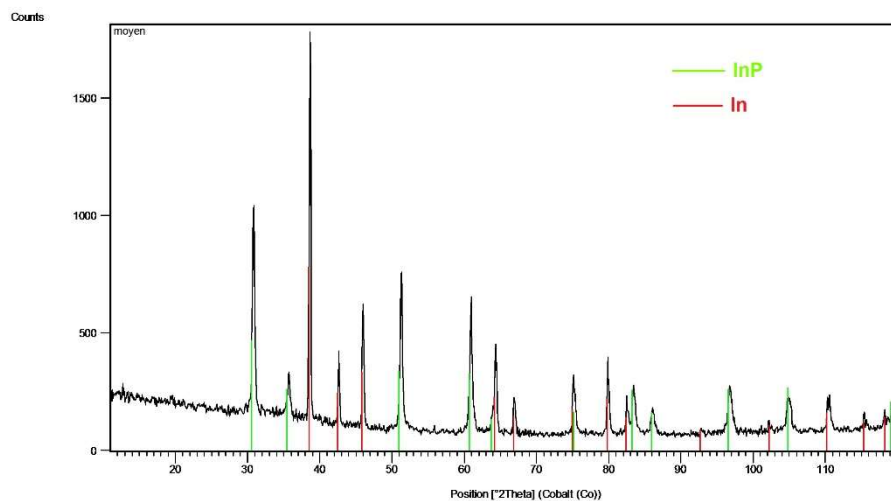


**Figure 62:** XRD spectra of **4-6c**. The XRD spectra of InP and In are included as comparison.

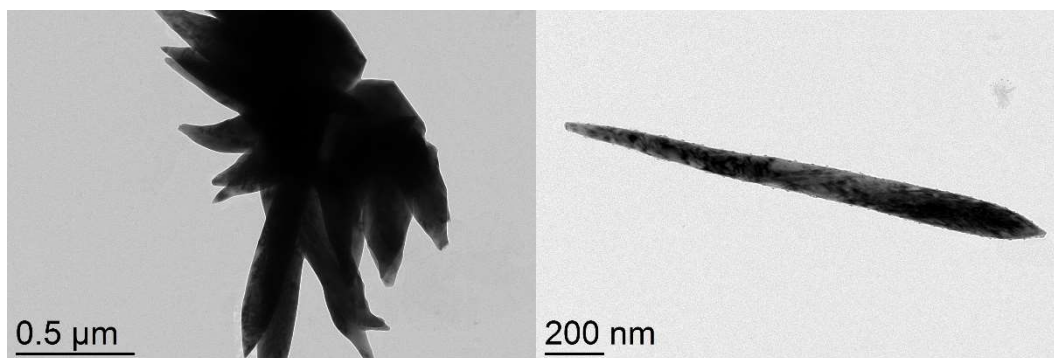


**Figure 63:** TEM images of **4-6c**.

#### 4.6.5. Thermogravimetric Analysis

The TGA was performed by Ulrike Schiessl at the Universität Regensburg, Institute of Inorganic Chemistry, Prof. Dr. Arno Pfitzner on a Thermowaage TG50 of Mettler Toledo. The heating rate was 10°C per minute.

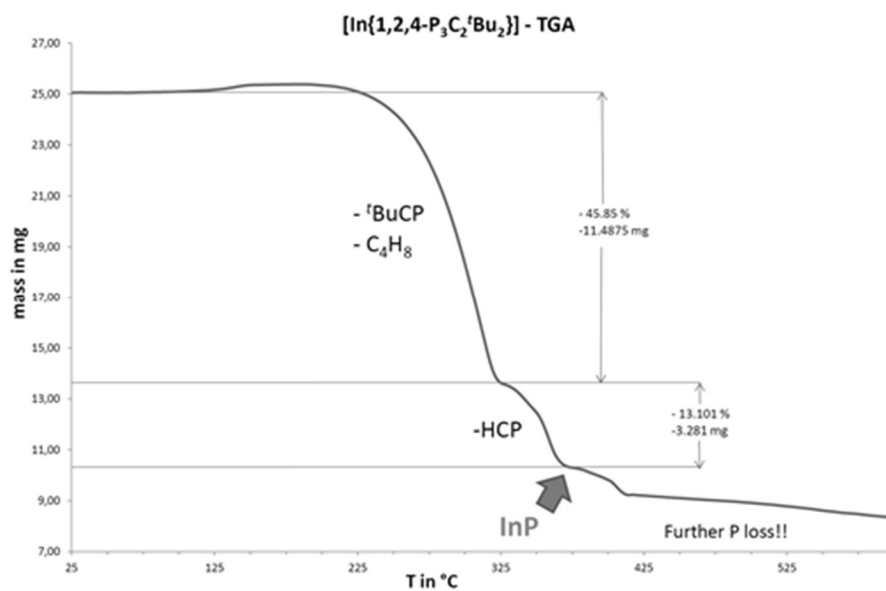


Figure 64: TGA of 4-1.

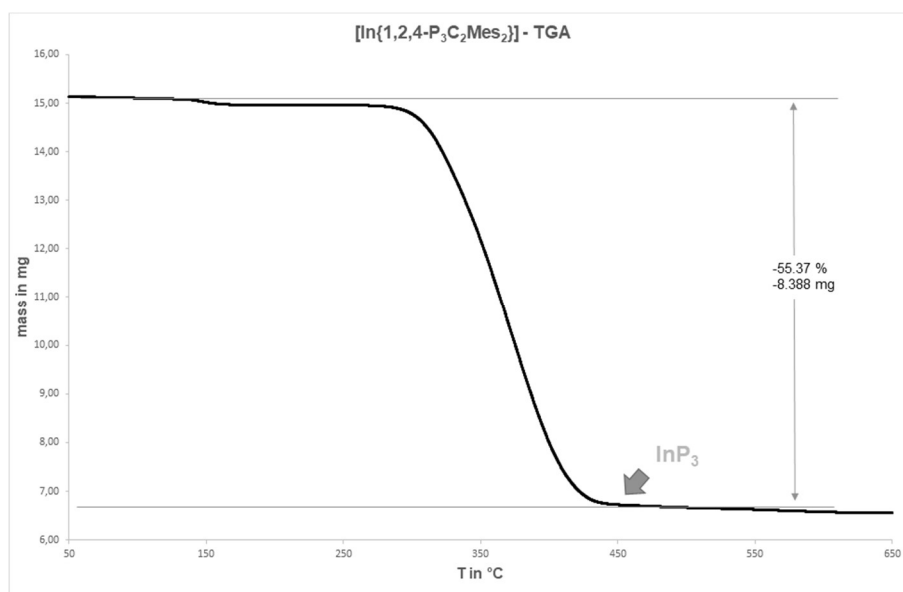


Figure 65: TGA of 4-5.



## 4.7. References

- [1] A. Iandelli, *Gazz. Chim. Ital.* **1941**, *71*, 58
- [2] R. Didchenko, J. E. Alix, R. H. Toeniskoetter, *J. Inorg. Nucl. Chem.* **1960**, *14*, 35-37.
- [3] K. Onuma, A. Kasahara, K. Kato, N. Aihara, T. Udagawa, *J. Cryst. Growth* **1991**, *107*, 360-364.
- [4] M. Usuda, K. Sato, R. Takeuchi, K. Onuma, T. Udagawa, *J. Electron. Mater.* **1996**, *25*, 407-409.
- [5] X. Yang, D. Zhao, K. S. Leck, S. T. Tan, Y. X. Tang, J. Zhao, H. V. Demir, X. W. Sun, *Adv. Mater.* **2012**, *24*, 4180-4185.
- [6] N. Kinomura, K. Terao, S. Kikkawa, H. Horiuchi, M. Koizumi, H. Setoguchi, *Mater. Res. Bull.* **1983**, *18*, 53-57.
- [7] H. Zhang, D.-H. Ha, R. Hovden, L. F. Kourkoutis, R. D. Robinson, *Nano Lett.* **2011**, *11*, 188-197.
- [8] O. I. Micic, C. J. Curtis, K. M. Jones, J. R. Sprague, A. J. Nozik, *J. Phys. Chem.* **1994**, *98*, 4966-4969.
- [9] O. I. Micic, J. R. Sprague, C. J. Curtis, K. M. Jones, J. L. Machol, A. J. Nozik, H. Giessen, B. Fluegel, G. Mohs, N. Peyghambarian, *J. Phys. Chem.* **1995**, *99*, 7754-7759.
- [10] A. A. Guzelian, J. E. B. Katari, A. V. Kadavanich, U. Banin, K. Hamad, E. Juban, A. P. Alivisatos, R. H. Wolters, C. C. Arnold, J. R. Heath, *J. Phys. Chem.* **1996**, *100*, 7212-7219.
- [11] O. I. Mičić, S. P. Ahrenkiel, A. J. Nozik, *Appl. Phys. Lett.* **2001**, *78*, 4022-4024.
- [12] L. Li, M. Protière, P. Reiss, *Chem. Mater.* **2008**, *20*, 2621-2623.
- [13] A. Cros-Gagneux, F. Delpech, C. Nayral, A. Cornejo, Y. Coppel, B. Chaudret, *J. Am. Chem. Soc.* **2010**, *132*, 18147-18157.
- [14] H. Borchert, S. Haubold, M. Haase, H. Weller, C. McGinley, M. Riedler, T. Möller, *Nano Lett.* **2002**, *2*, 151-154.
- [15] D. D. Lovingood, G. F. Strouse, *Nano Lett.* **2008**, *8*, 3394-3397.
- [16] S. Xu, J. Ziegler, T. Nann, *J. Mater. Chem.* **2008**, *18*, 2653-2656.
- [17] L. Li, P. Reiss, *J. Am. Chem. Soc.* **2008**, *130*, 11588-11589.
- [18] X. Yang, D. Zhao, K. S. Leck, S. T. Tan, Y. X. Tang, J. Zhao, H. V. Demir, X. W. Sun, *Adv. Mater.* **2012**, *24*, 4180-4185.
- [19] J. Gao, K. Chen, R. Luong, D. M. Bouley, H. Mao, T. Qiao, S. S. Gambhir, Z. Cheng, *Nano Lett.* **2012**, *12*, 281-286.
- [20] H. Virieux, M. Le Troedec, A. Cros-Gagneux, W.-S. Ojo, F. Delpech, C. Nayral, H. Martinez, B. Chaudret, *J. Am. Chem. Soc.* **2012**, *134*, 19701-19708.
- [21] N. Miao, B. Xu, N. C. Bristowe, J. Zhou, Z. Sun, *J. Am. Chem. Soc.* **2017**, *139*, 11125-11131.
- [22] Z. Li, M. Qian, L. Song, L. Ma, H. Qiu, X. C. Zeng, *PCCP* **2019**, *21*, 1285-1293.
- [23] S. L. Castro, S. G. Bailey, R. P. Raffaele, K. K. Banger, A. F. Hepp, *J. Phys. Chem. B* **2004**, *108*, 12429-12435.
- [24] N. L. Pickett, P. O'Brien, *Chem. Rec.* **2001**, *1*, 467-479 and references therein.
- [25] J. P. Carpenter, C. M. Lukehart, S. B. Milne, S. R. Stock, J. E. Wittig, B. D. Jones, R. Glosser, J. G. Zhu, *J. Organomet. Chem.* **1998**, *557*, 121-130.
- [26] M. D. Francis, P. B. Hitchcock, J. F. Nixon, H. Schnöckel, J. Steiner, *J. Organomet. Chem.* **2002**, *646*, 191-195.

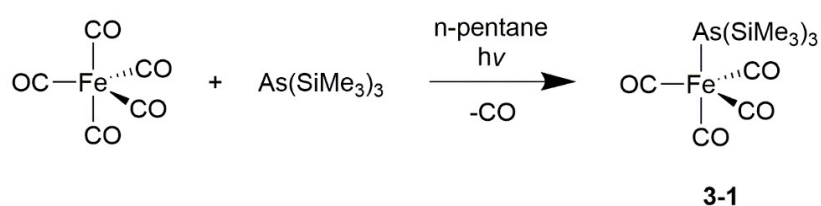


- 
- [27] F. G. N. Cloke, J. C. Green, P. B. Hitchcock, J. F. Nixon, J. L. Suter, D. J. Wilson, *Dalton Trans.* **2009**, 1164-1171.
- [28] C. Callaghan, G. K. B. Clentsmith, F. G. N. Cloke, P. B. Hitchcock, J. F. Nixon, D. M. Vickers, *Organometallics* **1999**, *18*, 793-795.
- [29] C. Heindl, S. Reisinger, C. Schwarzmaier, L. Rummel, A. V. Virovets, E. V. Peresykina, M. Scheer, *Eur. J. Inorg. Chem.* **2016**, *2016*, 743-753.
- [30] C. Heindl, A. Schindler, M. Bodensteiner, E. V. Peresykina, A. V. Virovets, M. Scheer, *Phosphorus, Sulfur, Silicon and Relat. Elem.* **2015**, *190*, 397-403.
- [31] S. M. Mansell, M. Green, R. J. Kilby, M. Murray, C. A. Russell, *CR Chim* **2010**, *13*, 1073-1081.
- [32] C. Müller, R. Bartsch, A. Fischer, P. G. Jones, R. Schmutzler, *J. Organomet. Chem.* **1996**, *512*, 141-148.
- [33] O. T. Beachley, J. C. Pazik, T. E. Glassman, M. R. Churchill, J. C. Fettinger, R. Blom, *Organometallics* **1988**, *7*, 1051-1059
- [34] These crystals were not suitable for X-ray crystallography.
- [35] C. E. Rowland, W. Liu, D. C. Hannah, M. K. Y. Chan, D. V. Talapin, R. D. Schaller, *ACS Nano* **2014**, *8*, 977-985.
- [36] F. Uhlig, R. Hummeltenberg, *J. Organomet. Chem.* **1993**, *452*, C9-C10.
- [37] C. Callaghan, G. K. B. Clentsmith, F. G. N. Cloke, P. B. Hitchcock, J. F. Nixon, D. M. Vickers, *Organometallics* **1999**, *18*, 793-795.
- [38] G. Recker, *Z. Anorg. Allg. Chem.* **1976**, *423*, 242-254.
- [39] CrysAlisPro Software System, Agilent Technologies UK Ltd, Yarnton, Oxford, **2014**
- [40] O. V. Dolomanov, L. J. Bourhis, R. J. Gildea, J. A. K. Howard, H. Puschmann, *J. Appl. Crystallogr.* **2009**, *42*, 339-341
- [41] G. M. Sheldrick, *Acta Crystallographica Section A* **2015**, *71*, 3-8
- [42] G. Sheldrick, *Acta Crystallographica Section C* **2015**, *71*, 3-8
- [43] C. A. Schneider, W. S. Rasband, K. W. Eliceiri, *Nature Methods* **2012**, *9*, 671-675.

## 5. Conclusion

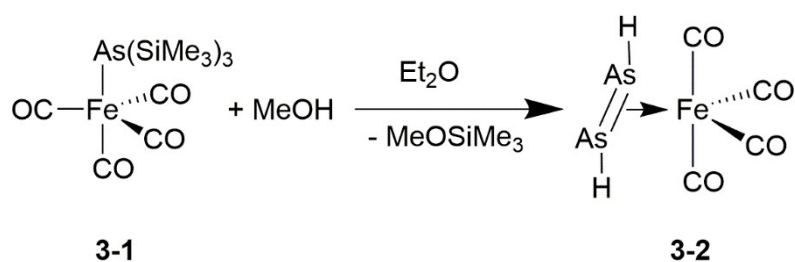
### 5.1. A Parent Diarsene $\text{HAs}=\text{AsH}$ Complex as AsH Unit Source to Novel Compounds

Recently, we reported the usage of the single-source precursor  $[\text{Fe}(\text{CO})_4(\text{PH}_3)]$  for the synthesis of iron phosphide nanoparticles and showed, that complexes containing exclusively labile CO ligands and hydrogen substituents on a pnictogenyl atom display suitable precursors for the synthesis of nanoparticles. Based on that work, it was intended to synthesise an As-containing analogue.



**Scheme 6:** Synthesis of **3-1**.

The irradiation of  $\text{Fe}(\text{CO})_5$  and  $\text{As}(\text{SiMe}_3)_3$  in pentane affords  $[\{\text{Fe}(\text{CO})_4\}\text{As}(\text{SiMe}_3)_3]$  (**3-1**) in 81% yield (Scheme 6). The discovery of Compound **3-1** closes the gap between the two already known analogues  $[\{\text{Fe}(\text{CO})_4\}\text{E}(\text{SiMe}_3)_3]$  ( $\text{E} = \text{P}, \text{Sb}$ ). Compound **3-1** has been fully characterised by  $^1\text{H}$  and  $^{13}\text{C}$  NMR, IR, MS and X-Ray structure analysis (Figure 66). To investigate the thermal decomposition pathway of **3-1**, a TGA and nanoparticle synthesis followed by TEM investigations were performed. Unfortunately, for **3-1**, no concrete indications of the suitability of compound **3-1** for nanoparticle synthesis could be obtained.



**Scheme 7:** Synthesis of **3-2**.

The methanolysis of **3-1** at low temperatures ( $-80\text{ }^\circ\text{C}$ ) and the following purification via sublimation result in the complex  $[\{\text{Fe}(\text{CO})_4\}\{\eta^2\text{-As}_2\text{H}_2\}]$  **3-2** in a yield of 86% (Scheme 2). Compound **3-2** is the first complex containing a  $\text{HAs}=\text{AsH}$  ligand stabilised by only one sterically non-demanding organometallic fragment. The methanolysis of **3-1** with deuterated methanol yielded the deuterated derivative **3-2D**. **3-2** has been fully characterised by  $^1\text{H}$  and  $^2\text{H}$  NMR spectroscopy, IR spectroscopy, MS and X-Ray structure analysis (Figure 66). DFT calculations revealed that the *trans* isomer is thermodynamically favoured. Additionally, **3-2** is best described as an olefin-like complex. Compound **3-2** is extremely air- and

moisture-sensitive and rapidly decomposes rapidly at temperatures above  $-20^{\circ}\text{C}$ . This is the reason why further investigations on the suitability of this compound for nanoparticle synthesis have not been performed.

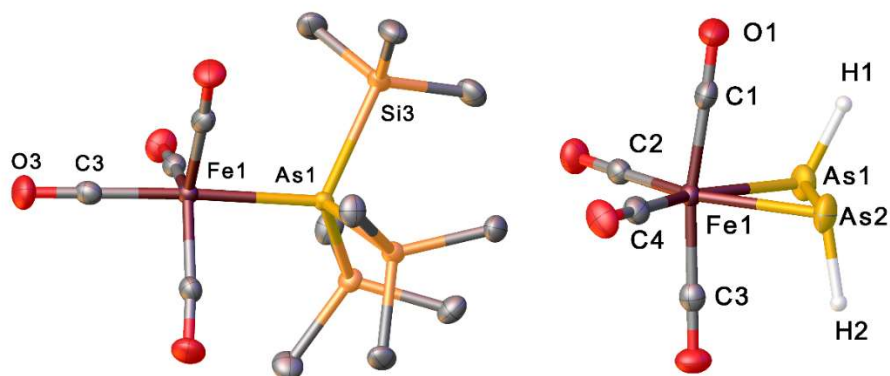
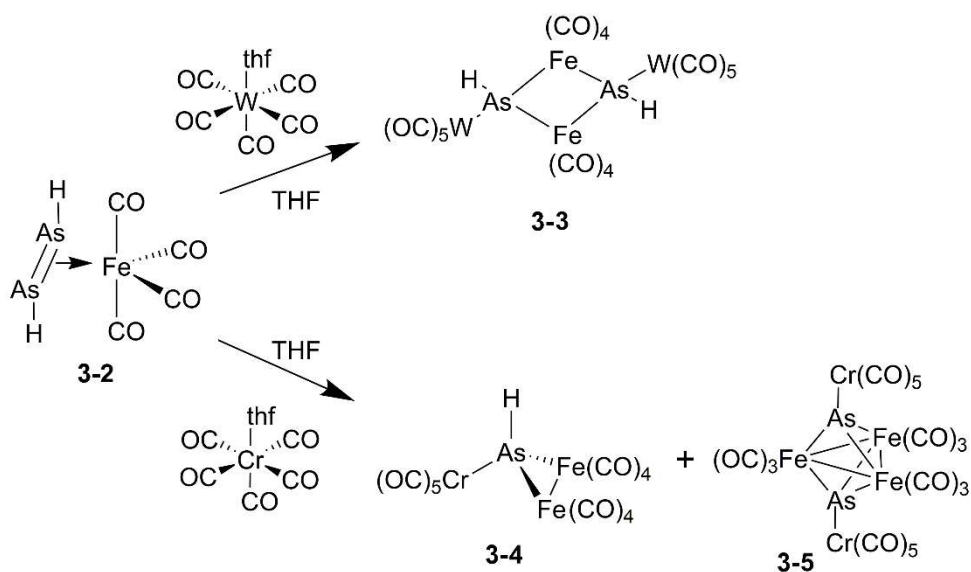


**Figure 66:** Molecular structure of **3-1** (left, hydrogen atoms are omitted for clarity) and **3-2** (right) with ellipsoids set at 50% probability.

To investigate the reaction behaviour of the unprotected  $\text{HAs}=\text{AsH}$  unit, synthesis with Lewis acids were performed. The reaction of **3-2** and  $[\text{W}(\text{CO})_5(\text{thf})]$  affords  $[\{\text{Fe}(\text{CO})_4\}\text{AsH}\{\text{W}(\text{CO})_5\}]_2$  (**3-3**) in 43% yield, which represents the first compound with a planar  $\text{As}_2\text{Fe}_2$  ring that has been structurally characterised (Scheme 8). The reaction with **3-2D** leads to the deuterated derivative **3-3D**. Compound **3-3** has been fully characterised by  $^1\text{H}$  and  $^2\text{H}$  NMR spectroscopy, IR spectroscopy, MS and X-Ray structure analysis (Figure 67). Despite the fact, that **3-3** exhibits the desired requirements for being a single-source precursor for nanoparticle synthesis, the yield (132 mg) was too low to perform a detailed study on the synthesis of nanoparticles.



**Scheme 8:** Reactivity of **3-2** towards the Lewis acids  $[\text{M}(\text{CO})_5(\text{thf})]$  ( $\text{M} = \text{Cr}, \text{W}$ ).

To investigate, if all group 6 elements react equally, further syntheses were performed. The reaction of **3-2** and  $[\text{Cr}(\text{CO})_5(\text{thf})]$  affords  $[\{\text{Fe}_2(\text{CO})_8\}\text{AsH}\{\text{Cr}(\text{CO})_5\}]$  (**3-4**) in 20% yield (Scheme 8), which show a different structure to **3-3**. In literature, there are only few complexes described containing AsH ligands in which the arsenic is tetrahedrally coordinated. The reaction with **3-2D** reveals an unexpected H/D exchange during the reaction. Compound **3-4** has been fully characterised by  $^1\text{H}$  NMR spectroscopy, IR spectroscopy, MS and X-Ray structure analysis (Figure 67). Like **3-3**, the new compound **3-4** exhibits the desired requirements for being a single-source precursor for nanoparticle synthesis, but the yield (33 mg) was too low to perform detailed nanoparticle investigations.

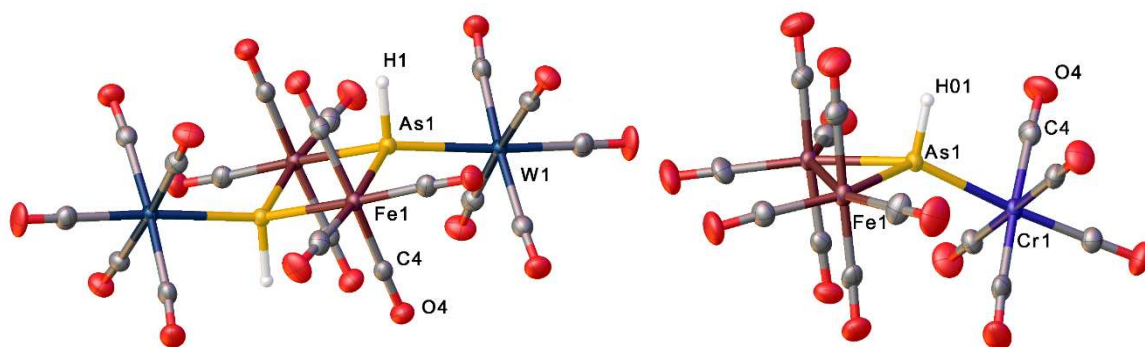


**Figure 67:** Molecular structure of **3-3** (left) and **3-4** (right) with ellipsoids set at 50% probability.

During the investigation of the reaction behaviour of the unprotected  $\text{HAs}=\text{AsH}$  unit towards Lewis acids, new synthetic routes for the known compounds  $[\text{Fe}_3(\text{CO})_9\{\mu_3\text{-AsCr}(\text{CO})_5\}_2]$  (**3-5**) and  $[\text{Fe}_3(\text{CO})_9\{\mu_3\text{-AsMnCp}(\text{CO})_2\}_2]$  (**3-6**) have been found by reacting **3-2** with  $[\text{Cr}(\text{CO})_5(\text{thf})]$  and  $[\text{MnCp}(\text{CO})_2(\text{thf})]$ .

## 5.2. Indium Triphospholyls Examined as Precursor for Nanoparticle Synthesis

Nixon *et al.* stated, that  $[\text{In}][1,2,4\text{-P}_3\text{C}_2^t\text{Bu}_2]$  (**4-1**) is a suitable precursor for crystalline indium phosphide nanoparticles under mild conditions. In this work, the preliminary study on this topic, done in our group by Susanne Bauer in cooperation with Bruno Chaudret, is summarised and brought into publication format. They investigated the multistep decomposition of **4-1** by TGA, performed nanoparticle synthesis in mesitylene with the stabilisers hexadecylamine (HDA) and oleic acid (OA) and investigated the obtained nanoparticles with TEM, HRTEM, EDX, XRD. The results of these analytics revealed, that these particles consist only on the shell of InP, the core is In.

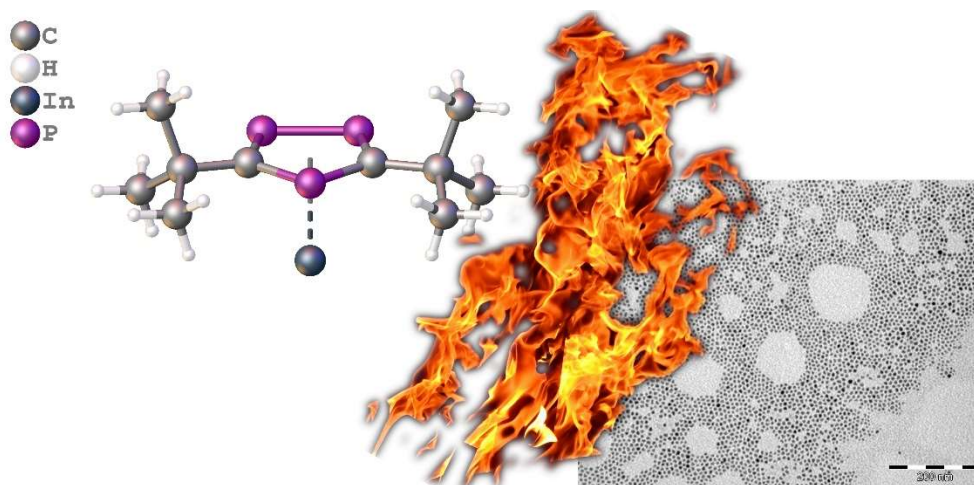
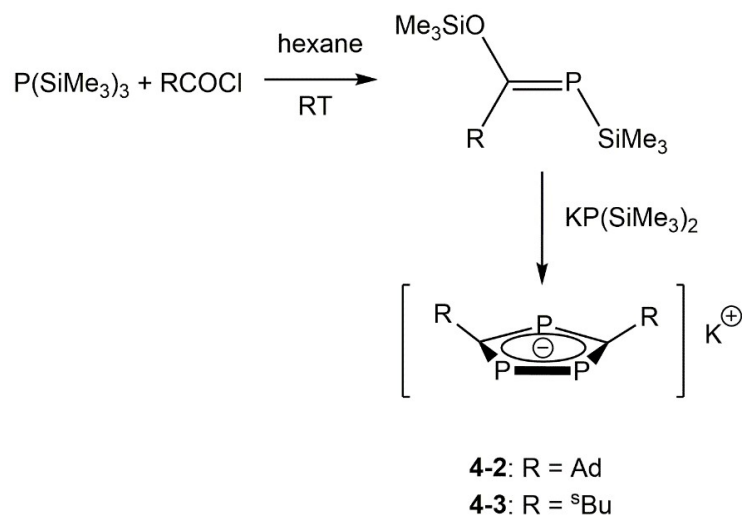


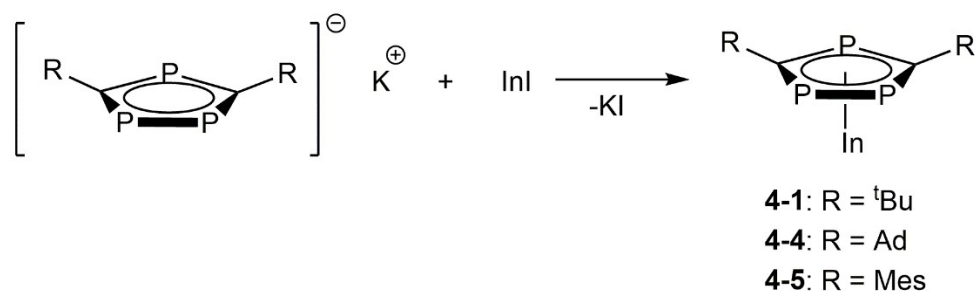
**Figure 68:** Grafically display, that the thermal decomposition of **4-1** leads to nanoparticles.

To increase the ratio of InP in the NPs, the substitution of the  $t$ Bu substituent of the triphospholyl ligand was performed. As starting materials, we present the reaction of  $[\text{K}][\text{P}(\text{SiMe}_3)_3]$  with  $\text{Me}_3\text{SiO}(\text{R})\text{C}=\text{P}(\text{SiMe}_3)_2$  leading to novel potassium triphospholyl salts  $[\text{K}][1,2,4\text{-P}_3\text{C}_2\text{R}_2]$  ( $\text{R} = \text{Ad}$  (**4-2**),  $t$ Bu (**4-3**)) in 57% (**4-2**) and 29% (**4-3**) yield, respectively (Scheme 9). Both compounds were characterised by  $^1\text{H}$  and  $^{31}\text{P}\{^1\text{H}\}$  NMR spectroscopy.



**Scheme 9:** Synthesis of potassium triphospholyls.

The reaction of **4-2** with InI lead to  $[\text{In}][1,2,4\text{-P}_3\text{C}_2\text{Ad}_2]$  (**4-4**), a novel indium triphospholy compound with adamantyl substituents, which was characterised by  $^{31}\text{P}\{^1\text{H}\}$  NMR and MS, but could not be further isolated (Scheme 10). The reaction of  $[\text{K}][1,2,4\text{-P}_3\text{C}_2\text{Mes}_2]$  with InI affords  $[\text{In}][1,2,4\text{-P}_3\text{C}_2\text{Mes}_2]$  (**4-5**) in 40% yield (Scheme 10). Besides compound **4-1**, compound **4-5** is the second fully characterised indium triphospholy. Additionally, it represents the indium triphospholy compound with the most sterically demanding substituents synthesised so far. Another feature is the new crystal packing. Compound **4-5** has been fully analysed by  $^1\text{H}$  and  $^{31}\text{P}\{^1\text{H}\}$  NMR spectroscopy, MS, EA and X-Ray structure analysis. The elimination of the phosphalkyne  $\text{P}\equiv\text{CMes}$  at the conditions given by the mass spectroscopy is appealing for NP investigations. To investigate the thermal decomposition pathway of **4-5**, a TGA was performed. It shows a one-step decomposition, leaving theoretically  $\text{InP}_3$ , which makes this compound a promising subject for further investigations.

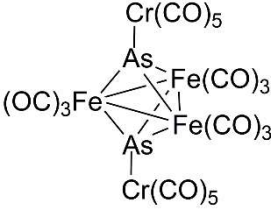
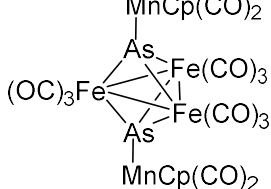
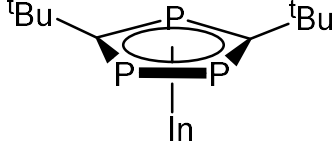
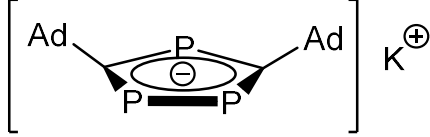
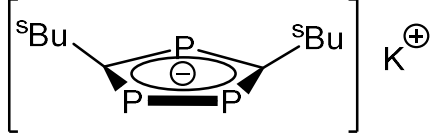
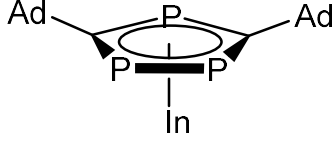
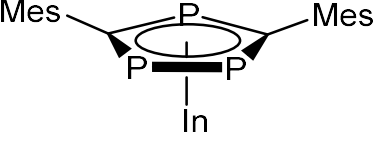


**Scheme 10:** Salt metathesis of 1,2,4-triphospholyls

## 6. Appendix

### 6.1. List of Numbered Compounds

Numbered compound	Structural formula or description
<b>3-1</b>	
<b>3-1a</b>	Decomposition product of <b>3-1</b> at 160°C without stabilisers
<b>3-1b</b>	Decomposition product of <b>3-1</b> at 160°C, stabilised with 1eq HDA
<b>3-1c</b>	Decomposition product of <b>3-1</b> at 160°C, stabilised with 1eq OA
<b>3-2</b>	
<b>3-2D</b>	
<b>3-3</b>	
<b>3-3D</b>	
<b>3-4</b>	

3-5	
3-6	
3-A	[[Tren <sup>TIPS</sup> U) <sub>2</sub> (As <sub>2</sub> H <sub>2</sub> )] (Tren <sup>TIPS</sup> = N(CH <sub>2</sub> CH <sub>2</sub> NSiPr <sub>3</sub> ) <sub>3</sub> )
3-B	[Fe(CO) <sub>4</sub> ]{η <sup>2</sup> -As <sub>2</sub> Ph <sub>2}}</sub>
3-C	[Fe <sub>2</sub> (CO) <sub>8</sub> ]AsPh{Cr(CO) <sub>5</sub> }
4-1	
4-2	
4-3	
4-4	
4-5	
4-6a	Decomposition product of <b>4-1</b> at 290°C stabilised with 1 eq HDA and 1 eq OA.
4-6b	Decomposition product of <b>4-1</b> at 170°C stabilised with 1 eq HDA and 1 eq OA.
4-6c	Decomposition product of <b>4-1</b> , hot injection method, stabilised with 1 eq HDA and 1 eq OA.



## 6.2. List of Abbreviations

A	Angstroem 1 Å = 1·10 <sup>-10</sup> m
acac	acetylacetonate
Ad	adamantly
AIM	atoms in molecules
bcc	body centered cubic
BCPs	Bond Critical Points
CVD	Chemical Vapour Deposition
D	Deuterium
d	doublet
DEP	Direct Exposure Probe
DFT	Discrete Fourier transform
DIP	Direct Insertion Probe
EDX	Energy dispersive X-ray spectroscopy
EI	Electron Ionisation
hCG	human chorionic gonadotropin
hcp	hexagonal close packed
HDA	hexadecylamine
HOMO	Highest Occupied Molecular Orbital
HRTEM	High Resolution Transmission Electron Microscopy
Hz	Hertz, s <sup>-1</sup>
<i>J</i>	coupling constant, Hz
LED	light emitting diode
LUMO	Lowest Unoccupied Molecular Orbital
[M] <sup>+</sup>	molecular ion peak
m	multiplet
m/z	mass to charge ratio
Mes	mesityl
MOCVD	Metal Organic Chemical Vapour Deposition
MOVPE	metalorganic vapour phase epitaxy
MS	Mass Spectrometry
MSP	Multi source precursor
NBO	Natural Bond Orbital
N <sub>H</sub> S <sub>4</sub>	2,2-bis(2-mercaptophenylthio)diethylamine
NM	Nanomaterial
NMR	Nuclear Magnetic Resonance
NP	Nanoparticles
OA	oleic acid
ppm	part per million
s	singlet
<sup>s</sup> Bu	secondary butyl
SEM	Scanning Electron Microscope

SMAD	Solvated Metal Atom Dispersion
SSP	Single-source precursor
t	triplet
<sup>t</sup> Bu	tertiary butyl
TEM	Transmission Electron Microscope
TGA	Thermogravimetric analysis
thf	tetrahydrofuran, C <sub>4</sub> H <sub>8</sub> O
TOPO	trioctylphosphine oxide
TREN <sup>Tipp</sup> s	N(CH <sub>2</sub> CH <sub>2</sub> NSiPr <sub>3</sub> ) <sub>3</sub>
WBI	Wiberg Bond Index
XRD	Powder X-ray diffraction
δ	chemical shift
ν	Wavenumber, cm <sup>-1</sup>



### 6.3. Danksagung

Ich möchte an dieser Stelle danken:

- Prof. Dr. Manfred Scheer für die Möglichkeit, meine Dissertation an seinem Lehrstuhl anzufertigen und die außerordentlich guten Arbeitsbedingungen.
- Dr. Gábor Balázs für die Hilfe während der ersten Hälfte meiner Promotion und die Durchführung der DFT Rechnungen.
- Michi für Alles! Danke für die sehr gute Aufnahme und Einarbeitung in das Labor, die ständige, selbstlose Hilfe, selbst wenn du besseres zu tun hattest. Für die produktiven und aufmunternden Gespräche, dass du sowohl Paper als auch Dissertation probegelesen hast. Dafür, dass du von einem Kollegen zu einem sehr guten Freund geworden bist.
- Christian und Stefan, danke dass ihr diese Dissertation probegelesen habt.
- Rudi, dass du den anstrengenden Weg der Promotion mitgegangen bist, mit mir über alles gesprochen hast und mir jederzeit mit Rat und Tat beigestanden bist.
- Dani, danke dass wir als Nanopartikel Subgroup so gut zusammengehalten haben und du mir immer hilfreich zur Seite gestanden bist. Du hast mir gezeigt, dass die Kreativität auch während einer Chemiepromotion nicht stirbt. Dein Lachen wird man nie vergessen.
- Tobi, wenn man gemeinsam durch eine schwere Zeit geht, schweißt das zusammen. Danke für die Tipps.
- Michi, Giuliano, Lena und Rudi für die sehr gute, saubere und produktive Laboratmosphäre.
- Andrea und Alexey für die produktive Atmosphäre im Schreibbüro.
- Schotti, dass er als Ausgleich den universitären Spieleabend ins Leben gerufen hat und in diesem Sinne Schotti, Tom, Michi, Giuliano, Sonja, Julian, Valli und Nicolo, dass ihr es mir ermöglicht habt, mein Hobby zu einer Leidenschaft zu formen, die mich geprägt hat.
- An alle ehemaligen und derzeitigen Mitglieder des Lehrstuhls Scheer, die mir bei den unterschiedlichsten Gelegenheiten geholfen haben oder mit denen ich sehr gute Unterhaltungen auf den Feiern führen konnte. Bei einigen wäre vermutlich das Potential einer guten Freundschaft da gewesen, aber leider haben sich die Leben zu wenig überschritten. Danke trotzdem, dass ich mich bei euch wohlfühlen konnte. Ich glaube, ich brauche keine Namen zu nennen, jeder der sich angesprochen fühlt, weiß es.
- Tom, Christian, Susi, Beuti und Matthias möchte ich auch Danke sagen. Wir haben das Studium von Anfang an zusammen bestritten, haben gemeinsam gelacht und gelernt. Ihr habt mit mir Regensburg erkundet und die Zeit innerhalb und außerhalb des Studiums verschönert.
- Karin Kilgert und Barbara Bauer, die mir immer freundlichst mit den verschiedensten Problemen geholfen haben.
- Georgine Stühler und Annette Schramm aus der NMR Abteilung für die Hilfe bei den NMR Messungen.

- Wolfgang Söllner für die sehr gute Betreuung aller massenspektrometrischen Fragen, die sich in der langen Zeit ergeben haben.
- Susanne, danke dass du mich in der finalen Phase der Promotion so gut unterstützt hast und mir gezeigt hast, dass auch kleine Schritte wichtig sind.
- Vielen Dank auch an meine Eltern, Resi und Alois Rund, für die unendliche Unterstützung. Ohne euch wäre diese Promotion nicht möglich geworden, weshalb ich sie euch gewidmet habe.